Charles University

Faculty of Science

Study program: Physical chemistry

Mgr. Michal Malý

Application of advanced models of electromigration by means of computer software
Softwarové aplikace pokročilých modelů elektromigrace

Dissertation thesis

Supervisor: Mgr. Pavel Dubský, Ph.D.

Prague 2020

This dissertation thesis summarizes research results that were achieved over the course of my doctoral studies at the *Electromigration and Chromatography* (ECHMET) group at the Department of Physical and Macromolecular Chemistry of the Faculty of Science of the Charles University.

This work was financially supported by GA UK grant no. 726716, GA ČR grant no. 15–18424Y and GA ČR grant no. 18–11776S.

Prohlašuji, že jsem tuto disertační práci zpracoval samostatně a že jsem uvedl všechny literární či jiné informační zdroje, které jsou v této práci použity. Tato disertační práce ani její podstatná část nebyly použity k získání jiného či stejného akademického titulu.

I hereby declare that I wrote this dissertation thesis myself and that I cited all literature and other sources of information that are used within this thesis. This thesis or any significant part of it have not been used to obtain the same or any other academic degree.

V Praze ....

podpis

Acknowledgements

Well, this will get awkward... Naturally, my biggest and greatest *thank you* goes to Pavel, my supervisor, mostly for putting up with me and my perpetual need to criticize and question everything we have accomplished during these four years. He also introduced me to the world of real science, powerful and daring enough to take an actual peek inside the black box known as the Universe.

I would like to thank Gabriel and Pablo of CIMEC. Collaboration across the Atlantic and multiple timezones is never easy but without you, PeakMaster 6 never would have been what it is!

Finally, I must thank to the entire ECHMET group for being such a great bunch of people. Yes, I am talking about you: The hopeless optimists, the moral beacons, those dangerously passionate about science, those with some strict ideas about beer in the workplace, the everyday sunshines, the protectors of individual privacy, the social rebels... you know who you are and I will truly miss all of you :'(

Keywords

AnglerFish, affinity capillary electrophoresis, capillary zone electrophoresis, complex-forming equilibria, Debye-Hückel, ionic effects, nonlinear theory of electromigration, Onsager-Fuoss, PeakMaster 6, software development

Klíčová slova

AnglerFish, afinitní kapilární elektroforéza, kapilární zónová elektroforéza, komplexační rovnováhy, Debye-Hückel, iontové efekty, nelineární teorie elektromigrace, Onsager-Fuoss, PeakMaster 6, vývoj softwaru

Abstract

Motion of ions under the influence of electric field has been a subject of scientific interest for many decades. Capillary electrophoresis in particular benefited greatly from this research and mathematical models of electromigration applicable to capillary electrophoresis have been developed. As the sophistication of the models grew, so did the computational demands to evaluate them. In order to fully exploit the possibilities of advanced mathematical models a computer implementation capable of solving non-trivial problems at sufficient speed is necessary.

This dissertation thesis explores applications of computer implementations of mathematical models related to electromigration in two different areas. The main focus of this thesis is on the topic of linear theory of electromigration. We discuss the extension of the linear theory of electromigration beyond of just acid-base equilibria and computer implementation of this extented theory which is specialized to include complex-forming equilibria in order to be able to deal with affinity capillary electrophoresis problems. Some technical aspects of the computer implementation are also discussed. This is followed upon by investigating certain selected affinity capillary electrophoresis systems. The purpose of this investigation is to re-derive some of the already known laws and rules valid in affinity capillary electrophoresis systems directly from the extended mathematical model and to provide insight into phenomena that were previously unknown or not sufficiently understood. We investigate some of the systems purely symbolically. However, in order to do that, these systems had to be considerably simplified. Although these simplifications do not compromise the insight gained by the symbolical investigation, numerical computer model was still necessary to design comparable "real-world" counterparts of these systems. We use these "real-world" systems to verify the validity of the used simplifications and for experimental verifications. Some of the phenomena we discuss are impossible to investigate at all without an appropriate computer model.

Later we focus on ionic effects with respect to how they affect effective mobility of an analyte in capillary zone electrophoresis experiments. Analysis of the effective mobility of a chemical compound in appropriately chosen set of background electrolytes can be used to determine pK_A and μ_{lim} constants of the compound. However, due to the ionic effects, pK_A and μ_{lim} constants determined in this way will not represent the true thermodynamic constants but rather some apparent constants valid only under the conditions where they were measured. This problem can be largely eliminated with proper treatment of the experimental data. We discuss the application of nonlinear fit and Debye-Hückel and Onsager-Fuoss laws to calculate true thermodynamic pK_A and μ_{lim} constants from effective mobility values measured in different background electrolytes. The procedure we describe has to evaluate a lengthy series of calculations. A specialized computer program is, therefore, required for the procedure to be fully effective. We introduce such a computer program.

Finally, we demonstrate the use of the data evaluation method described earlier to calculate pK_A and μ_{lim} values of 14 compounds that we then use as pI markers to characterize pH gradients in capillary isoelectric focusing experiments.

Abstrakt

Pohyb iontů v elektrickém poli je předmětem vědeckého výzkumu po mnoho desetiletí. Přínos tohoto výzkumu byl zvlášť významný pro kapilární elektroforézu, pro kterou byly vyvinuty matematické modely elektromigrace. S rostoucí sofistikovaností modelů rostla i náročnost výpočtů nutných k jejich vyřešení. Aby bylo možné plně využít možnosti pokročilých matematických modelů, je zapotřebí příslušná počítačová implementace schopná vyřešit netriviální problémy dostatečně rychle.

Tato disertační práce se zabývá aplikací počítačových implementací matematických modelů vztahujících se k elektromigraci ve dvou oblastech. Hlavním tématem této práce je lineární teorie elektromigrace. Je diskutována rozšířená teorie elektromigrace uvažující více rovnováh než pouze rovnováhy acidobazické a počítačová implementace této teorie, která je specializována pro rovnováhy komplexační, aby bylo možné řešit problémy afinitní kapilární elektroforézy. Jsou zmíněny i některé technické aspekty počítačové implementace. Dále jsou rozebrány vybrané systémy afinitní kapilární elektroforézy. Cílem tohoto rozboru bylo odvodit již dříve známé zákony platné v systémech afinitní kapilární elektroforézy pomocí rozšířené lineární teorie elektromigrace a objasnit tak jevy, které byly dříve nepozorované či nedostatečně vysvětlené. Některé systémy jsou rozebrány čistě symbolicky. To je však možné pouze v případě, že jsou příslušné systémy značně zjednodušeny. Ačkoliv použitá zjednodušení nedevalvují přínos objevů získaných symbolickým rozborem, numerický počítačový model je nutný k návrhu odpovídajících nezjednodušených systémů. Nezjednodušené systémy jsou použity k ověření oprávněnosti provedených zjednodušení a k praktickým experimentům. Některé námi studované systémy není možné bez vhodného počítačového modelu analyzovat vůbec.

Dále se zabýváme iontovými efekty a jejich vlivem na efektivní mobilitu analytů v kapilární zónové elektroforéze. Analýza efektivní mobility chemické látky ve vhodně zvolené sérii pracovních elektrolytů může být použita ke stanovení pK_A a μ_{lim} konstant této látky. Takto stanovené konstanty kvůli vlivu iontových efektů nepřestavují skutečné termodynamické konstanty ale pouze konstanty aparentní, platné pouze v podmínkách, ve kterých byly stanoveny. Tento problém lze do značné míry odstranit vhodným postupem při vyhodnocení experimentálních dat. Diskutujeme použití nelineárního fitu spolu s Debyeovým-Hückelovým a Onsagerovým-Fuossovým zákonem pro výpočet pravých termodynamických pK_A a μ_{lim} z efektivních mobilit změřených v různých pracovních elektrolytech. Postup, který popisujeme se sestává z náročné série výpočtů. Aby byl tento postup skutečně efektivní, je nutné jej implementovat ve formě počítačového programu. Tento program je představen.

Na závěr demonstrujeme použití výše popsané metody vyhodnocení dat k určení pK_A a μ_{lim} konstant 14 látek, které byly použity jako pI markery pro charakterizaci pH gradientu při experimentech kapilární isoelektrické fokusace.

Contents

List of used abbreviations and symbols

ACE	Affinity capillary electrophoresis
ALU	Arithmetic logic unit
BGE	Background electrolyte
CE	Capillary electrophoresis
CZE	Capillary zone electrophoresis
EMD	Electromigration dispersion
FPU	Floating point unit
HVL	Harrhoff-van der Linde
ICIEF	Imaging capillary isoelectric focusing
KRF	Kohlrausch regulating function
LTEM	Linear theory of electromigration
NLTEM	Nonlinear theory of electromigration
PDE	Partial differential equation
a_0	Area of HVL peak
a_1	Center of Gaussian component of HVL peak
a_2	Standard deviation of Gaussian component of HVL peak
$a_{3\delta}$	Measure of triangularity of HVL peak
$[A^z]$	Concentration of ionic form of constituent A and charge z
c_i	Total concentration of i-th constituent
$\tilde{c}$	$\tilde{c}(x,t)$, function of temporospatial concentration disturbances
$\vec{\tilde{c}}$	Column vector of $\tilde{c}$ functions
c_S	Selector concentration
C_i	Total concentration of i-th constituent
$D_{i,z}$	Diffusion coefficient of z-th ion of i-th constituent
$\boldsymbol{D}$	Diffusion matrix
E	Electric field intensity
F	Faraday constant
$[H^+]$	Concentration of H^+ ion
j	Current density
J_i	Total mass flux of i-th constituent
$J_{(g)}$	Mass flux of form g
$J_{(g)em}$	Electromigration contribution to mass flux of form g
$J_{(g)D}$	Diffusion contribution to mass flux of form g
$J_{(g)emdiff}$	Diffusion current contribution to mass flux of form g
K_A	Thermodynamic consecutive acid-base dissociation constant
K'_A	Apparent consecutive acid-base dissociation constant
K_S	Thermodynamic complexation stability (affinity) constant
K_W	Water dissociation constant

$L_{i,z}$	Thermodynamic total acid-base dissociation constant for z-th charge transition of i-th species
$L'_{i,z}$	Apparent total acid-base dissociation constant for z-th charge transition of i-th species
$\boldsymbol{M}$	Matrix form of the system of continuity equations
$\boldsymbol{M_0}$	Mobility matrix of the linearized model of electromigration evaluated at BGE composition (absolute Taylor term)
$\boldsymbol{M_1}$	Electromigration properties matrix (Štědrý's notation)
$\boldsymbol{M_2}$	Acid-base equilibria matrix
$\boldsymbol{M_{1,k}}$	k-th term of the total first Taylor expansion term (Hruška's notation)
n_i	Lowest charge of i-th constituent
p_i	Highest charge of i-th constituent
pI	Isoelectric point
pK_A	$-\log_{10} K_A$
pK'_A	$-\log_{10} K'_A$
t	Time
x	Spatial coordinate
$\alpha_{h,A}$	Molar fraction of form h with respect to total concentration of analyte A
$\alpha^0_{h,A}$	Molar fraction of form h at $\lim c_A \to 0$
γ_X	Activity coefficient of form X
κ	Specific conductivity
κ_{BGE}	Specific conductivity of the BGE
$\mu_{A,free}$	Limiting ionic mobility of free analyte
$\mu'_{A,free}$	Apparent ionic mobility of free analyte
μ_{AS}	Limiting ionic mobility of analyte-selector complex
μ'_{AS}	Apparent mobility of analyte-selector complex
μ'_X	Apparent ionic mobility of form X
$\mu_{lim}(A,z)$	Limiting mobility of constituent A at charge z
$\nu_{(g)i}$	Number of particles of i-th constituent in form g
ω_A	Set of all forms that contain constituent A
Ω	Set of all forms in a system

Main goals

1. Develop a computer implementation of chemical equilibrium solver capable of considering both acid-base and complex-forming equilibria. (Publication I)
2. Use the new insight provided by the ACE-capable NLTEM to investigate behavior of model ACE systems. (Publication II)
3. Implement nonlinear fit of effective electrophoretic mobility dependence that also considers Debye-Hückel and Onsager-Fuoss for ionic effects corrections. (publication III)
4. Investigate properties of compounds that may be used as pI markers to characterize pH gradients. (publication IV)

1 Capillary electrophoresis

Capillary electrophoresis (CE) is a separation technique that separates analytes by taking advantage of their different mobilities under the influence of electric field. A capillary electrophoresis experimental setup consists of a narrow capillary, usually tens of micrometers in diameter, filled with a solution of electrolytes. A solution consists of constituents where a constituent refers to a chemical compound such as sodium, acetic acid, β-cyclodextrin etc. Chemical interactions that take place in a solution give rise to individual forms of each constituent such as CH_3COO^{-1} and CH_3COOH^0 in case of acetic acid. Overall mobility of a constituent is a weighted sum of mobilities of all forms in which the constituent is present.

Capillary zone electrophoresis (CZE) is one of various modes of CE which achieved large adoption in analytical practice. In a CZE setup the entire capillary is uniformly filled with a solution of background electrolyte (BGE). A short plug of sample is injected at the inlet end of the capillary. When the sample is injected, voltage is applied, allowing the analytes in the sample to separate. Once the analytes separate from each other they form individual zones inside the separation space and travel independently of each other. A detector is placed near the outlet end of the capillary to observe concentration changes and detect the analytes as they pass through it. One peculiarity of CZE is the presence of so-called system zones. Unlike analyte zones, system zones are disturbances of the BGE concentration that do not contain any analyte. The total number of zones that form in a CZE system is the sum of number of analytes and BGE constituents.

1.1 Ionic effects in solutions of electrolytes

Ions in an electrolyte solution interact with each other via coulombic forces. Debye and Hückel [1, 2] introduced the theory of ionic atmosphere where an ion in a solution is surrounded by ions of opposite charge. Before two ions can initiate a chemical interaction, they have to break through the ionic atmosphere barrier. Thermodynamic equilibrium of most chemical reactions is a function of concentration of all participating constituents. Mathematical models that describe the equilibrium are usually derived for so-called ideal solutions. An ideal solution is a solution where any secondary effects affecting its chemical behavior, such as electrostatic interactions, may be neglected. Debye and Hückel worked out a mathematical model that expresses activity as a function of ionic strength of the solution. Activity, in general, can be perceived as an effective concentration of a constituent. Using activities instead of concentrations to calculate equilibrium in non-ideal solutions yields more accurate results.

Mobility of ions is also affected by electrostatic interactions. An extension of the Debye-Hückel theory proposed by Onsager and Fuoss [3] describes how the ionic atmosphere retards the electrophoretic motion of ions. Debye-Hückel and Onsager-Fuoss theories and their practical application are discussed further in chapter 5.

1.2 Affinity capillary electrophoresis

Affinity capillary electrophoresis (ACE) is a modification of CZE which uses chemical interaction to alter analyte mobility. This can help to achieve separation in cases where multiple analytes have mobilities very close to each other. The idea behind ACE is to have the analytes interact with a background constituent usually referred to as the selector. Separation can be achieved if mobility of at least one analyte-selector complex is sufficiently different from that of free analyte or if the affinity constants of the complexes are sufficiently different (or both of the above) and if the affinity constants of the complex-forming interactions are sufficiently large. ACE finds numerous applications in chiral separations of drugs and other natural compounds [4–6].

2 Conservation laws and continuity equations in electromigration

2.1 Brief historical overview

Description of motion of ions in solutions of electrolytes has been a subject of large scientific interest for over 100 years. Given the relative simplicity of this phenomenon, first basic set of continuity equations for one-dimensional channels were defined as early as in the late 19th century. One of the first works that derived some sort of conservation law was published by Kohlrausch [7] in 1897. This law became to be known as the Kohlrausch regulating function (KRF). The KRF had a limited scope of applicability and was not suitable for practical modeling of electromigration systems. Nevertheless, Kohlrausch's work demonstrated the possibilities of modeling of electromigration processes even though it was limited to very simple systems at that time. Some notable works on the topic of theory of electromigation came from Tiselius [8], Beckers [9, 10], Mikkers [11–13], Boček and Gebauer [14–17], Mosher and Thormann [18–21], Hirokawa [22–24] and Gaš [25, 26]. This eventually lead to development of sophisticated mathematical models which enabled in-depth investigations of electromigration processes.

2.2 Continuity equation

The continuity equation that describes the motion of an electrically charged particle under the influence of electric field is a nonlinear partial differential equation which includes an electromigration and diffusion term. Its original formulation considered only acid-base equilibria and can be written as equation 2.1

$$\frac{\partial c_i}{\partial t} = \frac{\partial}{\partial x} \sum_{z=n_i}^{p_i} \left(D_{i,z} \frac{\partial c_{i,z}}{\partial x} - \mathrm{sgn}(z) c_{i,z} \mu'_{i,z} E \right) - v_{EOF} \frac{\partial c_i}{\partial x} \tag{2.1}$$

In equation 2.1 c_i is total concentration of i-th constituent, t is time, x is spatial coordinate, n_i and p_i are the most negative and positive charges attainable by the i-th constituent, respectively, z is charge, $D_{i,z}$ is diffusion coefficient of the i-th form with charge z, $c_{i,z}$ is concentration of ionic form of the i-th constituent with charge z, $\mu'_{i,z}$ is apparent electrophoretic mobility of the ionic form of the i-th constituent with charge z, E is electric field intensity and v_{EOF} is velocity of advective flow.

Complete description of an electrophoretic system consists of a system of equations 2.1, one for each constituent. There is no known analytical solution of this system of equations and it has to be solved numerically. Numerical solutions are, however, rather time consuming even for simple systems. Furthermore, deducing any laws of broader applicability from numerical models alone is problematic, if not impossible. While the numerical models of electromigration have proven to be invaluable for understanding of the dynamics of electromigration, simplified solutions for the problem were sought for.

2.3 Linearization of the continuity equation

Poppe [27, 28] was the first to suggest that the system of equations 2.1 could be linearized. A linearized solution may be solved analytically which is beneficial in multiple ways. An analytical formulation of a problem enables us to find rules of general applicability by investigating the mathematical model, providing the true insight into the problem. Analytical solutions are also much faster to compute than numerical ones. Poppe showed that a linearized solution specific to CZE experimental setups leads to a matrix eigenvalue problem. The simplification is specific to CZE because the system is represented as uniformly distributed BGE whose concentration is disturbed at one point in space by the injection of sample. Štědrý [29–32] built upon this approach and formulated the problem in a compact form as equation 2.2.

$$\left(\frac{\partial\vec{\tilde{c}}}{\partial t}\right)_{em} = -\frac{j}{\kappa_{BGE}}\boldsymbol{M}\times\frac{\partial\vec{\tilde{c}}}{\partial x} \tag{2.2}$$

The $\boldsymbol{M}$ matrix is referred to as mobility matrix, κ_{BGE} is specific conductivity of the BGE. $\tilde{c} = \tilde{c}(x,t)$, meaning that $\tilde{c}$ is a function of concentration disturbances propagating in time and space. The term *disturbance* here refers to the concentration difference between the undisturbed BGE and the actual concentrations at the given point in time in space in the capillary. $\vec{\tilde{c}}$ is a column vector of these functions, one for each constituent. The initial condition ($\tilde{c}(x,0)$) assumes "reasonably small" disturbances at the point of the injection and no disturbances elsewhere. This implies that concentrations of analytes is zero in the entire separation space except for the sample plug. This is again in accordance with the CZE experimental setup. Eigenvalues of the matrix $\boldsymbol{M}$ are mobilities of all zones that can be observed in a given system, both analyte and system zones. The $\boldsymbol{M}$ matrix is a square matrix that can can be obtained as a product of two matrices referred to as $\boldsymbol{M_1}$ and $\boldsymbol{M_2}$ in Štědrý's original papers. Matrix $\boldsymbol{M_1}$ encodes electromigration properties of all ionic forms and matrix $\boldsymbol{M_2}$ encodes the equilibrium relationships that govern the system.

Each row in matrix $\boldsymbol{M_1}$ corresponds to one constituent and each column to one ionic form in the system. A general formula for each element is given by equation 2.3

$$\boldsymbol{M_1}(i,[k,z]) = -\frac{j}{\kappa}\operatorname{sgn}(z)\mu'_{k,z}\delta_{ik} + \left(\sum_{z=n_i}^{p_i}\frac{j}{\kappa^2}\operatorname{sgn}(z)\mu'_{i,z}c_{i,z}\right)F|z|\mu'_{k,z} \tag{2.3}$$

where i is the index of i-th constiuent and the row of the element, k is the index of the k-th constituent and z a charge of one of its forms. F is the Faraday constant and δ_{ik} the Kroenecker delta. Column of the element can be calculated using formula 2.4.

$$I_{k.z} = \sum_{l=0}^{k-1}(p_l + n_l) + z + n_k \tag{2.4}$$

Values of $c_{i,z}$ represent concentrations of the z-th ionic form of the i-th constituent. Important step that allows linearization of the continuity equation is setting concentrations of constituents that are analytes to zero.

Elements of matrix $\boldsymbol{M_2}$ are given by equation 2.5.

$$\boldsymbol{M_2}([k,z],i) = \frac{\partial c_{k,z}}{\partial c_i} \tag{2.5}$$

$c_{k,z}$ is the concentration of the z-th ion of k-th constituent and c_i the analytical concentration of i-th constituent. Indexation is similar to that of matrix $\boldsymbol{M_1}$ but transposed. Row of the element is now calculated by formula 2.4 and the column of the element is i. Since the model used by Štědrý considered acid-base equilibria only, Štědrý's papers present the derivatives that make up the matrix $\boldsymbol{M_2}$ directly in their analytical forms. Štědrý's matrices omit species with zero charge because they have no effect on the overall behavior of the system.

Hruška [33] later extended Štědrý's model by including the first nonlinear term into the linearized continuity equation. The equation then becomes 2.6.

$$\frac{\partial \vec{c}}{\partial t} = -\frac{j}{\kappa_{BGE}} \left(\boldsymbol{M_0} + \sum_{k=1}^{N} \boldsymbol{M_{1,k}} \check{c}_k \right) \times \frac{\partial \vec{c}}{\partial x} + \boldsymbol{D} \times \frac{\partial^2 \vec{c}}{\partial x^2} \tag{2.6}$$

where the sum of $\boldsymbol{M_{1,k}}$ is the first term of Taylor expansion. Unlike Štědrý, Hruška does not split the $\boldsymbol{M}$ matrix into two submatrices in his papers and reuses the $\boldsymbol{M_1}$ notation to denote the first term of Taylor expansion.

Hruška's $\boldsymbol{M_{1,k}}$ matrix is defined by equation 2.7.

$$\boldsymbol{M_{1,k}} = \frac{\partial \boldsymbol{M}}{\partial c_k} \tag{2.7}$$

Hruška's extension came to be known as the nonlinear theory of electromigration (NLTEM) [34], although the name could be seen as misleading because it is still just and extension of the linearized model and applicable to the CZE experimental setups only. The great advantage of NLTEM is its ability to predict not only positions and compositions of all zones but also the expected shapes of detector responses. The NLTEM provided solid mathematical proof that peaks observed in CZE experiments follow the profile given by the Haarhoff-van der Linde (HVL) function [35]. The HVL function is given by equation 2.8.

$$HVL_\delta(t) = \frac{\frac{a_0}{a_2 a_{3\delta}\sqrt{2\pi}} \exp\left[-\frac{1}{2}\left(\frac{t-a_1}{a_2}\right)^2\right]}{\frac{1}{\exp(a_{3\delta})-1} + \frac{1}{2}\left[1+\operatorname{erf}\left(\frac{t-a_1}{\sqrt{2}a_2}\right)\right]} \tag{2.8}$$

where a_0 is the total area of the peak, a_1 is center of symmetry of the gaussian component of the peak, a_2 the standard deviation of the gaussian component of the peak and $a_{3\delta}$ the degree of peak asymmetry. Depending on the value of the $a_{3\delta}$ parameter, the HVL function profile can be either a strictly gaussian peak ($\lim a_{3\delta} \to 0$) or a peak of asymmetric triangular shape. The triangularity of the peak increases with the absolute value of the $a_{3\delta}$ parameter, the orientation of the triangle (either a fronting or tailing peak) depends of the sign of $a_{3\delta}$. Peaks of such a shape occur very commonly in CZE as a result of electromigration dispersion (EMD) [34].

2.4 Addition of complex-forming equilibria

The possibility of extending the NLTEM to include complex-forming equilibria was investigated by Hruška [36] and Beneš [37]. Although the authors acknowledged the possibility that the NLTEM [36] could be extended with a general complex-forming model they opted for a simpler approach. Their work focused solely on how complexation affects behavior of the analyte. In their work only the analyte and one BGE component are allowed to interact. Moreover, one complexation partner must be fully charged and the other strictly neutral. While these limitations seem restrictive, they describe a very common ACE setup where a fully charged analyte interacts with a neutral selector in the BGE. Common examples of selectors that possess no electric charge are various cyclodextrins or crown-ethers. The authors use the Wren-Rowe equation [38] (equation 2.9) to calculate the analyte effective mobility.

$$\mu_{A,eff} = \frac{\mu'_{A,free} + K_S \frac{\gamma_S \gamma_A}{\gamma_{AS}} c_S \mu'_{AS}}{1 + K_S \frac{\gamma_S \gamma_A}{\gamma_{AS}} c_S} \tag{2.9}$$

$\mu_{A,eff}$ is effective mobility of analyte, $\mu'_{A,free}$ is apparent mobility of free (uncomplexed) analyte, μ'_{AS} apparent mobility of the analyte-selector complex, K_S is the affinity (stability, complexation) constant, c_S is concentration of the selector in BGE and γ_A, γ_S and γ_{AS} are activity coefficients of the respective forms.

Hruška's and Beneš's work use equation 2.9 directly instead of deriving it from NLTEM. Their work first explored the effect of complexation on analyte EMD by expressing each contributing factor in analytical form.

Despite the invaluable insights into analyte behavior in ACE provided by Hruška and Beneš, their work left a lot to be desired for in terms of complete description of ACE systems within the framework of the NLTEM theory.

2.5 The PeakMaster software

Linearized model of electromigration was implemented in a computer program PeakMaster. The original PeakMaster was not based on the LTEM but rather on a moving boundary theory [39, 40]. Later improvement known as PeakMaster 5 used LTEM for all electromigration calculations. PeakMaster 5 was later improved to include the NLTEM model [33] and simple complex-forming model [36]. Latest revision of the PeakMaster 5-series software at the time of writing of this thesis is PeakMaster 5.4.

3 Generalization of the NLTEM, its application to ACE and the PeakMaster 6 software (publication I)

The original NLTEM was developed only with the acid-base equilibria in mind. The question that needed answering was whether it is possible to extend the interactions that occur in the system beyond just acid-base equilibria and still keep the mathematical model in its linearized form. This question was thoroughly investigated in publication I [41].

One of the conditions that must be met in a system that we seek to solve with the linearized continuity equation is that all chemical interactions that take place in the system must happen "instantaneously". From the perspective of electromigration this means that the chemical equilibrium in the system must be reestablished much faster than the electrophoretic motion of particles in the system disturbs it. In other words the system must be in thermodynamic equilibrium at any point in time and space. Acid-base equilibria are an example of a chemical interaction that is fast enough to be used by NLTEM. Complex-forming equilibria are in principle also fast enough to be solvable by the linearized model. Other interactions that were previously studied by CZE such as enantiomer interconversion [42, 43] cannot be considered as "instantaneous" and therefore cannot be described by the linearized model.

The first step on the way to introduce chemical interactions other that acid-base equilibria is modification of the fundamental continuity equation (2.1). This has to be done because even the original continuity equation upon which (N)LTEM is based considers only acid-base equilibria. A general continuity equation that covers mass transport of arbitrary chemical species governed by arbitrary chemical equilibrium is given in equation 3.1.

$$\frac{\partial c_i}{\partial t} = \frac{\partial J_i}{\partial x} = -\sum_{g \in \Omega} \nu_{(g)i} \frac{\partial J_{(g)}}{\partial x} \tag{3.1}$$

Notice that the concrete term that describes the mass flux in equation 2.1 is now replaced by a generic mass flux term $\nu_{(g)i}\frac{\partial J_{(g)i}}{\partial x}$ which covers all processes that cause constituents in a system to move, including advection. The double summation over all charge states of all constituents is now replaced by a single summation over all elements of Ω set. The Ω contains all forms present in the system. Another notable difference is that the mass flux term is now multiplied by the $\nu_{(g)i}$ term to account for the fact that an individual chemical specie may transport more than one particle of a given constituent. For instance, a specie AB_2 would have the $\nu_{(g)i}$ set to 1 for the mass flux of A and to 2 for the mass flux of B. If a form g does not contain constituent i in any form, value of $\nu_{(g)i}$ is zero. For practical purposes the generic mass flux term has to be expressed in specific terms which describe the mass transport phenomena in the system we seek to investigate.

For the purposes of expanding the NLTEM, another notation update was desirable.

The electromigration matrix is now referred to as $\boldsymbol{M_\mu}$ and the equilibrium (or communication) matrix is referred to as $\boldsymbol{M_\partial}$. Elements of the generalized $\boldsymbol{M_\mu}$ are now defined according to equation 3.2

$$\begin{aligned} \boldsymbol{M_\mu}(i,h) &= \frac{\kappa_{BGE}}{\kappa}\left(\nu_{(h)i}\mu'_{(h)} - \frac{F}{\kappa}\sum_{g\in\Omega}\nu_{(g)i}\mu'_{(g)}c_{(g)}r_{(g)(h)}\right) \\ r_{(g)(h)} &= z_{(h)}\mu'_{(h)} - \frac{\kappa}{F}\frac{\partial \ln \mu'_{(g)}}{\partial c_{(h)}} + \sum_{f\in\Omega} z_{(f)}c_{(f)}\frac{\partial \mu'_{(f)}}{\partial c_{(h)}} \end{aligned} \tag{3.2}$$

If we assume that all ionic mobilities do not depend on concentration of any constituent, we can simplify the $r_{(g)(h)}$ term into

$$r_{(g)(h)} = z_{(h)}\mu'_{(h)} \tag{3.3}$$

The assumption of no concentration dependence of ionic mobilities is applicable if the ionic effects are neglected. In such a case, in addition to simplifying the $r_{(g)(h)}$ term we can replace all apparent mobilities with limiting ionic mobilities.

Substituting equation 3.3 into equation 3.2 effectively yields equation 2.3.

The overall layout of the matrix is equivalent to matrix $\boldsymbol{M_1}$ in Štědrý's notation. The matrix has $N \times |\Omega|$ dimension where N is the number of constituents and $|\Omega|$ the number of all forms in the system. Its i-th row can be thought of as referring to the i-th constituent and its h-th column referring to the h-th ionic form. Elements of the $\boldsymbol{M_\partial}$ matrix whose dimension is $|\Omega| \times N$ are now defined by equation 3.4

$$\boldsymbol{M_\partial}(h,q) = \frac{\partial c_{(h)}}{\partial c_q} \tag{3.4}$$

which is merely a restatement of the original $\boldsymbol{M_2}$ matrix definition using different indexation to accommodate the fact that the individual ionic forms are now referred to by their position in the Ω set instead of their charge.

3.1 Application to ACE

As was already stated, the generalization above may be applied to any CZE system that is governed by "fast enough" equilibria. The task of applying this generalized model to a specific class of systems mostly lies in expressing the terms of the $\boldsymbol{M_\partial}$ matrix explicitly and solving the respective equations. In case of ACE, mobility of every constituent in the system is, in general, governed by two interactions. First interaction is the acid-base equilibrium. Acid-base equilibrium controls the number of protons which a constituent exchanges with its environment. The general equation that describes this equilibrium is given by 3.5

$$K_A = \frac{[H^+]\gamma_{H^+}[A^{z-1}]\gamma_{A^{z-1}}}{[A^z]\gamma_{A^z}} \tag{3.5}$$

where $[H^+]$ is concentration of protons, $[A^{z-1}]$ is concentration of the dissociated acid (or conjugated base) that released the proton and $[A^z]$ is concentration of the acid (or conjugated base) that did not release the

proton in this step of dissociation and γ_{H^+}, $\gamma_{A^{z-1}}$ and γ_{A^z} are activity coefficients of the respective forms. Dissociation of species that can exchange more than one proton is described by a system of equations 3.5. A solution of constituents that undergo acid-base equilibria must be in equilibrium on the macroscopic scale. Therefore, the overall electric charge of the solution must add up to zero. This electroneutrality condition can be described by equation 3.6. In the works of Štědrý, equation 3.6 is referred to as the G-polynomial.

$$\sum_{i=1}^{N} c_i \sum_{z=n_i}^{p_i} \frac{z L'_{i,z} ([H^+]\gamma_{H^+})^z}{\sum_{z'=n_i}^{p_i} L'_{i,z} ([H^+]\gamma_{H^+})^{z'}} + [H^+]\gamma_{H^+} - \frac{K_W}{[H^+]\gamma_{H^+}\gamma_{OH^-}} = 0 \tag{3.6}$$

$$L'_{i,z} = \begin{cases} \prod_{z'=z}^{-1} K_{i,z'} \frac{\gamma_{Az'+1}}{\gamma_{H^+}\gamma_{Az'}} & z < 0 \\ 1 & z = 0 \\ \prod_{z'=0}^{z-1} \left(K_{i,z'} \frac{\gamma_{Az'+1}}{\gamma_{H^+}\gamma_{Az'}} \right)^{-1} & z > 0 \end{cases}$$

$L'_{i,z}$ is the apparent total dissociation constant for the respective dissociation step (the K_A constants are consecutive) and γ_{H^+}, γ_{OH^-}, $\gamma_{Az'+1}$ and $\gamma_{Az'}$ are activity coefficients of the respective forms. Equation 3.6 is universal and valid for arbitrarily complex aqueous solution that contains chemical species which undergo only acid-base equilibria. It can be shown that equation 3.6 is monotonic for positive values of $[H^+]$. This allows us solve the equation for $[H^+]$ by various numerical methods such as bisection or Newton-Raphson method. A model that considers acid-base equilibria only can use equation 3.6 and its derivatives, which are available in analytical form, to calculate the elements of matrices $\boldsymbol{M_\mu}$ and $\boldsymbol{M_\partial}$, construct the $\boldsymbol{M_0}$ matrix and find its eigenvalues. This exact approach is used by the PeakMaster 5-series software.

Inclusion of complex-forming equilibria complicates the situation. The general equation that describes a complex-forming equilibrium between two species is given by 3.7.

$$K_S = \frac{[AS]\gamma_{AS}}{[A]\gamma_A[S]\gamma_S} \tag{3.7}$$

where K_S is the affinity constant and $[A]$, $[S]$ and $[AS]$ are concentrations of the respective forms and γ_A, γ_S and γ_{AS} are activity coefficients of the respective forms. Equation 3.7 is equivalent to equation 3.5 for acid-base equilibria. An acid-base equilibrium can be, at least from the point of view of thermodynamics, seen as a special case of complex-forming equilibrium with the $[H^+]$ as the ligand and the completely deprotonated form of the other chemical specie as the second complexation partner [44]. To illustrate the increase of complexity, let us consider two simple systems. First system contains just a weak monovalent acid in water. Concentration equilibrium of all species in this system can be completely described by set of equations 3.8.

$$\begin{aligned} K_W &= [H^+]\gamma_{H^+}[OH^-]\gamma_{OH^-} \\ K_A &= \frac{[H^+]\gamma_{H^+}[A^-]\gamma_{A^-}}{[HA]\gamma_{HA}} \\ c_A &= [HA] + [A^-] \\ 0 &= [H^+] - [OH^-] - [A^-] \end{aligned} \tag{3.8}$$

where the terms in square brackets represent concentrations of there respective forms and γ_{H^+}, γ_{OH^-}, γ_{A^-} and γ_{HA} are activity coefficients of the respective forms. This system of equations leads to the final

equation 3.9.

$$[H^+]^3 + [H^+]^2 K_A \frac{\gamma_{HA}}{\gamma_{H^+}\gamma_{A^-}} - [H^+]\left(\frac{K_W}{\gamma_{H^+}\gamma_{OH^-}} + K_A \frac{\gamma_{HA}}{\gamma_{H^+}\gamma_{A^-}} c_A\right) + K_W K_A \frac{\gamma_{HA}}{\gamma_{H^+}^2 \gamma_{OH^-}\gamma_{A^-}} = 0 \quad (3.9)$$

This equation is a function of just one variable, $[H^+]$, and its solution can be found analytically. Now let us consider a second system which, in addition to a weak monovalent acid also contains a complex-forming substance. For the sake of simplicity, let us assume that the complex-forming substance interacts only with the $[A^-]$ form of the acid and that it does not participate in acid-base equilibria. The complete set of equations that describes such a system is now given by 3.10. For the sake of readability, activity coefficients are omitted in this section.

$$\begin{aligned} K_W &= [H^+][OH^-] \\ K_A &= \frac{[H^+][A^-]}{[HA]} \\ c_A &= [HA] + [A^-] + [A^-S] \\ K_S &= \frac{[A^-S]}{[A^-][S]} \\ c_S &= [S] + [A^-S] \\ 0 &= [H^+] - [OH^-] - [A^-] - [A^-S] \end{aligned} \quad (3.10)$$

The final equation 3.11 now has a rather daunting form

$$\begin{aligned} &[H^+]^5 (-1 + K_A K_S) \\ +&[H^+]^4 (-c_A K_A K_S - K_A (1 + c_S K_S - K_A K_S)) + {K_A}^2 K_S {K_W}^2 \\ +&[H^+]^3 (c_A K_A (1 + c_S K_S - 2K_A K_S) + (1 - 2K_A K_S) K_W) \\ +&[H^+]^2 (-K_A (-1 - c_S K_S + 2K_A K_S) K_W + c_A K_A K_S (c_A K_A + KW)) \\ +&[H^+] \left(2c_A {K_A}^2 K_S K_W + K_A K_S {K_W}^2\right) \\ &= 0 \end{aligned} \quad (3.11)$$

Addition of just two more equations to the system (mass balance of the selector and its complex-forming equilibrium) leads to a polynomial of 5th degree. This demonstrates that inclusion of another kind of interaction that acts orthogonally to acid-base equilibria greatly complicates the solution of the overall equilibrium even if we limit ourselves to very simple cases.

3.2 PeakMaster 6 software

Equation 3.6 is particularly useful because its terms are straightforward to formulate. Formulation of an equivalent equation for complex-forming systems is far more complicated because its terms depend not only on the constituents' dissociation states but also the complex-forming interactions. While it is possible to construct a "complex-forming-aware" equivalent of equation 3.6, practicality of such an approach had to be considered as well because one of the main goals of this work was to create a computer implementation of the theoretical model. The final implementation expresses the total equilibrium as a

system of equations where each equation describes one particular equilibrium. Additional equations include the mass balances of all constituents and the water ionic product. Such a system of equations can be solved efficiently by means of Newton-Raphson method. Because the Newton-Raphson method is a numerical method, additional steps had to have been taken to maximize the chance that the solver will converge to the correct solution. All equilibrium equations have been rewritten as their logarithmic forms where equation 3.5 becomes equation 3.12.

$$pK_A = pH + pA^- - \log \gamma_{A^-} - pHA + \log \gamma_{HA} \tag{3.12}$$

The same transformation applies for complex-forming equilibria as well. Working with negative logarithms of concentrations and the respective stability constants has multiple advantages. Since the logarithm of a real number is defined only in the positive domain, using logarithms of concentrations instead of the actual values prevents the solver from straying towards solutions with negative concentrations. Such solutions, while mathematically valid, have no physical meaning. Another advantage is of purely technical nature. Since logarithmic forms of equations replace multiplication and division with addition and subtraction, respectively, computer implementation of the logarithmic system may provide better performance because addition and subtraction are usually evaluated faster than multiplication and especially division on common computer microprocessors.

The Newton-Raphson solver requires an initial estimate that has to be sufficiently close to the correct solution in order to converge. This estimate is calculated by treating the system as if it involved only acid-base equilibria at first, calculating the equilibrium concentrations using equation 3.6 and using these concentrations to calculate initial estimates of concentration of complexes.

One drawback of the aforementioned approach involves the construction of the matrix $\boldsymbol{M_\partial}$. Because we describe the concentration equilibrium of the system as a system of equations, we can no longer express the derivatives that make up the matrix $\boldsymbol{M_\partial}$ in analytical form. The obvious alternative is to calculate these derivatives numerically using the well-known equation 3.13.

$$\Delta = \frac{f(x+h) - f(x-h)}{2h} \tag{3.13}$$

and for the second derivative equation 3.14

$$\Delta^2 = \frac{f(x+h) - 2f(x) + f(x-h)}{h^2} \tag{3.14}$$

In order for the equations 3.13 and 3.14 to provide sufficiently accurate results the value of h has to be small. When we seek to implement a numerical derivatives solver in a computer, some aspects of computer floating-point arithmetic must be considered. The IEEE 754 standard defines a series of binary representations of decimal numbers. The commonly used *single* and *double* representations use a fixed number of bits to represent a decimal number. This limits both the range of numbers that can be represented and the number of digits of precision. In the case of the *double* format, 53 bits are used to store the fractional part of the number, giving approximately 16 digits of precision. This precision turned out to be insufficient to calculate the derivatives in the matrix $\boldsymbol{M_\partial}$ and matrices $\boldsymbol{M_{1,k}}$ reliably. To overcome the problem, the computer implementation uses arbitrary-precision arithmetic to calculate the derivatives. This comes at the expense of considerably degraded performance. Most computer microprocessors contain a dedicated circuitry (commonly referred to as the FPU) that performs operations on decimal numbers stored in the *single* or *double* precision representation. Arbitrary-precision arithmetic relies entirely on

software implementation and has to be processed by the general-purpose ALU unit of the microprocessor. To alleviate the performance impact of the arbitrary-precision arithmetic, the computer implementation takes advantage of parallel processing. More importantly, computation power of current microprocessors is more than sufficient to compensate for the additional overhead of the arbitrary-precision arithmetic.

The goal of this work was not only to extend the capabilities of PeakMaster with general complex-forming equilibria but also to provide a set of libraries with implementations of algorithms that solve common problems related to theory of electrolyte solutions and capillary electrophoresis. A set of libraries called ECHMETCoreLibs [45] was devised to solve the following problems

- Define a chemical system in terms of its constituents, their physico-chemical parameters, complex-forming interactions and concentrations.
- Calculate equilibrium composition of a chemical system and the derivatives required by the NLTEM model.
- Implement Debye-Hückel and Onsager-Fuoss laws to calculate activities and actual ionic mobilities.

The generalized NLTEM model was implemented in a separate library called LEMNG [46]. The LEMNG library is responsible for

- Constructing the respective matrices.
- Calculating the eigenvalues and eigenvectors needed to construct the predicted electrophoregrams.
- Representing the predicted electrophoregrams as arrays of X,Y values.

ECHMETCoreLibs and LEMNG are available as reusable open-source libraries.

The PeakMaster 6 software itself is the graphical user interface for data entry and display. The general layout remained similar to PeakMaster 5 with some adjustments to accommodate the addition of complex-forming equilibria and the fact that the NLTEM instead of LTEM is now used by default to draw peak shapes.

4 Investigation of ACE systems with the NLTEM (publication II)

The NLTEM model even in its extended form can be solved symbolically for simple systems. While the simplifications required to obtain solutions in symbolic form are quite restrictive, the insight provided by examining the symbolical expressions is extremely valuable. This analysis was done thoroughly in publication II [47].

4.1 Proof of the Wren-Rowe equation

The Wren-Rowe equation (2.9) has been a matter of debate amongst scientists for years. The Wren-Rowe equation is based upon equation 3.7 which works with actual concentrations of free analyte $[A]$ and selector $[S]$. The Wren-Rowe equation, on the other hand, works with the total (analytical) concentration of the selector c_S. The assumption is that since concentration of the analyte is usually very small the consumption of the selector through complexation is negligible, allowing to set $[S] = c_S$. The scope of applicability of this assumption was being questioned and various attempts to fix the Wren-Rowe equation have been made [48–50]. With the extended NLTEM we may attempt to obtain the effective mobility of the analyte as eigenvalue of the mobility matrix and confront the result with the Wren-Rowe equation.

Let us consider a simple system with two strong BGE components X and Y, analyte A and selector S which is also present in the BGE. In order to be able to obtain the analyte eigenmobility in a symbolic form, acid-base equilibria have to be neglected. Neglecting the acid-base equilibria is equivalent to considering a system composed only of strong electrolytes or non-electrolytes. In this case, we assume X, Y and A to be strong monovalent electrolytes and S to be a non-electrolyte. The respective matrices then look as follows (4.1 and 4.2). For the sake of simplicity, concentrations of constituents X, Y and S are considered equal and denoted by common variable c.

$$\boldsymbol{M_\mu} = \begin{pmatrix} \mu_X - \frac{\mathrm{sgn}(z_X)\mu'_X F}{\kappa_{BGE}}\mu'_X c & -\frac{\mathrm{sgn}(z_Y)\mu'_Y F}{\kappa_{BGE}}\mu'_X c & -\frac{\mathrm{sgn}(z_A)\mu'_A F}{\kappa_{BGE}}\mu'_X c & -\frac{\mathrm{sgn}(z_{AS})\mu'_{AS} F}{\kappa_{BGE}}\mu'_X c & 0 \\ -\frac{\mathrm{sgn}(z_X)\mu'_X F}{\kappa_{BGE}}\mu'_Y c & \mu'_Y - \frac{\mathrm{sgn}(z_Y)\mu'_Y F}{\kappa_{BGE}}\mu'_Y c & -\frac{\mathrm{sgn}(z_A)\mu'_A F}{\kappa_{BGE}}\mu'_Y c & -\frac{\mathrm{sgn}(z_{AS})\mu'_{AS} F}{\kappa_{BGE}}\mu'_Y c & 0 \\ 0 & 0 & \mu'_A & \mu'_{AS} & 0 \\ 0 & 0 & 0 & \mu'_{AS} & 0 \end{pmatrix} \tag{4.1}$$

$$\boldsymbol{M_\partial} = \begin{pmatrix} 1 & 1 & 0 & 0 \\ 1 & 1 & 0 & 0 \\ 0 & 0 & \frac{1}{1+K_{AS}\frac{\gamma_A-\gamma_S}{\gamma_{AS}}c_S} & 0 \\ 0 & 0 & \frac{K_{AS}\frac{\gamma_A-\gamma_S}{\gamma_{AS}}c_S}{1+K_{AS}\frac{\gamma_A-\gamma_S}{\gamma_{AS}}c_S} & 0 \\ 0 & 0 & 0 & 1 \end{pmatrix} \tag{4.2}$$

The $\boldsymbol{M_0}$ matrix is then given by 4.3

$$\boldsymbol{M_0} = \begin{pmatrix} 0 & 0 & m_{13} & 0 \\ 0 & 0 & m_{23} & 0 \\ 0 & 0 & \frac{\mu'_A+c_S K_{AS}\frac{\gamma_A-\gamma_S}{\gamma_{AS}}\mu'_{AS}}{1+c_S K_{AS}\frac{\gamma_A-\gamma_S}{\gamma_{AS}}} & 0 \\ 0 & 0 & m_{43} & 0 \end{pmatrix} \tag{4.3}$$

Elements m_{13}, m_{23} and m_{43} are generally non-zero but their values do not have to be expressed specifically in this case. Regardless of the values of the m terms, eigenvalues of the matrix 4.3 are always equal to 4.4.

$$\lambda(\boldsymbol{M_0}) = \left\{ \begin{matrix} 0 \\ 0 \\ \frac{\mu'_A+c_S K_{AS}\frac{\gamma_A-\gamma_S}{\gamma_{AS}}\mu'_{AS}}{1+c_S K_{AS}\frac{\gamma_A-\gamma_S}{\gamma_{AS}}} \\ 0 \end{matrix} \right\} \tag{4.4}$$

Set 4.4 tells us that our example system shall have three stationary system zones and an analyte zone whose mobility is given by the only non-zero term of the set 4.4. This term corresponds exactly to the Wren-Rowe equation 2.9, conclusively proving that the original formulation by Wren and Rowe is correct. Further investigation can show that the actual concentration profiles of analyte and selector inside the analyte zone (and the corresponding deviation from $c_A \to 0$) contributes only to electromigration dispersion of the zone. The zone, however, always contains a point whose mobility corresponds exactly to that predicted by the Wren-Rowe equation. This point represents the true effective analyte mobility.

4.2 Analyte mobility in interacting BGE

A situation where the selector interacts both with the analyte and some BGE component is usually avoided in practice. The problem is, however, still interesting from a theoretical point of view and the solution has a practical application [51]. Let us consider a system similar to the one above but at this time the selector is allowed to form a complex with the analyte and one of the BGE components. The structure of the matrix is too complicated for a purely symbolical evaluation, therefore, a roundabout approach was devised. Taking advantage of the fact that (N)LTEM requires that concentrations of all analytes be

set to zero, one can attempt to guess the corresponding eigenvalue from the system of equations 4.5.

$$\begin{aligned} K_{AS} &= \frac{[AS]\gamma_{AS}}{[A]\gamma_A[S]\gamma_S} \\ K_{XS} &= \frac{[XS]\gamma_{XS}}{[X]\gamma_X[S]\gamma_S} \\ c_X &= [X] + [XS] \\ c_S &= [S] + [XS] \end{aligned} \tag{4.5}$$

Solving the system 4.5 for $[S]$ and substituting c_S for $[S]$ in the original Wren-Rowe equation 2.9 yields the "interacting" Wren-Rowe equation 4.6.

$$\mu_{A,eff} = \frac{\mu'_{A,free} + \frac{1}{2}K_{AS}\frac{\gamma_A\gamma_S}{\gamma_{AS}}\mu'_{AS}\left(\frac{\sqrt{\left(K_{XS}\frac{\gamma_X\gamma_S}{\gamma_{XS}}c_X - K_{XS}\frac{\gamma_X\gamma_S}{\gamma_{XS}}c_S - 1\right)^2 + 4K_{XS}\frac{\gamma_X\gamma_S}{\gamma_{XS}}c_X} - 1}{K_{XS}\frac{\gamma_X\gamma_S}{\gamma_{XS}}} - c_X + c_S\right)}{1 + \frac{1}{2}K_{AS}\frac{\gamma_A\gamma_S}{\gamma_{AS}}\left(\frac{\sqrt{\left(K_{XS}\frac{\gamma_X\gamma_S}{\gamma_{XS}}c_X - K_{XS}\frac{\gamma_X\gamma_S}{\gamma_{XS}}c_S - 1\right)^2 + 4K_{XS}\frac{\gamma_X\gamma_S}{\gamma_{XS}}c_X} - 1}{K_{XS}\frac{\gamma_X\gamma_S}{\gamma_{XS}}} - c_X + c_S\right)} \tag{4.6}$$

The actual shape of equation 4.6 depends on the values of K_{XS}, c_S and c_X. Evidence obtained from evaluating equation 4.6 with sensible affinity constants indicates that in common cases the curve keeps the hyperbolic shape, making it difficult to discover that there is a parasitic interaction between the selector and a BGE component. This can lead to error in determination of complexation affinity constant of the analyte as the publication II also discusses.

In order to confirm that the guessed equation 4.6 is actually valid, effective mobilities predicted by equation 4.6 were compared against those calculated by the extended NLTEM model. Effective mobility predicted by equation 4.6 and the extended NLTEM are in perfect agreement.

4.3 The Tiselius' equation

The Tiselus' equation 4.7 [8] defines the effective mobility of an analyte as

$$\mu_{eff,A} = \sum_{h \in \omega_A} \alpha_{h,A}\mu_h \tag{4.7}$$

where ω_A is the set of all forms that contain the analyte A, $\alpha_{h,A}$ molar fraction of form h with respect to total concentration of analyte A and μ_h mobility of the form h. It turns out that the Tiselius' equation can be derived from the NLTEM model. Assuming the extended NLTEM model, one can derive the Tiselius equation using the following steps.[1]

First, let us rewrite the definition of the $\boldsymbol{M_\mu}$ elements as follows (ionic effects are neglected).

$$\boldsymbol{M_\mu}(i,h) = \begin{cases} h \in \omega_i, \frac{\kappa_{BGE}(\mu_h + z_h\mu_h\Sigma_i)}{\kappa} \\ h \notin \omega_i, \frac{\kappa_{BGE}z_h\mu_h\Sigma_i}{\kappa} \end{cases} \tag{4.8}$$

[1]Even though the text speaks of NLTEM, the first-order nonlinear expansion is not necessary to derive the Tiselius' equation.

$$\Sigma_i = \frac{-F}{\kappa}\left(\sum_{g\in\omega_i}\mu_g\alpha_{g,i}\right)C_i \tag{4.9}$$

Note that concentrations of forms are expressed via molar fraction with respect to total concentration of the given analyte where C_i is the total concentration. When evaluated at the BGE concentrations, row vector of $\boldsymbol{M_\mu}$ matrix for each analyte has a general form

$$\boldsymbol{M_\mu}(A,*) = (0\ldots0, \mu_{1,A}\ldots\mu_{N,A}, 0\ldots0) \tag{4.10}$$

where $\mu_{1,A}\ldots\mu_{N,A}$ are mobilities of all forms that contain the analyte A.

Similarly, we evaluate the $\boldsymbol{M_\partial}$ matrix at the BGE concentration.

$$h\in\omega_A : \frac{\partial c_h}{\partial C_i} = \begin{cases} i = A, \alpha^0_{h,A} \\ i \neq A, 0 \end{cases} \tag{4.11}$$

$\alpha^0_{h,A}$ is the molar fraction of form h at $\lim c_A \to 0$

The entire matrix $\boldsymbol{M_\partial}$ is then

$$\boldsymbol{M_\partial} = \begin{pmatrix} & & \underline{\ldots} & \underline{\ldots} & \underline{A} & \underline{\ldots} \\ \vdots & | & \ddots & \vdots & \vdots & \vdots \\ h & | & 0 & 0 & \alpha^0_{h,A} & 0 \\ h+1 & | & 0 & 0 & \alpha^0_{h+1,A} & 0 \\ h+. & | & 0 & 0 & \alpha^0_{h+.,A} & 0 \\ h+N & | & 0 & 0 & \alpha^0_{h+N,A} & 0 \\ \vdots & | & \vdots & \vdots & \vdots & \ddots \end{pmatrix} \tag{4.12}$$

where all elements, except those explicitly stated, may be nonzero.

The product of A-th row of matrix $\boldsymbol{M_\mu}$ and matrix $\boldsymbol{M_\partial}$ yields the A-th row of matrix $\boldsymbol{M_0}$. Zero elements in the A-th row of $\boldsymbol{M_\mu}$ matrix cancel out all non-zero elements in rows of matrix $\boldsymbol{M_\partial}$. Conversely, zero elements in columns of $\boldsymbol{M_\partial}$ matrix cancel out nonzero elements of the A-th row of $\boldsymbol{M_\mu}$ matrix. The only element that does not get canceled is the diagonal element.

$$\boldsymbol{M_0}(A,A) = \sum_{h\in\omega_A}\alpha^0_{h,A}\mu_h \tag{4.13}$$

This diagonal element is one of the eigenvalues of the $\boldsymbol{M_0}$ matrix and according to the NLTEM theory it represents the true analyte mobility. The Tiselius' equation derived in this way holds only for cases where the complex-forming equilibrium stoichiometry is 1:1. More general complex forming stoichiometry would require further adjustments to the derivation procedure sketched above but the general principle would remain the same. This further demonstrates the validity of the Wren-Rowe equation in its original formulation.

4.4 The selector package

Past experimental evidence revealed that the total concentration of the selector in the analyte zone can be different than that in the BGE. It was suggested that this happens as a result of the analyte movement through the BGE. While these effects have been observed experimentally [52, 53], no systematic investigation of the nature of this phenomenon had been done. The extended NLTEM model provides all the necessary tools to explore this phenomenon by predicting the experimental results and verifying them experimentally.

Intuitive insight into the principles of ACE suggests that in the case of a neutral selector interacting with a charged analyte, the selector concentration in the analyte zone will always increase as the selector is dragged along with the analyte in the form of its complex. This intuitive prediction was corroborated by numerical simulations in Simul 5 Complex [54] and conclusively verified by the extended NLTEM. An experiment where MAPH-β-cyclodextrin was used as the selector was conducted to gather data for experimental verification. This particular cyclodextrin was used because it is visible on the UV detector. UV detection is necessary to convert the observed signal trace to concentration scale. The shape of the analyte peak observed in the experiment and the shape of the analyte zone predicted by the extended NLTEM are in very good agreement.

5 Addressing the issue of ionic effects (publication III)

Theoretical predictions of CE experiments require input parameters which describe the physico-chemical nature of the system and its composition. In the case of CE, two parameters that describe a chemical compound are of particular interest, the acid-base dissociation constant K_A and limiting mobility of the compound at a given charge $\mu_{lim}(A, z)$. Both of these parameters are thermodynamic constants and can be measured experimentally. Experimentally obtained values are, however, affected by the environment in which the measurements are conducted. The effects in question are commonly known as ionic effects. The nature of ionic effects stems from the fact that ions in an electrolyte solution interact with each other via coulombic forces. Coulombic forces affect molecules' ability to dissociate and ions' ability to move through the solution under the influence of electric field. True thermodynamic pK_As and limiting mobilities are defined to infinitely diluted solutions where the coulombic interactions are not present. True thermodynamic values of these constants are therefore experimentally unavailable and some mathematical correction of the experimentally obtained apparent values must be used.

Models describing the ionic effects in a quantitative way have been a matter of scientific interest for a long time. As was discussed in the introdution, Deybe and Hückel proposed a theory of ionic atmosphere and activity coefficients [1, 2]. Their theory uses ionic strength as the measure of magnitude of coulombic interactions. Ionic strength is defined by equation 5.1

$$I = \frac{1}{2}\sum_{i=1}^{N} c_i z_i^2 \tag{5.1}$$

where N is the total number of ions in the system. Ionic strength has the dimension of concentration. The Debye-Hückel model uses only the value of ionic strength and certain parameters of the solvent to calculate activity coefficients. Activity coefficients can be used to calculate the apparent dissociation constant from true thermodynamic constant or vice versa.

Dependence of ionic mobility on the environment surrounding the ion is more complicated. The solution has to consider the dynamics of the formation of the ionic atmosphere and its deformation when the reference ion is in motion. Onsager and Fuoss [3] devised a theory that considers this dynamics and it can be used to calculate the apparent mobilities of all ions in a solution. Input parameters for the Onsager-Fuoss model consist of concentrations of all ions in the system and their limiting mobilities.

A common CZE-based method for determination of pK_As and limiting mobilities relies on taking a series of measurements at different pH and constructing a pH vs. effective mobility dependence [55–57]. This

dependence has the form of the Henderson-Hasselbalch curve and can be described by equation 5.2

$$\mu'_{eff} = \frac{\sum_{z=n}^{p} \mu'_z 10^{-\left(\sum_{j=n}^{z} pK'_{A,z} - (z-n)pH\right)}}{\sum_{z=n}^{p} 10^{-\left(\sum_{j=n}^{z} pK'_{A,z} - (z-n)pH\right)}} \tag{5.2}$$

where n and p are the lowest and highest charge of the analyte, respectively, and $pK'_{A,n} = 0$. This theoretical equation can be used to fit the experimental data to obtain both pK_A and ionic mobilities. This approach was first suggested by Cai [55] and used to determine pK_As of many compounds [56, 57]. pK_A and mobility values obtained directly from the fit are only apparent (pK'_A and μ' rather than pK_A and μ_{lim}) and therefore valid only under conditions sufficiently similar to those where they were measured. Some mathematical treatment must be used to calculate the true thermodynamic values. Correcting pK_A values for ionic strength with the Debye-Hückel model is quite straightforward [57] and commonly used. Because the fit uses pH vs. mobility dependence and the correction is done after the fit, it is necessary to perform all experiments at the same ionic strength for the correction to yield meaningful results.

Since the dependence of apparent ionic mobility on buffer composition is more complicated, only a few attempts to correct fitted ionic mobilities were made [58–60], first proposed by Šlampová. This approach used a rather simple equation from the classical physical chemistry textbook by Robinson and Stokes [61]. This equation is valid only for weak monovalent compounds and does not consider the actual composition of the buffer in which the measurements were conducted. As useful as this method is, its inability to work with anything else but monovalent analytes is rather limiting because the higher the charge, the more pronounced is the difference between apparent and limiting mobility and therefore the need to apply some form of correction. This method also requires to perform all measurements in buffers of the same ionic strength.

The aim of publication III [62] was to devise an improvement upon the aforementioned method. The principal idea was to replace the commonly used pH vs. effective mobility dependence with *buffer composition vs. effective mobility* dependence. This approach has two major advantages. Using the entire buffer composition as the independent variable enables the use of the original Onsager-Fuoss equation which is far less restrictive and approximative than the formula suggested by Robinson and Stokes. Using the buffer composition as input also lifts the limitation to perform all measurements at the same ionic strength because ionic strength is merely a property of the buffer.

While the less sophisticated method can be processed by general-purpose tools such as MATLAB or Origin, the complex nature of the approach proposed in publication III requires a specialized computer program to be fully effective. Primary goal of publication III was to devise such a program. The program named AnglerFish reuses the infrastructure provided by ECHMETCoreLibs and user interface elements of PeakMaster 6. Use of common building blocks enables easy data exchange between AnglerFish and PeakMaster 6 and provides mutually consistent results. The user enters composition of all buffers that were used to measure the effective mobility dependence curve, effective mobilities measured in each buffer, dissociation states and estimated pK_As and limiting mobilities as input. A Levenberg-Marquardt algorithm is then used to fit the experimental data points. The overall logic is shown in diagram 5.1. The most noteworthy feature of the algorithm is that it internally always works with true thermodynamic values of the fitted parameters. While it may seem unnecessary to recreate the *buffer + analyte* system in every step of the calculation, the ECHMETCoreLibs data model does not allow modifications of physico-chemical parameters of constituents once the `ChemicalSystem` object has been initialized.

AnglerFish was validated against the classical Cai's procedure which was programmed into Origin. pK_As from the classical fit were corrected for ionic strength with the Debye-Hückel formula. Additionally, ionic mobilities were corrected for ionic effects by hand with assistance of the PeakMaster software. This procedure is described in detail in publication III. Both procedures yield comparable results in terms of precision and accuracy. The procedure performed by AnglerFish is considerably less time consuming and error prone because it is completely automated. In principle it is also more accurate because the *ex-post* limiting mobilities correction of classically fitted data can be done only for one conveniently chosen data point[1].

[1]The "one-point correction" procedure is outlined in more detail in publication III

Figure 5.1: AnglerFish fit logic diagram

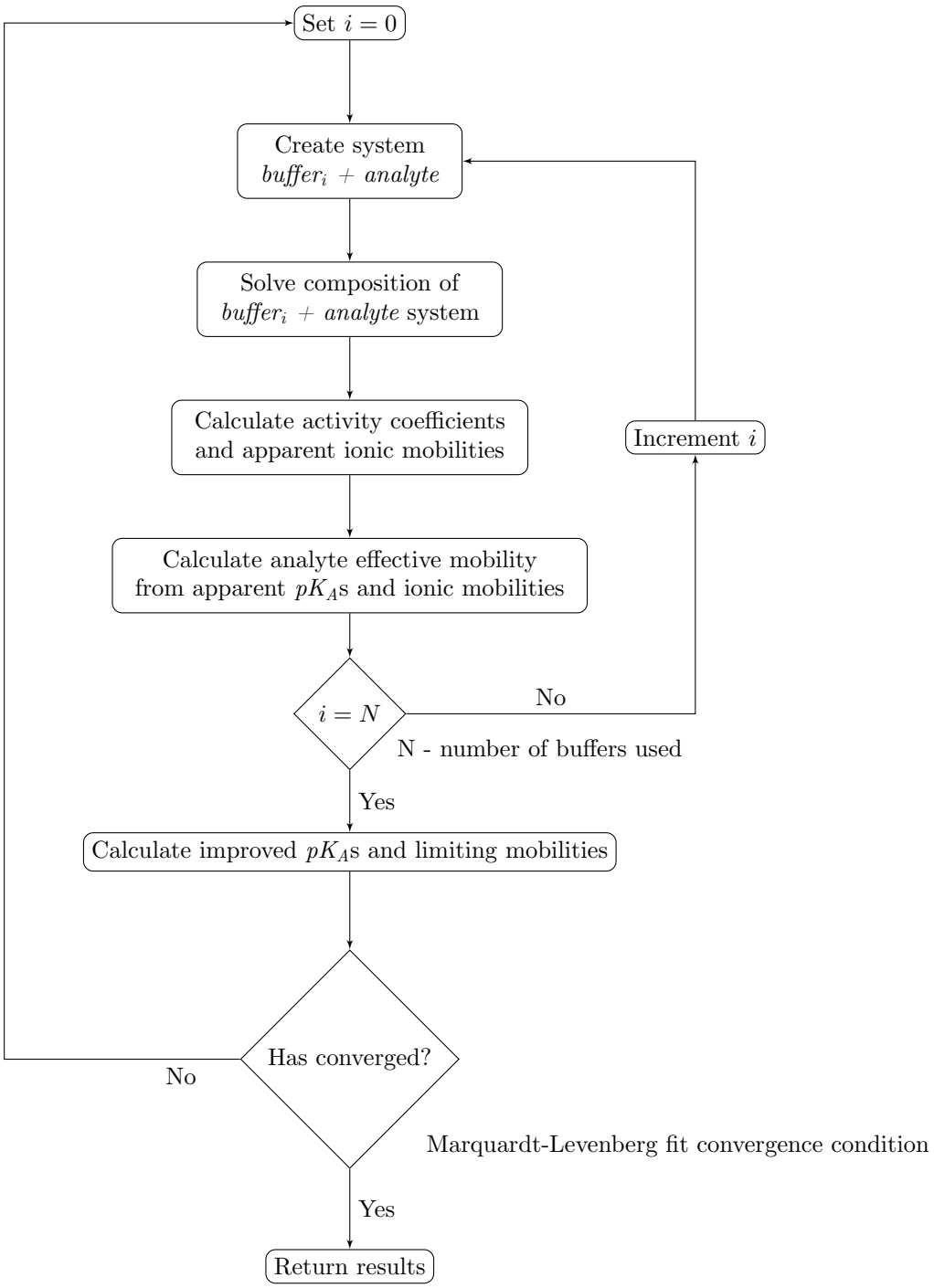

6 Determination of pK_A and limiting mobilities of pI markers for accurate pH gradient characterization (publication IV)

The isoelectric point (pI) is an important characteristic of complex chemical compounds such as proteins and other biomolecules. Methods based on electrophoresis are excellent tools for determination of the pI. When a CZE-based method is used a pH gradient can be established in the capillary. Position of the analyte along the pH gradient represents its pI value. For this to work, the slope of the pH gradient must be known. pI markers are chemical compounds with convenient electromigration properties that allow them to be used to characterize pH gradients. Initial research of pH gradients in capillary electrophoresis was done by Rilbe [63, 64]. Rilbe formed some elementary rules that have to be met for a stable pH gradient to form inside the separation space. In publication IV [65] a set of 14 compounds was identified as potential candidates for pI markers. A viable candidate has to be an ampholyte with at most two weakly acidic and basic groups, its structure must be well known and they are either readily commercially available or are easy to prepare in the laboratory with adequate purity.

Values of pI marker candidates pK_As were first estimated from their chemical structures to assess whether a given compound can be a viable pI marker. Estimates were calculated with SPARC and ChemSketch software. The actual values of pK_As and limiting mobilities were measured by means of CZE. Data was evaluated with the AnglerFish software to obtain true thermodynamic values of pK_As and limiting ionic mobilities.

Out of the 14 candidate pI markers only 12 absorb UV light at 280 nm wavelength. Actual behavior of these 12 selected pI markers was investigated experimentally by means of imaging capillary isoelectric focusing (ICIEF). In ICIEF the entire separation space is scanned by a UV/VIS detector. Therefore, exact positions of analytes in the capillary can be observed at any point in time. The separation space was filled with a commercial mixture of carrier ampholytes (SH AES) with pH range 3–10 and the 12 selected pI markers. Precise composition of the SH AES mixture is not declared by the manufacturer. Since the pI values of all used markers was known, it was possible to determine the actual shape of the pH gradient that formed inside the separation space. Contrary to common expectations, the gradient showed considerable deformation both at the anodic and cathodic end.

To complement the practical experiment a numerical simulation was run in Simul 5 Complex computer program [54]. The simulation used an artificial set of 181 ampholytes with -1 to $+1$ charge span and pK_As ranging from 3.5 to 10.8. The pK_A step between two consecutive ampholytes was 0.0406. The simulation showed trends very similar to those that were observed experimentally. Deformation of the pH gradient was less pronounced because artificial set of carrier ampholytes that were used for the simulation is closer to ideal carrier ampholyte mixture than the real SH AES ampholyte mixture. Additionally, the simulation does not consider any additional disruptive effects such as local heating, electroosmotic flow etc.

7 Conclusion and future outlook

This dissertation thesis discussed the utility of advanced mathematical models that deal with electromigration problems when they are backed with a computer implementation. Computer implementation of specialization of the extended NLTEM allowing to solve affinity capillary electrophoresis problems was developed and implemented into PeakMaster 6 computer program. Various affinity capillary electrophoresis systems were investigated. The Wren-Rowe and Tiselius' equation were re-derived directly from the extended NLTEM model. Behavior of analytes in systems where the analyte and a BGE component compete for a selector was investigated. A previously observed but insufficiently described change of selector concentration in the analyte zone was successfully predicted by the extended NLTEM and verified experimentally.

Nonlinear Marquardt-Levenberg fit coupled with Debye-Hückel and Onsager-Fuoss laws was successfully used for accurate determination of true thermodynamic pK_A and μ_{lim} constants of various compounds by measuring their effective mobilities in series of BGEs. Compounds characterized in this way were then used for pH gradient characterization in ICIEF experiments.

We expect that PeakMaster 6 will find practical applications in design and optimizations of ACE methods because of its unique ability to accurately calculate positions of all zones in ACE systems, regardless of their complexity. Its advanced equilibrium model opens the possibilities to study systems where the complex-forming interaction goes beyond 1:1 stoichiometry. The underlying engine is generic enough that it can be used as a basis of other software.

Bibliography

(1) Debye, P.; Hückel, E. *Physik Zeitschrift* **1923**, *24*, 185–206.

(2) Debye, P.; Hückel, E. *Physik Zeitschrift* **1923**, *24*, 305–325.

(3) Onsager, L.; Fuoss, R. M. *The Journal of Physical Chemistry* **1932**, *36*, 2689–2778.

(4) Neaga, I. O.; Hambye, S.; Bodoki, E.; Palmieri, C.; Ansseau, E.; Belayew, A.; Oprean, R.; Blankert, B. *Analytical and bioanalytical chemistry* **2018**, *410*, 4495–4507.

(5) Solinova, V.; Mikyskova, H.; Kaiser, M. M.; Janeba, Z.; Holy, A.; Kasicka, V. *Electrophoresis* **2016**, *37*, 239–247.

(6) Olabi, M.; Stein, M.; Waetzig, H. *Methods* **2018**, *146*, 76–92.

(7) Kohlrausch, F. *Annalen der Physik* **1897**, *298*, 209–239.

(8) Tiselius, A. The moving boundary method of studying the electrophoresis of proteins., 1930.

(9) Beckers, J., 1973.

(10) Everaets, F.; Beckers, J.; Verheggen, P., *Isotachophoresis - Theory, Instrumentation and Application*; Elsevier: 1976.

(11) Mikkers, F.; Everaets, F.; Peek, J. *Journal of Chromatography* **1979**, *168*.

(12) Mikkers, F.; Everaets, F.; Peek, J. *Journal of Chromatography* **1979**, *168*.

(13) Mikkers, F.; Everaets, F.; Peek, J.; Verheggen, P. *Journal of Chromatography* **1979**, *169*.

(14) Boček, P.; Gebauer, P. *Journal of Chromatography* **1981**, *217*.

(15) Boček, P.; Gebauer, P. *Journal of Chromatography* **1981**, *219*.

(16) Gebauer, P.; Boček, P. *Journal of Chromatography* **1982**, *242*.

(17) Gebauer, P.; Boček, P. *Journal of Chromatography* **1983**, *267*.

(18) Thormann, W.; Mosher, R. A. *Trans. Soc. Computer Simulation* **1984**, *1*.

(19) Thormann, W.; Mosher, R. A.; Bier, M. *Electrophoresis* **1985**, *6*.

(20) Thormann, W.; Mosher, R. A. *Electrophoresis* **1985**, *6*.

(21) Mosher, R. A.; Thormann, W. *Electrophoresis* **1985**, *6*.

(22) Hirokawa, T.; Nakahara, K.; Kiso, Y. *Journal of Chromatography* **1989**, *463*.

(23) Hirokawa, T.; Nakahara, K.; Kiso, Y. *Journal of Chromatography* **1989**, *470*.

(24) Hirokawa, T.; Nishino, M.; Aoki, N.; Kiso, Y.; Sawamoto, Y.; Yagi, T.; Akiyama, J. *Journal of Chromatography* **1983**, *271*.

(25) Gaš, B., 1975.

(26) Gaš, B.; Vacík, J.; Zelenský, I. *Journal of Chromatography* **1991**, *545*, 225–237.

(27) Poppe, H. *Journal of Chromatography* **1990**, *506*, 13TH INTERNATIONAL SYMP ON COLUMN LIQUID CHROMATOGRAPHY (CLC 89),STOCKHOLM, SWEDEN, JUN 25-30, 1989, 45–60.

(28) Poppe, H. *Analytical Chemistry* **1992**, *64*, 1908–1919.

(29) Štědrý, M.; Jaroš, M.; Gaš, B. *Journal of chromatography a* **2002**, *960*, 187–198.

(30) Štědrý, M.; Jaroš, M.; Včelákova, K.; Gaš, B. *Electrophoresis* **2003**, *24*, 536–547.

(31) Štědrý, M.; Jaroš, M.; Hruška, V.; Gaš, B. *Electrophoresis* **2004**, *25*, 3071–3079.

(32) Jaroš, M.; Hruška, V.; Štědrý, M.; Zusková, I.; Gaš, B. *Electrophoresis* **2004**, *25*, 3080–3085.

(33) Hruška, V.; Riesová, M.; Gaš, B. *Electrophoresis* **2012**, *33*, 923–930.

(34) Dvořák, M.; Dubský, P.; Dovhunová, M.; Gaš, B. *Electrophoresis*, *40*, 668–682.

(35) Haarhoff, P. C.; Van der Linde, H. J. *Analytical Chemistry* **1966**, *38*, 573–582.

(36) Hruška, V.; Svobodová, J.; Beneš, M.; Gaš, B. *Journal of chromatography a* **2012**, *1267*, 102–108.

(37) Beneš, M.; Svobodová, J.; Hruška, V.; Dvořak, M.; Zusková, I.; Gaš, B. *Journal of chromatography a* **2012**, *1267*, 109–115.

(38) Wren, S.; Rowe, R. *Journal of chromatography* **1992**, *603*, 235–241.

(39) Gaš, B.; Coufal, P.; Jaroš, M.; Muzikář, J.; Jelínek, I. *Journal of Chromatography A* **2001**, *905*, 269–279.

(40) Jaroš, M.; Včeláková, K.; Zusková, I.; Gaš, B. *Electrophoresis*, *23*, 2667–2677.

(41) Malý, M.; Dovhunová, M.; Dvořák, M.; Gerlero, G. S.; Kler, P. A.; Hruška, V.; Dubský, P. *Electrophoresis* **2019**, *40*, 683–692.

(42) Dubský, P.; Svobodová, J.; Gaš, B. *Journal of chromatography b-analytical technologies in the biomedicaland life sciences* **2008**, *875*, 30–34.

(43) Dubský, P.; Svobodová, J.; Tesařová, E.; Gaš, B. *Journal of chromatography b-analytical technologies in the biomedicaland life sciences* **2008**, *875*, 35–41.

(44) Svensson, H. *Acta chemica scandinavica* **1948**, *2*, 841–855.

(45) Malý, M.; Dubský, P. ECHMETCoreLibs. `https://github.com/echmet/ECHMETCoreLibs` (accessed 12/03/2019).

(46) Malý, M.; Dubský, P. LEMNG. `https://zenodo.org/record/1461522` (accessed 12/03/2019).

(47) Dovhunová, M.; Malý, M.; Dubský, P.; Gerlero, G. S.; Kler, P. A. *Journal of Chromatography A* **2019**, DOI: `https://doi.org/10.1016/j.chroma.2019.460595`.

(48) Boonleang, J.; Stobaugh, J. F. *ELECTROPHORESIS* **2013**, *34*, 1232–1240.

(49) Penn, S. G.; Bergstroem, E. T.; Knights, I.; Liu, G.; Ruddick, A.; Goodall, D. M. *The Journal of Physical Chemistry* **1995**, *99*, 3875–3880.

(50) Penn, S. G.; Bergstrom, E. T.; Goodall, D. M.; Loran, J. S. *Analytical Chemistry* **1994**, *66*, PMID: 7978295, 2866–2873.

(51) Beneš, M.; Riesová, M.; Svobodová, J.; Tesařová, E.; Dubský, P.; Gaš, B. *Analytical Chemistry* **2013**, *85*, PMID: 23895553, 8526–8534.

(52) Poppe, H. *Journal of Chromatography A* **1999**, *831*, 105–121.

(53) Almeida, V. K.; Larive, C. K. *Magnetic Resonance in Chemistry* **2005**, *43*, 755–761.

(54) Hruška, V.; Beneš, M.; Svobodová, J.; Zusková, I.; Gaš, B. *Electrophoresis* **2012**, *33*, 938–947.

(55) Cai, J.; Smith, J. T.; Rassi, Z. E. *Journal of High Resolution Chromatography* **1992**, *15*, 30–32.

(56) Poole, S. K.; Patel, S.; Dehring, K.; Workman, H.; Poole, C. F. *Journal of Chromatography A* **2004**, *1037*, Estimation of Physicochemical Properties by Chromatographic and Electrophoretic Techniques, 445–454.

(57) Šolínová, V.; Kašička, V.; Koval, D.; Česnek, M.; Holý, A. *Electrophoresis* **2006**, *27*, 1006–1019.

(58) Šlampová, A.; Boček, P. *Electrophoresis* **2008**, *29*, 538–541.

(59) Šlampová, A.; Křivánková, L.; Gebauer, P.; Boček, P. *Journal of Chromatography A* **2008**, *1213*, 25–30.

(60) Šlampová, A.; Křivánková, L.; Gebauer, P.; Boček, P. *Journal of Chromatography A* **2009**, *1216*, 16th International Symposium on Capillary Electroseparation Techniques, Catania, ITALY, AUG 31-SEP 04, 2008, 3637–3641.

(61) Robinson, R. A.; Stokes, R. H., *Electrolyte solutions*; Mineola, NY : Dover Publications: 2002.

(62) Malý, M.; Boublík, M.; Pocrnić, M.; Ansorge, M.; Lorinčíková, K.; Svobodová, J.; Hruška, V.; Dubský, P.; Gaš, B. *Electrophoresis*, DOI: 10.1002/elps.201900283.

(63) Rilbe, H. *Annals of the new york academy of sciences* **1973**, *209*, 11–22.

(64) Rilbe, H. *Electrophoresis* **1984**, *5*, 1–17.

(65) Ansorge, M.; Gaš, B.; Boublík, M.; Malý, M.; Šteflová, J.; Hruška, V.; Vigh, G. *Electrophoresis*, DOI: 10.1002/elps.201900381.

Publication I

Michal Malý[1]
Magda Dovhunová[1]
Martin Dvořák[1]
Gabriel S. Gerlero[2]
Pablo A. Kler[2,3]
Vlastimil Hruška[4]
Pavel Dubský[1]

[1]Faculty of Science, Department of Physical and Macromolecular Chemistry, Charles University in Prague, Prague, Czech Republic
[2]Centro de Investigación de Métodos Computacionales (CIMEC, UNL-CONICET), Santa Fe, Argentina
[3]Departamento de Ingeniería en Sistemas de Información, FRSF-UTN, Santa Fe, Argentina
[4]Liquid Phase Separations Division, Agilent Technologies Deutschland GmbH & Co. KG, Waldbronn, Germany

Received September 22, 2018
Revised December 4, 2018
Accepted December 5, 2018

Research Article

Generalized model of the linear theory of electromigration and its application to electrokinetic chromatography: Theory and software PeakMaster 6—Next Generation

The linear theory of electromigration, including the first-order nonlinear approximation, is generalized to systems with any equilibria fast enough to be considered instantaneous in comparison with the timescale of peak movement. For example, this theory is practically applied in the electrokinetic chromatography (EKC) mode of the CZE. The model enables the calculation of positions and shapes of analyte and system peaks without restricting the number of selectors, the complexation stoichiometry, or simultaneous acid–base equilibria. The latest version of our PeakMaster software, PeakMaster 6—Next Generation, implements the theory in a user-friendly way. It is a free and open-source software that performs all calculations and shows the properties of the background electrolyte and the expected electropherogram within a few seconds. In this paper, we mathematically derive the model, discuss its applicability to EKC systems, and introduce the PeakMaster 6 software.

Keywords:
Capillary zone electrophoresis / Electrokinetic chromatography / Linear theory of electromigration / PeakMaster

DOI 10.1002/elps.201800400

Additional supporting information may be found online in the Supporting Information section at the end of the article.

1 Introduction

Continuity laws, which describe the motion of charged particles under electric field effects in a one-dimensional channel, are not particularly difficult to formulate. The basic set of continuity equations was introduced by Kohlrausch [1], in 1897. Kohlrausch discovered the existence of specific conservation laws that may apply in electrophoretic systems [2]. Unfortunately, these laws have a limited scope of applicability and cannot be used to describe the behavior of an arbitrary electromigration system. The complete set of electromigration continuity equations is inherently nonlinear and must be numerically solved because no analytical closed form of the equations is known. Various computer implementations of numerical solvers of electromigration continuity laws have been developed since 1980s. Currently, advanced simulators such as Simul 5 [3], GENTRANS [4], and SPRESSO [5] are capable of solving 1D CE equations.

Finding an approximate solution to the continuity equations, valid under restrictions applicable to a given electromigration system, is an alternative to performing computer simulations. When available, an approximate solution provides the advantage of fast computation and often enables drawing more general conclusions about the given mode of electrophoresis. As first suggested by Poppe [6, 7], electromigration continuity equations can be linearized, and the solution leads to a matrix eigenvalue problem in CZE experimental setups. Using this approach, Štědrý et al. [8–10] later developed the linear theory of electromigration (LTEM). Štědrý et al. introduced the term *eigenmobility*, which is a number obtained as an eigenvalue of a mobility matrix. *Eigenmobility* means the true electromigration mobility of an

Correspondence: Dr. Pavel Dubský, Faculty of Science, Department of Physical and Macromolecular Chemistry, Charles University in Prague, Faculty of Science, Albertov 6, CZ-128 43 Prague 2, Czech Republic
E-mail: pavel.dubsky@natur.cuni.cz

Abbreviations: EKC, electrokinetic chromatography; **EMD**, electromigration dispersion; **HVL**, Haarhoff–van der Linde; **IS**, ionic strength; **LTEM**, linear theory of electromigration; **NLTEM**, first-order nonlinear theory of electromigration; **PDE**, partial differential equation; **PM6**, PeakMaster 6—Next Generation software; **R-FLU**, R-Flurbiprofen

Color online: See the article online to view Figs. 1–3 in color.

analyte or a system peak detectable in a CZE experiment. The model was able to predict the positions of all peaks in a CZE system containing an arbitrary number of analytes and a BGE consisting of any number of electrolytes. All constituents in a system could be general ampholytes. The model was implemented in PeakMaster 5 [11] software.

The linearized model provides previously unavailable insight into the behavior of CZE systems and can be fully resolved in a matter of seconds on an ordinary PC. Hruška et al. [12] later expanded the original model by including first nonlinear term in the linearized equation, herein referred to as the first-order nonlinear theory of electromigration (NLTEM) model. This enabled the model to predict not only the positions of all peaks but also their shapes. Although the practice of fitting distorted peaks by electromigration dispersion (EMD) with the Haarhoff–van der Linde (HVL) function [13, 14] was already recommended [15], the NLTEM model provided mathematical bases for such an approach. In addition, this practice demonstrated the time dependence of the fitted parameters that should be considered when analyzing peaks naturally detected in the time domain. The HVL function is a solution for an initial condition of an infinitely narrow injection plug. The function therein referred to as a HVLR function was shown to be the solution for a rectangular pulse initial condition. This model was included in PeakMaster 5.3.

Analytical demands of high-performance separations have led to the development of CZE techniques that achieve or improve separation through interactions between an analyte and an agent present in the background buffer. In electrokinetic chromatography (EKC) setups, the agent, usually referred to as the *selector*, forms a complex with the analyte, altering its electromigration properties. The equation used to calculate the expected change in analyte mobility as a function of its affinity to the selector and of the selector concentration was first proposed by Wren and Rowe [16]. The original Wren–Rowe equation was expanded by Rawjee, Williams, and Vigh [17] and Lelièvre and Gareil [18] to account for weak monovalent analytes and later by Dubský et al. [19, 20] to account for a mixture of selectors competing with each other for an analyte. All these models assume 1:1 stoichiometry and overlook possible interferences caused by interactions between a selector and other BGE constituents.

In terms of computer simulations, both GENTRANS [4] and Simul 5 [21] have been updated to simulate systems with one selector interacting with an arbitrary number of other constituents in a 1:1 stoichiometric ratio. All complexing components can be general ampholytes or neutral compounds. The complex-forming equilibria, nevertheless, also demands longer computational times for simulations. A limited complex-forming equilibrium model was also implemented in PeakMaster 5.3 Complex [22]. The model can handle a single selector that exclusively interacts with an analyte in a 1:1 ratio. Interactions between the selector and other BGE constituents are not allowed. Another constraint is that both analyte and selector can only be either neutral or fully charged species. In spite of these limitations, the model demonstrated for the first time that interactions between an analyte and a selector can have additional EMD-like effects on the analyte [23], and PeakMaster 5.3 Complex software can predict the extent of this dispersion.

The primary aim of this paper is to develop a comprehensive NLTEM model that describes complexation equilibria along with acid–base equilibria in CZE and EKC. In order to complete the theory, we further generalize the NLTEM model by formulating it in terms of any equilibria in which chemical species in solution decay or assemble to various forms with rates fast enough to consider that the equilibrium state is instantaneously achieved in comparison to the timescale of peak movement [23]. Generalized NLTEM is described in the first part of the paper, whereas PeakMaster 6—Next Generation software (PM6) is introduced in the second part of this paper.

The numerical implementation of the new model requires adopting a strategy different from that used in previous versions of PeakMaster in many aspects. This has led us to completely reimplementing the computational core and to developing an entirely new version of the PeakMaster software. PM6 is inevitably limited to a subset of the virtually unlimited number of chemical systems covered by the generalized NLTEM model. Nevertheless, our new model can handle all practically relevant systems of complex-forming equilibria with a 1:L stoichiometry in EKC, without restricting the number of selectors, wherein all BGE and analyte constituents can be general ampholytes, and any selector can interact with any number of analytes or other BGE constituents. Therefore, our new model makes it possible to characterize analyte and system peaks in a wide range of common EKC systems for the first time.

2 Theory

The original LTEM was built entirely around acid–base equilibria. In that case, the mutual relationships between partial differential equations (PDEs) that describe mass transport of every individual constituent in the system can be traced down to a single independent variable of the concentration of hydroxonium ions. This significantly simplifies the way in which (N)LTEM is formulated. The simplicity cannot be maintained in EKC where other equilibria can affect the system besides the acid–base ones. Addition of a neutral selector and the influence it has on analyte peak mobility and concentration distribution (peak shape) as revealed by PeakMaster 5.3 Complex calculations [22] is a particular example of an EKC system where complexation-related effects act independently of the acid–base-related effects.

On the other hand, when a single neutral/ fully charged selector interacts with a fully charged/neutral analyte (and no BGE constituents) in EKC—as previously implemented in the "5.3 Complex" version of PeakMaster—system peaks remain unaffected (up to a presence of the fully charged selector as a noninteracting species, if applicable), and the chemical equilibrium between the analyte and the selector

can be easily solved. Hence, an extension of the classical (N)LTEM model to such systems required only redefining a few analyte peak parameters [21]. The implementation of a more advanced complex-forming model was deemed complicated [21] due to the need for a new formulation of the theory and to the technical nature of the equilibrium solver used by the software at that time. Therefore, the implementation of the whole NLTEM model had to be changed to receive the general complex-forming equilibria solver.

2.1 Continuity equations

A one-dimensional model of electromigration consists of N continuity equations in which N is the number of chemical constituents of the system. Constituents can be general ampholytes or strictly neutral species, any of which can be present in various forms. The perception of forms is intuitive in simple CZE systems, as covered by the original theory, wherein every form belongs to exactly one constituent, such as the four (including neutral) forms of phosphoric acid, which belong to the phosphoric acid constituent. The only exceptions are water ions, H_3O^+ and OH^-, which are treated separately. The simple assignment of forms and constituents is lost when other equilibria compete with acid–base equilibria. For example, if both forms of a monovalent weak acid (A^- and HA) form complexes with a neutral selector S, all possible forms, SA^-, SAH, A^-, and AH, belong to the acid constituent, while the two forms, SA^- and SAH, simultaneously belong to the selector constituent.

Thus, a set (Ω) of all forms present in the system must be defined, regardless of constituent to which they belong. Additionally, the set (Ω) must now also include the water ions, herein referred to as H and OH. In contrast to simple CZE systems, a constituent may appear more than once in a single form; for example, the constituent S appears two times in a hypothetical complex form S_2A. We signify this with a coefficient $\nu_{(g)i}$, wherein the subscript (g) refers to the form g and the subscript i refers to the i-th constituent. If, for example, the selector, S, and the analyte, A, constituents are referred to with indexes $i = \{1; 2\}$, respectively, then $\nu_{(S_2A)1} = 2$ and $\nu_{(S_2A)2} = 1$. Thus the coefficient $\nu_{(g)i}$ is equivalent to the stoichiometric coefficient of the i-th constituent in the form g, although its definition is extended for the purpose of this theory so that

$$\nu_{(g)i} = 0 \text{ , if the form } g \text{ does not belong to the } i\text{-}th \text{ constituent.} \quad (1)$$

For example, $\nu_{(S_2A)3} = 0$, provided that we add a third constituent to the aforementioned example system. The relationships between the constituents and their forms can be thus generally expressed by the mass balance relation

$$c_i = \sum_{g\in\Omega} \nu_{(g)i} c_{(g)} \text{ ,} \quad (2)$$

where c_i stands for the net (analytical) concentration of the i-th constituent, $c_{(g)}$ stands for the concentration of the form g, and the summation includes the entire set of forms, Ω. Importantly, the forms that do not belong to the i-th constituent are inevitably excluded from the summation due to Eq. (1), which is a principle that applies to various equations throughout this article.

A concise introduction to continuity equations describing the mass conservation in electrophoresis can be found in the original paper on NLTEM [12]. The spatiotemporal development of concentration profile of each constituent, $c_i \equiv c_i(x, t)$, is given by

$$\frac{\partial c_i}{\partial t} = -\frac{\partial J_i}{\partial x} = -\sum_{g\in\Omega} \nu_{(g)i} \frac{\partial J_{(g)}}{\partial x}, \quad (3)$$

where $J_i \equiv J_i(x, t)$ is the mass flux[1] of the i-th constituent consisting of the mass fluxes, $J_{(g)}$, of the individual forms g that belong to this constituent in accordance with Eq. (2). Every mass flux is decomposed into three components,

$$J_{(g)} = J_{(g)em} + J_{(g)D} + J_{(g)emdiff}, \quad (4)$$

the electromigration component, the diffusion component, and the diffusion-potential-related component, respectively. It should be noted that the last component is somewhat artificial because it emerged from the electromigration flux by excluding a part that accounts for the diffusion potential (cf. [12]). A previous study [12] has demonstrated that merging the diffusion-potential-related term of the resulting continuity equation with the diffusion term is more advantageous than hiding it within the original electromigration term. Nevertheless, for the purposes of our discussion, we will continue differentiating all three contributors to the overall mass flux, according to Eq. (4).

The electromigration flux reads

$$J_{(g)em} = \frac{j}{\kappa} \mu_{(g)} c_{(g)}, \quad (5)$$

where j is the current density (cf. footnote 1), $\kappa \equiv \kappa(x, t)$ is the conductivity, and $\mu_{(g)} \equiv \mu_{(g)}(x, t)$ is the electrophoretic mobility of the form g. In contrast to the original theory [8–12], we do not work with electrophoretic mobility as a constant. We rather consider it a spatiotemporal variable because electrophoretic mobility depends on IS. We discuss this issue in more detail in Supporting Information. For mathematical convenience, we also switch from using unsigned mobilities, $u_{(g)}$, to using signed mobilities $\mu_{(g)} = sign(z_{(g)})u_{(g)}$, where $z_{(g)}$ is the charge of the form g. The diffusion flux is given by

$$J_{(g)D} = -D_{(g)} \frac{\partial c_{(g)}}{\partial x}, \quad (6)$$

where $D_{(g)}$ is the diffusion coefficient of the form g, which is considered constant (i.e., independent of IS, cf. Supporting information) herein. Finally,

$$J_{(g)emdiff} = \frac{j_{diff}}{\kappa} \mu_{(g)} c_{(g)}, \quad (7)$$

[1]Technically, mass flux, as shown in Eq. (2), is a signed quantity numerically equal to the only component of the one-dimensional vector $\vec{J}_i$.

where $j_{diff} \equiv j_{diff}(x, t)$ is the diffusion current density. The conductivity and the diffusion current density equal

$$\kappa = F \sum_{f \in \Omega} z_{(f)} c_{(f)} \mu_{(f)}, \tag{8}$$

where F is the Faraday constant, and

$$j_{diff} = -F \sum_{f \in \Omega} z_{(f)} D_{(f)} \frac{\partial c_{(f)}}{\partial x}. \tag{9}$$

2.2 Generalization of the linear theory of electromigration beyond the acid–base equilibria

Eq. (3) and Eqs. (4)–(9) form a set of N vastly interrelated nonlinear partial differential equations for N constituents. LTEM aims to decoupling the set of PDEs. This is primarily achieved by focusing on the migration flux only and by expressing the resulting PDEs in a matrix form of

$$\left(\frac{\partial \vec{\mathbf{C}}}{\partial t}\right)_{em} = -\frac{j}{\kappa_{BGE}} \mathbf{M} \times \frac{\partial \vec{\mathbf{C}}}{\partial x}, \tag{10}$$

where $\vec{\mathbf{C}} \equiv (c_1, \ldots, c_N)^T$ is a column vector of the concentrations of all constituents, κ_{BGE} is the conductivity of the BGE, and $\mathbf{M} \equiv \mathbf{M}(\vec{\mathbf{C}}(x, t))$ is the target matrix.

The elements of the matrix $\mathbf{M}$ were evaluated by Štědrý et al. for strong [8], weak univalent [9], and multivalent [10] electrolytes. Nevertheless, these derivations were always specialized to the inspected case of weak electrolytes, and no derivation concerned complex-forming equilibria in CZE. The general structure of the matrices is also unclear in the original papers. Using the generalized form of the continuity equations (cf. Section 2.1) allows us to reformulate LTEM to cover electrophoretic systems comprising any chemical equilibrium so that equilibrium reactions are fast enough to instantaneously reach equilibrium. In practical terms, the time scale of every reaction is negligible in comparison with that of the separation process (notice that the latter is measured as the time needed for a peak to travel the peak width, and not as the time of the entire separation [24]). Therefore, at any time and position in the capillary, the concentration of every form can be expressed as an algebraic function of concentrations of all constituents

$$f \in \Omega: \; c_{(f)} \equiv c_{(f)}(c_1, \ldots, c_N). \tag{11}$$

Because $J_{i,em}$ is a function of only concentrations of individual forms, which in turn are functions of concentrations of constituents, Eq. (11), we can easily assume, based on Eq. (10), that the elements of the matrix, $\mathbf{M}$, become

$$\mathbf{M}: m(i, q) = \left(\frac{\kappa_{\mathrm{BGE}}}{j} \frac{\partial J_{i,\mathrm{em}}}{\partial c_q}\right). \tag{12}$$

We provide a more detailed analysis in Supporting Information in which we further show that Eq. (12) leads to the matrix $\mathbf{M}$ decomposition into two matrices $\mathbf{M}_{\boldsymbol{\mu}}$ and $\mathbf{M}_{\partial}$,

$$\mathbf{M} = \mathbf{M}_{\boldsymbol{\mu}} \times \mathbf{M}_{\partial}. \tag{13}$$

The first matrix

$$\mathbf{M}_{\boldsymbol{\mu}}: \; m_{\mu}(i, h) = \frac{\kappa_{\mathrm{BGE}}}{\kappa} \left(\nu_{(h)i} \mu_{(h)} - \frac{F}{\kappa} \sum_{g \in \Omega} \nu_{(g)i} \mu_{(g)} c_{(g)} r_{(g)(h)}\right) \tag{14}$$

$$r_{(g)(h)} = \left(z_{(h)} \mu_{(h)} - \frac{\kappa}{F} \frac{\partial \ln \mu_{(g)}}{\partial c_{(h)}} + \sum_{f \in \Omega} z_{(f)} c_{(f)} \frac{\partial \mu_{(f)}}{\partial c_{(h)}}\right)$$

has an $N \times |\Omega|$ size, its elements have a dimension of electrophoretic mobility, and its i-th row can be regarded as referring to the i-th constituent, whereas its h-th column can be regarded as referring to the h-th form in the separation system. For this purpose, the set Ω is presumed arbitrarily, albeit uniquely, ordered, and we use the symbol h to express either the form h or its index in set Ω. Importantly, every i-th row of the matrix contains columns for all forms (h), even if that form does not belong to the i-th constituent, in which case $\nu_{(h)i} = 0$, in accordance with Eq. (1). Additionally, the matrix contains two special columns for the water ion "forms," which do not belong to any constituent, that is, $\nu_{(H)i} = 0$, $\nu_{(OH)i} = 0$ for every i.

The second matrix

$$\mathbf{M}_{\partial}: \; m_{\partial}(h, q) = \frac{\partial c_{(h)}}{\partial c_q} \tag{15}$$

has a size $|\Omega| \times N$ and its elements are dimensionless. We call it the "communication matrix" because it describes how constituents communicate with each other through the various equilibria present in the system. The communication matrix can be viewed as the central point in the linearization procedure because it reflects interconnections between individual mass conservation equations, Eq. (3), and thus is prerequisite for extracting the matrix, $\mathbf{M}$, Eq. (10), from the coupled set of PDEs. Simultaneously, the communication matrix could not be extracted from the coupled set of PDEs if Eq. (11) did not apply to every form $f \in \Omega$. Accordingly, the need for formulating the communication matrix limits the generalized LTEM model to infinitely fast equilibria.

The communication matrix converts the constituent concentration vector, $\vec{\mathbf{C}}$, into a vector of form concentrations, $(c_{(1)}, \ldots, c_{(|\Omega|)})^T = \mathbf{M}_{\partial} \times \vec{\mathbf{C}}$. Thus, the communication matrix is equivalent to the matrix $\mathbf{M}_2$ introduced for weak monovalent electrolytes in the appendix of [9] and further used in [10] for general ampholytes. Consequently, the matrix $\mathbf{M}_{\boldsymbol{\mu}}$ is equivalent to that therein referred to as the matrix $\mathbf{M}_1$. Nevertheless, matrices $\mathbf{M}_{\boldsymbol{\mu}}$ and $\mathbf{M}_{\partial}$ are not expressed identically to matrices $\mathbf{M}_1$ and $\mathbf{M}_2$, respectively, and the latter pair of matrices cannot be straightforwardly applied to complex-forming or similar equilibria.

Matrices $\mathbf{M}_{\boldsymbol{\mu}}$ and $\mathbf{M}_{\partial}$, as prescribed by Eqs. (14) and (15), respectively, enable us to express the LTEM matrix, $\mathbf{M}$, for systems with arbitrary fast equilibria. The diagonalization procedure and the introduction of the first-order nonlinear term, and thus the formulation of NLTEM for such systems, are identical to a previously published procedure [8–10, 12]. We refer the reader to Supporting Information for a complete theory, including several essential technical details that may not be clear in the original papers. Our second paper published in this special issue [25] provides a concise

summary of (N)LTEM (yet in simple CZE systems only). In short, the mathematical analysis reveals that BGE forms an environment in which N independent wave functions, $\tilde{w}_i$, tend to propagate with velocities ($\frac{j}{\kappa_{BGE}}\lambda_i$). λ_i are eigenvalues of a matrix $\mathbf{M}_0 = \mathbf{M}(\vec{\mathbf{C}}_{\mathrm{BGE}})$ evaluated at the composition of BGE. It should be noted that the vector $\vec{\mathbf{C}}_{\mathrm{BGE}}$ also contains analyte constituents, whose concentration is set to zero therein. Wave functions represent system peaks and analyte peaks, whose position can be easily obtained from the velocities. The chemical composition of the peaks can also be calculated from LTEM [26]. Peak concentration distributions are approximated through NLTEM as the HVL or HVLR function [12].

NLTEM requires expressing a few additional terms that we provide below for consistency purposes. The key step in NLTEM is the Taylor expansion of matrix $\mathbf{M}$. Taylor expansion approximates the matrix in a specific region, $\vec{\mathbf{C}}_{\mathrm{BGE}} + \vec{\tilde{c}}$, wherein $\vec{\tilde{c}}$ is a sufficiently small disturbance in the otherwise homogeneous distribution of the BGE. In the frame of NLTEM, the matrix $\mathbf{M}_0$ is understood as a zero-order Taylor term of the expansion of the matrix $\mathbf{M}$, and the first-order term is added to the electromigration expression as

$$\left(\frac{\partial \vec{\mathbf{C}}}{\partial t}\right)_{em} \cong -\frac{j}{\kappa_{BGE}}\left(\mathbf{M}_0 + \sum_{k=1}^{N} \mathbf{M}_{1,k}\tilde{c}_k\right) \times \frac{\partial \vec{\mathbf{C}}}{\partial x}, \tag{16}$$

where

$$\mathbf{M}_{1,k} = \frac{\partial \mathbf{M}}{\partial c_k}\left(\vec{\mathbf{C}}_{BGE}\right) \tag{17}$$

Solving Eq. (16) requires additionally extending it with the diffusion term

$$\frac{\partial \vec{\mathbf{C}}}{\partial t} \cong -\frac{j}{\kappa_{BGE}}\left(\mathbf{M}_0 + \sum_{k=1}^{N} \mathbf{M}_{1,k}\tilde{c}_k\right) \times \frac{\partial \vec{\mathbf{C}}}{\partial x} + \mathbf{D}\frac{\partial^2 \vec{\mathbf{C}}}{\partial x^2}, \tag{18}$$

where $\frac{\partial^2 \vec{\mathbf{C}}}{\partial x^2} = (\frac{\partial^2 c_1}{\partial x^2}, \ldots, \frac{\partial^2 c_N}{\partial x^2})^T$, and $\mathbf{D}$ is the constant matrix to be approximated from the diffusion and from the diffusion-potential-related fluxes, which originate from Eq. (3). When generalized to the fast equilibria, the diffusion matrix results in a form that differs from that formulated in simple CZE systems, namely by the $\nu_{(g)i}$ coefficients (cf. Supporting Information)

$$\mathbf{D} = \mathbf{D}_d \times \mathbf{M}_\partial, \tag{19}$$

where

$$\mathbf{D}_d : d_d\ (i,h) = \left(\nu_{(h)i} D_{(h)} - \frac{F z_{(h)} D_{(h)}}{\kappa} \sum_{g \in \Omega} \nu_{(g)i} \mu_{(g)} c_{(g)}\right) \tag{20}$$

and $\mathbf{M}_\partial$ is the communication matrix given by Eq. (15). Finally, the matrix $\mathbf{D}$ is evaluated at the composition of BGE, $\mathbf{D} \equiv \mathbf{D}(\vec{\mathbf{C}}_{\mathrm{BGE}})$.

LTEM transforms the original set of coupled electromigration-term PDEs in the concentration domain, Eq. (5), into a fully equivalent set of decoupled PDEs in the domain of the wave functions, $\tilde{w}$. In contrast, NLTEM requires discarding some higher-order nonlinear terms when deriving Eq. (19). Moreover, the diagonalization procedure is incomplete when applied to the first-order Taylor expansion term and to the diffusion term. Thus, for diagonalization purposes, the effects of propagating waves on each other are disregarded. This assumption—termed the assumption of an immediate separation of zones [12]—is equivalent to discarding the off-diagonal elements of the two "diagonalized" matrices that originate from NLTEM. All approximations adopted within NLTEM are elaborated to detail in Supporting Information.

This suggests that the HVL and HVLR distributions can represent the exact solution to the set of PDEs, Eq. (3), only to a limited extent. Nevertheless, NLTEM has thus far proved to be in a very good agreement with both experimental data and numerical solutions to the factual set of equations (Eq. (3)) [22, 27], and—in contrast to full numerical solutions—it provides results straightforwardly. When a more exact solution of the peak shape is required, the disturbances $\tilde{c}_i$ are too large to satisfy the Taylor expansion limits, or the assumption of the immediate separation of waves (i.e., analyte or system peaks) is far from reality, the full numerical solution, for example, by means of Simul [20], has to be used.

3 Results and discussion

Despite the strong formal similarities between the old and the new formulations of the NLTEM model, the evaluation of the new model requires adopting a strategy significantly different from that used in the case of simple CZE systems. The original PeakMaster was written as a monolithic piece of code, which allowed the rapid development and quick addition of new features. However, such design made it difficult to introduce changes at a more fundamental level. PM6 involves a completely new implementation of NLTEM, which now includes general complex-forming equilibria. The code has been split into modules to facilitate code reuse and long-term maintainability. The entire code base is now built on top of free and open source tools and is available to the scientific community from https://github.com/echmet/PeakMasterNG (https://doi.org/10.5281/zenodo.1461507).

3.1 Computation engine

The inclusion of complex-forming equilibria in the model requires a different approach to calculating the equilibrium composition of a solution. In the former version of PeakMaster, the concentration of the hydroxonium ions, $c_{(H)}$, was first evaluated as the only positive root of the *G-polynomial* [10]. Consequently, the individual concentrations of all other ionic forms at a given pH of the system can be easily calculated when considering only acid–base equilibria. However, the *G-polynomial* can no longer be used because the equilibrium is now a function of more than one variable. Our new equilibrium solver instead constructs a system of equations in which each equation represents an individual equilibrium.

The system is numerically solved using the Newton–Raphson method. To prevent the solver from reaching mathematically correct but physically meaningless solutions with negative concentrations, we transform all equations into their logarithmic forms.

However, this transition to a numerical solver has a considerable disadvantage: the loss of the ability to analytically express the concentration derivatives of equilibrium composition (cf. the communication matrix, Eq. (15), and the first-order Taylor term, Eq. (17)). This was a problem because the *double floating*-point precision (per IEEE754 naming) turned out to be insufficient to correctly and consistently calculate the concentration derivatives. Thus, we calculate these derivatives using an arbitrary-precision floating-point arithmetic provided by GNU GMP library [28] (https://gmplib.org/). Higher-level mathematical functions operating with arbitrary precision are supplied by GNU MPFR library [29] (https://www.mpfr.org) and MPReal C++ wrapper [Holoborodko, P., MPFR C++, 2008] (http://www.holoborodko.com/pavel/mpfr/). Matrix algebra is provided by Eigen library [Benoît J., Gaël G., et al., Eigen v3, 2010] (http://eigen.tuxfamily.org/). Although the use of arbitrary-precision arithmetic decreases performance, and even though all numeric derivatives must be done in software, the computation is still completed within a few seconds.

The equilibrium solver is implemented as a separate module within a package termed ECHMETCoreLibs (https://github.com/echmet/ECHMETCoreLibs). The ECHMETCoreLibs package is a more general set of libraries for calculating the properties of chemical solutions with no particular focus on CZE. IS correction can be applied to the equilibrium composition through an iterative calculation. The NTLEM itself is implemented in another module termed LEMNG (https://github.com/echmet/LEMNG, https://doi.org/10.5281/zenodo.1461522). The LEMNG module uses ECHMETCoreLibs to create an internal description of a chemical system, to solve its equilibrium composition, and then it calculates the true ionic mobilities applying Onsager–Fuoss [30] IS correction. These data are used to generate the respective NTLEM matrices and to calculate the electrophoretic properties of the system, as described in the Section 2.

3.2 Complexation mode

The most prominent improvement in PM6 over its predecessors is the inclusion of a very general complex-forming model. However, some design compromises had to be made because developing a completely general complex-forming model is a daunting task, in terms of computer implementation. The logic of the complex-forming model implemented in ECHMETCoreLibs is based on a "nucleus-ligand" scheme designed with the specifics of EKC experimental setups in mind.

In this scheme, the tree of complex forms is built around ionic forms of nuclei, which can bind an arbitrary amount

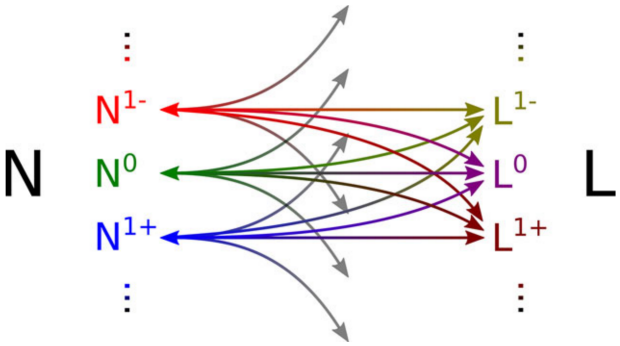

Figure 1. Schematic depiction of interactions allowed within ECHMETCoreLibs nucleus-ligand scheme.

of ionic forms of any ligands. The rationale of this scheme is shown in Fig. 1. The allowed stoichiometry of complex-forming relationships between nucleus and "ligand" ionic forms is 1:L in which L is an arbitrary natural number. In other words, a specific complex form may contain only one ionic form of a nucleus and an arbitrary number of ligand ionic forms of multiple ligands. Relationships between two ionic forms of a nucleus or ligand type are not allowed. We illustrate how these rules work in practice in a few other examples given in Supporting Information.

The nucleus-ligand scheme allows the formation of mixed complexes with multiple ligand ionic forms simultaneously bound to a single nucleus. EKC experimental setups typically do not involve these complexes. Instead, selectors compete for analytes or BGE constituents and exclusively bind to them. To simplify the user interface, PM6 currently prevents users from entering systems in which mixed complexes would occur.

3.3 PeakMaster 6 software

The basic layout of the UI remained similar to that of Peakmaster 5. The most notable changes include the possibility to enter the exact composition of BGE and sample solutions directly from the main window, the simplification of the chart (shapes of system peaks are directly displayed in the main window), and the rearrangement of some control elements.

Limiting ionic mobilities and dissociation constants are available in a database based on Hirokawa's data [31–35]. There is no database available for complexation parameters—the number of possible interactions is exceedingly high, and the complexation parameters are often measured for specific conditions only. However, user can save the composition of their system, including the entered complexation parameters.

PeakMaster 6 offers several corrections for nonideal ionic behavior in solution, including corrections for IS, specifically the Onsager–Fuoss and Debye–Hückel model [36]. Both of these are enabled by default. In addition, correction for viscosity can be enabled [23]. Importantly, the applicability of any of these corrections may be compromised in systems containing bulky and/or highly charged selectors, especially

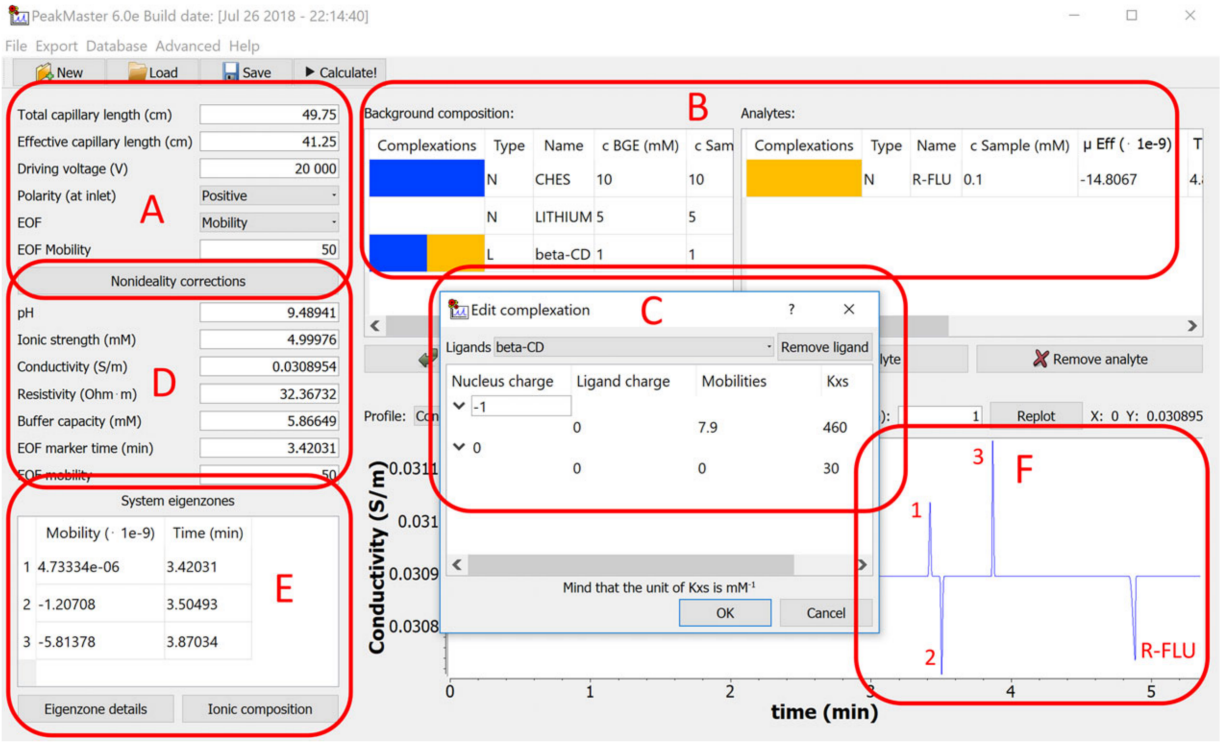

Figure 2. Screenshot of the PM 6 software. Model system described in Table 1. See text for detailed description of regions (A) to (F).

Table 1. Model system composition and characteristics

Composition	BGE	Sample
CHES concentration (mM)	10	10
Lithium concentration (mM)	5	5
β-CD concentration (mM)	1	1
R-FLU concentration (mM)	0.00	0.1
Electrophoretic properties (charge)	Mobility/ 10^{-9} m^2 s^{-1} V^{-1}	pK_a
CHES (–1)	25	9.55
Lithium (+1)	40.1	13.8
R-FLU (–1)	22.23	4.19
Complexes with β-CD	Mobility/ 10^{-9} m^2 s^{-1} V^{-1}	Complexation constant
CHES (–1)	7.9	460
CHES (0)	0	30
R-FLU (–1)	10.14	5 000
R-FLU (0)	0	10 000[a)]

a) The complexation constant of R-FLU(0)/β-CD complex was set to an arbitrary number. The true value does not matter because R-FLU exists almost exclusively in the (–1) acid–base form at the pH of 9.5.

at high selector concentrations. Such selectors (typically cyclodextrins) are quite common in EKC applications, although the relevant theory that would allow for exact IS or viscosity effects corrections has not been formulated yet [23].

Figure 2 shows the PM6 user interface. The model system specified in Table 1 is inspected. The mobilities and dissociation constants of CHES and Lithium were taken from the PM6 database, and those of R-Flurbiprofen (R-FLU) and the complexation parameters for R-FLU/β-CD complex and CHES/β-CD complex were taken from our previous study [37, 38]. System parameters are entered into region A and chemical composition into region B. Color coding in region B indicates constituents that form complexes. In our case, β-CD is considered the "ligand" that forms a complex with the R-FLU "nucleus" (orange) and another complex with the CHES "nucleus" (blue). The complexation parameters are specified in the complexation dialog, in region C. We show the complexation dialog for the CHES/β-CD complex (cf. Table 1). The dissociation constants of the complex forms require no specification [39]. After the calculation, basic characteristics of the analyte zone are further displayed in region B, and physical–chemical properties of BGE can be found in region D. Region E shows the emerging system peaks and their (eigen)mobilities, whereas a detailed description of zones and equilibria is provided in separate dialogs. Lastly, the predicted electropherogram is displayed in region F. We added numbers matching the system eignezones table (region E) and the name of the analyte to the peaks in the electropherogram.

The same model system from Table 1 was also simulated using Simul [20] (a developer version that numerically solves the full set of continuity equations, cf. Section 2.1, and utilizes the ECHMETCoreLibs for calculations of chemical equilibria at every simulation step). Figure 3 compares the calculated and simulated results without (A) and with (B) complexation between β-CD and the other constituents (CHES and R-FLU) applied. β-CD is present in BGE in both cases but is not set to form any complex in (A). Predicted

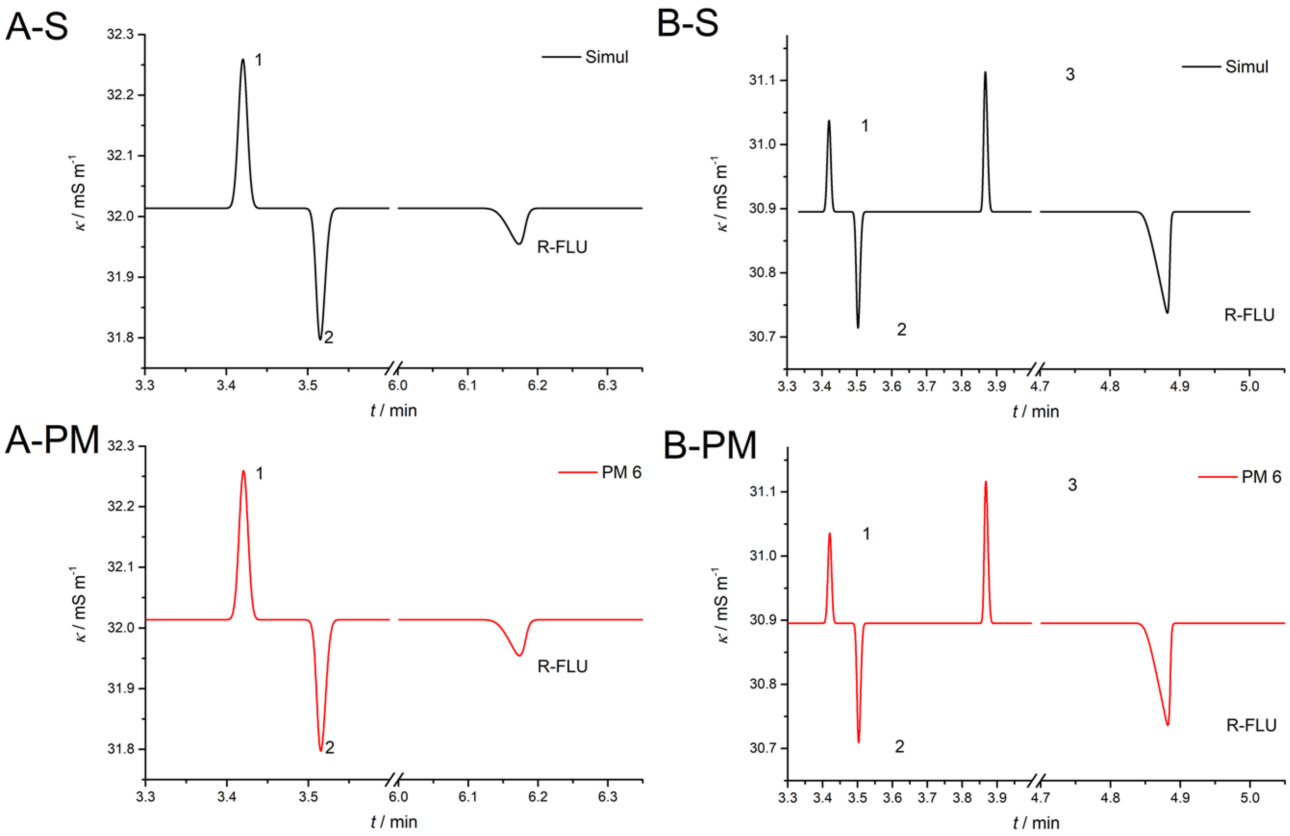

Figure 3. Electropherograms predicted by PM 6 (A-PM and B-PM) and by Simul (A-S and B-S) for the model system described in Table 1. (A-PM and A-S) Complexation between β-CD and CHES and β-CD and R-FLU is temporarily switched off. (B-PM and B-S) Complexation between β-CD and CHES and β-CD and R-FLU is switched on. Time axis is split for betted visibility of the peak shapes. Evaluation of the electropherogram is provided in Table 2.

electropherograms were evaluated using our software CEval [40] (https://echmet.natur.cuni.cz/software/download#ceval) and their numerical characteristics are given in Table 2.

Because β-CD is a neutral compound, the results (A) are equivalent to those observed in the previous versions of PeakMaster in simple CHES/Lithium buffer. Without the complexation, only two system peaks are apparently present, whereas three system peaks are actually present (as expected in systems with three BGE constituents), although two of them have exactly zero and almost zero mobilities (cf. Table 2) and thus coalesce. The system peak with exactly zero mobility arises due to the presence of the neutral noninteracting constituent (β-CD) in BGE. When the selector starts forming a complex with another BGE constituent (CHES), the system peak may become mobilized and visible (case (B)). Similarly, the effective mobility of the R-FLU analyte is altered by complexation with β-CD, as expected. As shown in Table 2 and Fig. 3, PM6 findings perfectly match the simulations. A detailed inspection of EKC systems using the generalized NLTEM and the verification of PM6 calculations will be reported in another paper (under preparation).

4 Concluding remarks

The generalized linear theory of electromigration was developed, including the first-order nonlinear approximation. The new theoretical model describes the behavior of electrophoretic systems with any equilibrium as long as the equilibrium reaction rates are fast enough to instantaneously reach the equilibrium state. The applicability of the model is shown, specifically in electrokinetic chromatography, which requires using complexing agents (selectors). Adding selectors to the system introduces additional complex equilibria that had not been implemented in the theory yet. Our model can describe the behavior of electrophoretical systems with any number of complexing agents, regardless of their charge or complexation stoichiometry. This model was implemented in the new generation of the PeakMaster software, which allows users to calculate the properties of electrophoretic systems and to predict the resulting electropherograms.

This work was supported by the Czech Science Foundation, under Grant No. 15–18424Y, by the Charles University Research Centre, under program No. UNCE/SCI/014, by the Charles

Table 2. BGE properties predicted by PM 6 for the model system specified in Table 1. Coding ((A-PM), (B-PM), (A-S), and (B-S)) corresponds to subparts of Figure 3

BGE characteristics (PM6)	Without complexation[c)]	With complexation[c)]
pH	9.54	9.49
Ionic Strength (mM)	5.00	5.00
Conductivity (mS/m)	32.0	30.9
Signed [a)] mobilities (PM6) (10^{-9} m^2 s^{-1} V^{-1})	Without complexation (A-PM)[c)]	With complexation (B-PM)[c)]
System peak 1	4.89×10^{-6}	4.73×10^{-6}
System peak 2	−1.38	−1.21
System peak 3	0.00	−5.81
Analyte peak R-FLU	−22.23	−14.81
Signed[a)] mobilities (Simul) (10^{-9} m^2 s^{-1} V^{-1})	Without complexation (A-S)[d)]	With complexation (B-S)[d)]
System peak 1	0.00	0.00
System peak 2	−1.38	−1.22
System peak 3	0.00	−5.83
Analyte peak R-FLU	−22.228	−14.77
Asymmetry[b)] (PM6)	Without complexation (A-PM)[d)]	With complexation (B-PM)[d)]
System peak 1	0.03	0.13
System peak 2	1.10	1.16
System peak 3	0.03	1.94
Analyte peak R-FLU	−5.30	−16.54
Asymmetry[b)] Simul	Without complexation (A-S)[d)]	With complexation (B-S)[d)]
System peak 1	0.01	−0.08
System peak 2	1.22	1.14
System peak 3	0.01	1.92
Analyte peak R-FLU	−5.13	−17.33

a) Positive/negative mobility corresponds to a movement of the peak toward the cathode/anode, respectively.
b) Measured as the $a_{3\delta}$ parameter of the HVL function [14].
c) PM6 output.
d) Evaluation of predicted electropherogram by means of CEval software [40].

University Grant Agency, through grants No. GA UK 726716 and No. GA UK 116217, Czech Republic, by the National Scientific and Technical Research Council (Agencia Nacional de Promoción Científica y Tecnológica – ANPCyT), through grant PICT-2016-0640, and by the National Technological University (Universidad Tecnológica Nacional – UTN), through grant PID ASUT-NFE0004475), Argentina.

The authors have declared no conflict of interest.

5 References

[1] Kohlraush, F., *Ann. Phys.* 1897, *62*, 209–239.

[2] Hruška, V., Gaš, B., *Electrophoresis* 2007, *28*, 3–14.

[3] Hruška, V., Jaroš, M., Gaš, B., *Electrophoresis* 2006, *27*, 984–991.

[4] Breadmore, M. C., Kwan, H. Y., Čáslavská, J., Thormann, W., *Electrophoresis* 2012, *33*, 958–969.

[5] Bercovici, M., Lele, S. K., Santiago, J. G., *J. Chromatogr. A* 2009, *1216*, 1008–1018.

[6] Poppe, H., *J. Chromatogr. A* 1990, *506*, 45–60.

[7] Poppe, H., *Anal. Chem.* 1992, *64*, 1908–1919.

[8] Štědrý, M., Jaroš, M., Gaš, B., *J. Chromatogr. A* 2002, *960*, 187–198.

[9] Štědrý, M., Jaroš, M., Včeláková, K., Gaš, B., *Electrophoresis* 2003, *24*, 536–547.

[10] Štědrý, M., Jaroš, M., Hruška, V., Gaš, B., *Electrophoresis* 2004, *25*, 3071–3079.

[11] Jaroš, M., Hruška, V., Štědrý, M., Zusková, I., Gaš, B., *Electrophoresis* 2004, *25*, 3080–3085.

[12] Hruška, V., Riesová, M., Gaš, B., *Electrophoresis* 2012, *33*, 923–930.

[13] Haarhoff, P. H., Van der Linde, H. J., *Anal. Chem.* 1966, *38*, 573–582.

[14] Dubský, P., Dvořák, M., Müllerová, L., Gaš, B., *Electrophoresis* 2015, *36*, 655–661.

[15] Erny G. L., Bergström, E. T., Goodall, D. M., *Anal. Chem.* 2001, *73*, 4862–4872.

[16] Wren, S. A. C., Rowe, R. C., *J. Chromatogr. A* 1992, *603*, 235–241.

[17] Rawjee, Y. Y., Williams, R. L., Vigh., G., *J. Chromatogr. A* 1993, *652*, 233–245.

[18] Lelièvre, F., Gareil, P., *Anal. Chem.* 1997, *69*, 385–392.

[19] Dubský, P., Svobodová, J., Gaš B., *J. Chromatogr. B* 2008, *875*, 30–34.

[20] Dubský, P., Müllerová, L., Dvořák, M., Gaš B., *J. Chromatogr. A* 2015, *1384*, 142–146.

[21] Hruška, V., Beneš, M., Svobodová, J., Zusková, I., Gaš, B., *Electrophoresis* 2012, *33*, 938–947.

[22] Hruška, V., Svobodová, J., Beneš, M., Gaš, B., *J. Chromatogr. A* 2012, *1267*, 102–108.

[23] Beneš, M., Svobodová, J., Hruška, V., Dvořák, M., Zusková, I., Gaš, B., *J. Chromatogr. A* 2012, *1267*, 109–115.

[24] Dubský P., Dvořák M., Ansorge M., *Anal. Bioanal. Chem.* 2016, *408*, 8623–8641.

[25] Dvořák, M., Dubský, P., Dovhunová, M., Gaš, B., *Electrophoresis*. https://doi.org/10.1002/elps.201800444

[26] Hruška, V., Štědrý, M., Včeláková, K., Lokajová, J., Tesařová, E., Jaroš, M, Gaš, B., *Electrophoresis* 2006, *27*, 4610–4617.

[27] Riesová, M., Hruška, V., Gaš, B., *Electrophoresis* 2012, *33*, 931–937.

[28] Granlund, T., GMP Development Team, GNU MP 6.0 Multiple Precision Arithmetic Library, Samurai Media Limited, Hong Kong 2015.

[29] Fousse, L., Guillaume, H., Lefévre, V., Pélissier, P, Zimmermann, P., *ACM Trans. Math. Softw.* 2007, *33*, 13.

[30] Onsager, L., Fuoss, R.M., *J. Phys. Chem.* 1932, *36*, 2689–2778.

[31] Hirokawa, T., Kiso, Y., *J. Chromatogr.* 1982, *248*, 341–362.

[32] Hirokawa, T., Nishimo, M., Aoki, N., Kiso, Y., Sawamoto, Y., Yagi, T., Akiyama, J., *J. Chromatogr.* 1983, *271*, D1–D106.

[33] Hirokawa, T., Gojo, T., Kiso, Y., *J. Chromatogr.* 1986, *369*, 59–81.

[34] Hirokawa, T., Gojo, T., Kiso, Y., *J. Chromatogr.* 1987, *390*, 201–223.

[35] Hirokawa T., Kiso Y., Gaš B., Zusková I., Vacík J., *J. Chromatogr.* 1993, *628*, 283–308.

[36] Bahga S. S., Bercovici M., Santiago J. G., *Electrophoresis* 2010, *31*, 910–919.

[37] Beneš M., Riesová M., Svobodová J., Tesařová E., Dubský P., Gaš B., *Anal. Chem.* 2013, *85*, 8526–8534.

[38] Riesová M., Svobodová J., Ušelová K., Tošner Z., Zusková I., Gaš B., *J. Chromatogr. A* 2014, *1364*, 276–288.

[39] Lelièvre F., Gareil P., Jardy A., *Anal. Chem.* 1997, *69*, 385–392.

[40] Dubský, P., Ördögová, M., Malý, M., Riesová M., *J. Chromatogr. A* 2016, *1445*, 158–165.

Publication II

Journal of Chromatography A 1610 (2020) 460595

Contents lists available at ScienceDirect

Journal of Chromatography A

journal homepage: www.elsevier.com/locate/chroma

Generalized model of the linear theory of electromigration and its application to electrokinetic chromatography: Capillary zone electrophoretic systems with complex-forming equilibria

Magda Dovhunová[a], Michal Malý[a], Pavel Dubský[a,*], Gabriel S. Gerlero[b], Pablo A. Kler[b,c]

[a] Faculty of Science, Department of Physical and Macromolecular Chemistry, Charles University, Hlavova 8, 128 43, Prague 2, Czech Republic
[b] Centro de Investigación de Métodos Computacionales (CIMEC, UNL-CONICET), Colectora RN 168 Km 472, S3000GLN, Santa Fe, Argentina
[c] Departamento de Ingeniería en Sistemas de Información, FRSF-UTN, Lavaise 610, S3004EWB, Santa Fe, Argentina

ARTICLE INFO

Article history:
Received 7 July 2019
Revised 27 September 2019
Accepted 30 September 2019
Available online 2 October 2019

Keywords:
Elektrokinetic chromatography
Cyclodextrin
Linear theory of electromigration
PeakMaster
Tiselius' equation

ABSTRACT

We discuss several possible phenomena in electrophoretic systems with complexing agents present in the background electrolyte. In our previous work, we extended the linear theory of electromigration with the first-order nonlinear term, which originally applied to acid-base equilibria only, by generalizing it to any fast chemical equilibria. This extension provides us with a fresh insight into the well-established technique of elecktrokinetic chromatography (EKC). We combine mathematical analysis of the generalized model with its solution by means of the new version of our software PeakMaster 6, and experimental data. We re-examine the fundamental equations by Wren and Rowe and Tiselius in the frame of the generalized linear theory of electromigration. Besides, we show that selector concentration can increase inside the interacting-analyte zone due to its complexation with the analyte, which contradicts the generally accepted idea of a consumption of a portion of the selector inside the zone. Next, we focus our discussion on interacting buffers (i.e., buffer constituents that form a complex with the selector). We demonstrate how such side-interaction of the selector with another buffer constituent can influence measuring analyte-selector interactions. Finally, we describe occurrence and mobilities of system peaks in these EKC systems.

We investigate systems with fully charged analytes and neutral cyclodextrins as selectors. Although the theory is not limited in terms of the charge and/or the degree of (de)protonation of any constituent, this setup allows us to find analytical solutions to generalized model under approximate, yet realistic, conditions and to demonstrate all important phenomena that may occur in EKC systems. An occurrence of system peaks in a system with fully charged selector is also investigated.

1. Introduction

Electrokinetic chromatography (EKC) is a widely used method involving a capillary zone electrophoresis (CZE) setup and complexing agents (selectors), such as micelles, cyclodextrins or crown-ethers [1–3]. The interaction between selector and analyte leads to the formation of a complex approximately as large as the selector (usually much larger than the analyte). This complex can also bear charge different from the charge of the analyte, if the selector is not a neutral compound. Due to changes in these properties, the analyte effective electrophoretic mobility also changes, thereby making it possible to separate neutral compounds or enantiomers, which would otherwise be inseparable in common CZE mode [3,4].

Analyte effective electrophoretic mobility in EKC can be described using a mathematical model first introduced by Wren and Rowe [5]. The original model is limited to 1:1 stoichiometry. Even though not every complex-forming equilibria will follow this stoichiometry, 1:1 is the preferred stoichiometry of many selector–analyte complexes, especially cyclodextrin complexes [6,7]. If this condition is fulfilled, the analyte-selector equilibrium is described as

$$A + S \rightleftharpoons AS, K'_{AS} = \frac{c_{(AS)}}{c_{(A)}c_{(S)}} \quad (1)$$

where $c_{(A)}$, $c_{(S)}$ and $c_{(AS)}$ represent the free analyte, the free selector and the analyte–selector complex concentrations in the solution, respectively, and K'_{AS} is the apparent complexation constant.

* Corresponding author at: Mgr. Pavel Dubský, Charles University, Faculty of Science, Albertov 6, CZ-128 43, Prague 2, Czech Republic.
E-mail address: pavel.dubsky@natur.cuni.cz (P. Dubský).

https://doi.org/10.1016/j.chroma.2019.460595
0021-9673/

If we accept the following approximation for the concentration of the free (uncomplexed) selector $c_{(S)}$,

$$c_{(S)} = C_S \tag{2}$$

where C_S represents the total (analytical) selector concentration, apparent complexation constant becomes approximately equal to

$$c_{(S)} \to C_S: \; K'_{AS} = \frac{c_{(AS)}}{c_{(A)}C_S} \tag{3}$$

This assumption is fulfilled if the selector is present in a sufficient excess over the analyte so that the amount of the selector captured in the complex, $c_{(AS)}$, is negligible to its total amount, C_S. Then, the effective electrophoretic mobility of the analyte can be expressed as published by Wren and Rowe [5],

$$\mu_{\text{eff}.A} = \frac{\mu_{(A)} + \mu_{(AS)}K'_{AS}C_S}{1 + K'_{AS}C_S} \tag{4}$$

where $\mu_{(A)}$ and $\mu_{(AS)}$ are the respective mobilities (we use signed mobilities, i.e., positive for cations and negative for anions, throughout this paper). However, this model is limited to the interaction between one analyte and one selector only, and it does not include acid-base equilibria. In 1993, this model was extended to monovalent weak acidic and basic analytes by Rawjee, Williams and Vigh [8,9], and the overall model for multiple complexation was introduced by Dubský et al. in 2015 [10].

In general CZE (without complexation), a linear theory of electromigration (LTEM) [11–15] has succeeded in predicting the fundamental properties of the separation system, namely development (expected mobilities and composition) of system zones (zones unrelated to any analyte in the sample) and analyte zones. The calculation was implemented into PeakMaster software [16] for convenient usage by the wide electrophoretic community. The theory was later advanced with a first-order non-linear term, resulting in the first-order nonlinear approximation to the linear theory of electromigration (NLTEM) [17]. NLTEM added to LTEM information on distribution (shapes) of the system and analyte zones [18] and was implemented into the next version of PeakMaster, PeakMaster 5.3 [17]. Since LTEM is naturally included in NLTEM, we do not distinguish between the two in our discussion and use the single acronym NLTEM throughout this paper.

NLTEM was later also extended to specific complex-forming equilibria [19]. The extension enabled evaluation of characteristics that describe concentration distribution (shape) of analyte peak, provided that one neutral/charged complexing agent forms a complex with charged/neutral analyte. The calculation was based on the original NLTEM model (without complexation) and, as such, neglected complexation equilibria between the selector and other BGE constituents and was not further extendable to more general EKC systems. However, it helped in understanding how complexation can cause electromigration dispersion (EMD) of the analyte peak, even when using a neutral selector [20], and the calculation was implemented into PeakMaster 5.3 Complex [19]. Besides the effects the complexation can cause to the analyte peak, interactions between the selector and other background electrolyte (BGE) components may substantially affect the BGE properties, e.g. pH [21]. Thus, other BGE properties, such as ionic strength or conductivity, will also be affected. Additionally, complexation with BGE components may cause changes in the mobility of system peaks [22]. However, these effects have not been further studied since.

Analyte and system peak electrophoretic mobilities in CZE depend not only on physical-chemical properties of constituents but also on ionic strength (IS) and Joule heating effects. From its early versions, PeakMaster software applies ionic effects corrections to its input parameters. By default, PeakMaster uses true thermodynamic pKa constants and limiting mobilities as input parameters. Once the equilibrium composition of the solution is calculated, pKa constants are corrected for ionic strength using the Debye-Hückel law [23,24]. Since the equilibrium composition, IS, and the apparent pKa values are mutually dependent, the whole procedure is performed iteratively until IS of the buffer levels out. IS-corrected equilibrium composition of the solution is then used to calculate actual ionic mobilities using the Onsager-Fuoss model [25]. In PM 6, the Debye-Hückel correction also applies to the complexation constants. Alternatively, apparent pKa constants and ionic mobilities, determined for the given buffer, can be entered and the ionic effects corrections can be switched off.

Corrections to Joule heating are not implemented in PM software. In contrast to IS, Joule heating is considered as an external effect not related to the chemical composition of the system. Such correction would require an assessment of the inner temperature in the capillary [26,27], which makes its algoritmization particularly difficult. Next, both electrophoretic mobilities and pKa and complexation constants must be adjusted to the given temperature. 2% mobility increase per 1 °C can serve as an approximate correction factor to the electrophoretic mobilities. Correction of pKa constants and complexation constants is not so straightforward since it would require a large number of experiments for the determination of the corresponding thermodynamic functions. Thus, the input parameters for PM must be always provided at the given temperature (25 °C by default) and the temperature should be well controlled by performing the experiment under low currents (power) or via the rational cooling adjustment strategy [27,28].

Another approach to studying EKC is using numerical simulations. Only few papers have been dedicated to simulation software that includes 1:1 complex-forming equilibria, such as Gentrans [29,30] or Simul [31]. Both of these were extended with algorithms that describe 1:1 chemical equilibria between solutes and a buffer additive, even micelles in case of GENTRANS [32]. In this paper, we use numerical simulations from Simul 5 Complex for verification of the presented data.

In our previous paper [33], we have introduced the generalized NLTEM model. This model was implemented in the new generation of PeakMaster software–PeakMaster 6 (PM 6) [33]. In contrast to the simulation software, PeakMaster calculation is based on matrix algebra and the solution to the problem is obtained within few seconds. On the other hand, it is essentially limited to CZE setup with a narrow zone of sample injected into the otherwise homogeneous BGE. The generalized NLTEM model enables us to draw theoretical considerations about the way the selector and the analyte and/or other BGE constituents influence each other in EKC for the first time. Leaving the more complex systems for future investigations, the aim of this paper is to describe the behavior of typical complexing electrophoretic systems. First, we show the effect of complex-forming equilibria on the analyte zone – both in BGE where none of the components interacts with the selector (non-interacting BGE) and in BGE where at least one of the components forms a complex (interacting BGE). Second, we discuss the effect of complexation in the interacting BGE on the system peaks. PM 6 calculations presented in this study are supported with experimental data and with numerical simulations.

2. Experimental section

2.1. Chemicals

All chemicals were of analytical grade purity. Lithium hydroxide monohydrate was purchased from Fluka (Steinheim, Germany). [Tris(hydroxymethyl)methyl]glycine (tricine), N-cyclohexyl-2-aminoethanesulfonic acid (CHES), benzoic acid, acetic acid, (*R*)-(−)-2fluoro-α-methyl-4-biphenylacetic acid (R-flurbiprofen, R-FLU),

S,S-hydrobenzoin (HB), dimethylsulfoxide (DMSO) and β-cyclodextrin (β-CD) were purchased from Sigma Aldrich (Steinheim, Germany). 6-monodeoxy-6-mono(3–hydroxy)propylamino-β-CD chloride (PA-β-CD) was obtained from CycloLab (Budapest, Hungary). 6-monoaminophenyl-β-cyclodextrin (MAPH-β-CD) was purchased from Cyclodextrin-Shop (Tilburg, Netherlands). Water for solution preparation was deionized using the Watrex Ultrapur system (Prague, Czech Republic).

2.2. Instrumentation

CE experiments were performed using the Agilent ^{3D}CE capillary electrophoresis instrument operated by ChemStation software from Agilent Technologies (Waldbronn, Germany). Detection was performed with the built-in diode array detector (DAD) and the contactless conductivity detector (CCD). Uncoated fused silica capillaries with an i.d. of 50 μm and an o.d. of 375 μm (Polymicro Technologies, Phoenix, AZ) were used for all electrophoretic experiments. CE measurements were performed at 25 °C, and the samples were injected hydrodynamically (individual injection conditions are reported for each set of experiments below). A new capillary was flushed with deionized water for 20 min and conditioned with actual running buffer before each run. All running buffers were filtered with 0.45-μm Minisart syringe filters (Sartorius Stedim Biotech, Goettingen, Germany). The PHM240 pH/ion meter (Radiometer, Copenhagen, Denmark) calibrated with standard IUPAC buffers, pH 1.679, pH 7.000, pH 10.012, and pH 12.450 (Radiometer Analytical, Lyon, France) was used for pH measurements.

2.2.1. Neutral selector interacting with the analyte only / with analyte and one BGE component (analyte part)

These experimental data were retrieved from our previous paper [22]. In the cited study, the selector β-CD, 0 – 10 mM concentration range, was dissolved directly in running buffers. Tricine/Li, 10.0/5.15 mM, running buffer was used as the buffer not interacting with the cyclodextrin. CHES/Li, 10.0/5.15 mM, running buffer was used as the buffer interacting with the cyclodextrin. The injected sample was 0.3 mM R-FLU and 0.15% DMSO. The samples were injected hydrodynamically at 100 mbar × s. The total capillary length (L_{tot}) and the length to DAD (L_{det}) were 49.75 and 41.25 cm, respectively. The applied voltage was 20 kV (cathode at the detector side).

2.2.2. The cyclodextrin package

The BGE of the model system contained 5.0 mM LiOH, IS 4.96 mM, pH 11.70. MAPH-β-CD was dissolved directly in running buffer in a concentration range of 0 – 3 mM. Samples contained 1.0 mM CHES, 2.5 mM LiOH and MAPH-β-CD at half the concentration of BGE dissolved in water. The composition of the sample was again designed by PeakMaster 6 to obtain sufficient amplitude of the cyclodextrin peak.

The samples were injected hydrodynamically at 80,150 mbar × s. The Ltot and Ldet were 48.9 51.2 and 40.442.7 cm, respectively. The driving voltage was 105 kV (cathode at the detector site). UV detection of the cyclodextrin package was performed by DAD at a wavelength of 245 nm.

2.2.3. Selector interacting with the analyte and with one BGE component (system peaks part)

The BGE of the model system contained 5.0 mM benzoic acid and 3.0 mM LiOH, IS 3.04 mM, pH 4.39. β-CD was dissolved directly in running buffer at a concentration range of 0 – 10 mM. Samples contained neither analyte nor EOF marker; only disturbed BGE was injected to generate system peaks. The compositions of the disturbances at the particular β-CD concentration are summarized in Table S1 (Supplementary material). They were designed by PM 6 to obtain convenient shapes, polarities, and amplitudes of system peaks.

The samples were injected hydrodynamically at 15 mbar × s. The L_{tot} and L_{det} were 79.2 and 70.7 cm, respectively. The driving voltage was 20 kV (cathode at the detector site). Indirect UV detection of system zones was performed by DAD at a wavelength of 200 nm.

The BGE of the second model system consisted of 30.0 mM acetic acid, 15.0 mM LiOH, 0.3 HB and 25 mM PA-β-CD · HCl, IS 40.02 mM, pH = 4.61. Samples contained neither analyte nor EOF marker; only disturbed BGE (30 mM acetic acid and 15 mM LiOH) was injected to generate system peaks.

The samples were injected hydrodynamically at 15,350 mbar × s. The Ltot and Ldet were 79.249.7 and 70.741.2 cm, respectively. The driving voltage was 20 kV (cathode at the detector site). Indirect detection of system zones was performed by CCD and DAD at a wavelength of 214 nm.

2.3. Software

Wolfram Mathematica 11 (Wolfram Research, Inc.) was used for symbolic calculations. PM 6 [33] was used for full NLTEM solution and generation of predicted electropherograms. Numerical simulations were run in a novel in-development computational core of Simul software (based on our original Simul 5 Complex [31]). The programs CEval [34], Origin 2018 (OriginLab Corporation, Northampton, MA) and Microsoft Office Excel 2017 were used for data evaluation. Our software CEval, Simul 5 Complex and PeakMaster 6 are available for free at https://echmet.natur.cuni.cz/software/download.

3. Results & discussion

The NLTEM model leads to a matrix eigenvalue problem. A specific matrix called mobility matrix, $\mathbf{M_0}$, is constructed as a product of a migration matrix and a communication matrix. While the migration matrix encodes electromigration properties of all the constituents in the given system, the communication matrix describes equilibrium interactions of constituents that make up the system. Specifically, the communication matrix describes how a change of concentration of one constituent affects the overall distribution of ionic and complex forms in the system. Eigenvalues of the final mobility matrix, $\mathbf{M_0}$, represent electrophoretic mobilities of all zones (both analyte and system zones) that occur in the given system. The NLTEM model and how it was derived is described in detail in our previous paper [33]. In [33] we have also shown how the interactions among constituents can be extended beyond the acid-base equilibria covered by the previous theory. The NLTEM model implemented in PeakMaster 6 software makes use of this extension by considering both acid-base and complex-forming equilibria.

We use NLTEM to investigate a series of common CZE systems that involve complex-forming interaction. In the article we always show only the resulting eigenvalues of the mobility matrix that describes a particular model system. More detailed derivation of the mobility matrices is available in Supplementary material.

3.1. Selector interacting with analyte only

3.1.1. Analytical solution

Analytical solution to the eigenvalues of the mobility matrix, $\mathbf{M_0}$, can be found only under some simplifications. Štědrý et al. adopted a strategy of neglecting the presence of water ions, H_3O^+ and OH^-, if the system consists of solely strong electrolytes in their seminal paper on NLTEM (LTEM precisely here) [12]. Considering a presence of strong BGE ion X, strong BGE counter-ion Y and a strong electrolyte analyte A, the eignevalues resulted as

$\lambda(\mathbf{M}_0) = \{0; 0; \mu_{(A)}\}$. Notice that the number of eigenvalues matches that of the constituents (X, Y, A) present in the system, which is the rule of thumb introduced within (N)LTEM. The two zero eigenvalues, which correspond to the mobilities of system peaks, suggest that only a stationary zone can exist in such systems. The third eigenvalue is the mobility of the analyte.

In the following model system, we further let a neutral selector (S) form a complex (AS) with the strong electrolyte analyte (A) (with 1:1 stoichiometry). This interaction is described by the complexation constant K'_{AS}, Eq. (1). Taking the same assumption of neglecting the presence of the water ions, so that the complexation is the only equilibrium that takes place in the system, and applying the assumption of the selector in excess, Eq. (3), eigenvalues of a mobility matrix, $\mathbf{M}_{0[AS]}$, result from the generalized NLTEM as:

$$\lambda\left(\mathbf{M}_{0[AS]}\right) = \left\{0; 0; 0; \frac{\mu_{(A)} + C_S K'_{AS}\mu_{(AS)}}{1 + C_S K'_{AS}}\right\}.$$

Detailed mathematical derivation can be found in Supplementary material. The subscript [*AS*] denotes that we treat the system of an analyte interacting with a selector. The number of the eigenvalues is in line with the general expectation that the number of peaks (both system and analyte peaks) should match the number of constituents. The constituents are X, Y, A, and S, the selector, in our example. Notice that the complex AS is not a separate constituent but it is rather a form of the analyte and selector constituents. Thus its presence does not contribute to the number of eigenvalues (zones) in EKC systems, yet it influences their values (mobilities of peaks).

Two of the system peaks with the zero mobility are those as expected in systems with exclusively strong electrolytes. The third system peak has also zero mobility. This corresponds to the selector *S* be a neutral compound added to the BGE. The fourth eigenvalue prescribes the mobility of the analyte zone and it matches exactly the formula for the effective electrophoretic mobility as derived by Wren and Rowe, Eq. (4).

3.1.2. Tiselius' equation

The previous paragraph illustrates how the effective mobility of an analyte in the environment of the given BGE results from the analysis of the eigenvalues of the mobility matrix, $\mathbf{M}_0$. The general formula for the effective mobility of the analyte was indeed published by Tiselius already in 1930 [35]. Provided that the chemical equilibria among various forms of a chemical species *A* is established in much shorter time than is the characteristic time of the separation process, the effective mobility of the species *A* equals,

$$\mu_{\text{eff, }A} = \sum_{(h)\in\omega_A} \alpha_{(h)A}\mu_{(h)} \tag{5}$$

where ω_A is a set of all forms of the constituent *A* and $\alpha_{(h)A}$ are molar fractions of the form (h) with respect to the total (analytical) concentration of the constituent *A* (cf. Supplementary material). Tiselius introduced Eq. (5) in the context of acid-base equilibria, albeit it has been taken for granted in complexation as well as mixed complexation/acid-base systems [2] later on. Specifically, Wren and Rowe derived their equation, Eq. (4), based on Tiselius's equation, Eq. (5). The degree of complexation, i.e., the values of $\alpha_{(h)A}$ for the free and the complexed form of the analyte, is governed by Eq. (1). However an unknown concentration of the free selector, $c_{(S)}$, inside the zone of the travelling peak appears in Eq. (1). Thus applicability of Wren and Rowe's equation, Eq. (4), and all its variants for mixtures of selectors and coupled acid-base equilibria is typically considered as limited to a sufficient excess of the selector, when its consumption by the complexation equilibrium is presumably negligible, and Eqs. (2) and (3) apply. The same result is observed in NLTEM as demonstrated in the previous section. Some authors tried to calculate the free amount of the selector, $c_{(S)}$, in the sample zone in an attempt to compensate for the selector consumption in Eq. (4) [36–38]. On the other hand, we argued [2] that the consumption of the free selector in the analyte zone by the complexation equilibrium should result in a peak deformation rather than affecting its effective electrophoretic mobility, $\mu_{\text{eff},A}$. This latter opinion was also supported by an experimental evidence [20,39], though no theory was available that could prove one or the other hypothesis.

The structure of (generalized) NLTEM matrices allows us to clarify the original Tiselius' equation (see Supplementary material) and express it in a form of

$$\mu_{\text{eff, }A} = \sum_{(h)\in\omega_A} \alpha^0_{(h)A}\mu_{(h)} \tag{6}$$

where $\alpha^0_{(h)A} = \lim_{C_A\to 0} \alpha_{(h)A}$. This number, Eq. (6), becomes one of the eigenvalues of the matrix $\mathbf{M}_0$, and describes the effective electrophoretic mobility of the peak of the analyte. We did not need to make any assumptions about the nature of the equilibria on the way to Eq. (6). The derivation has general applicability to any CZE/EKC system, as far as 1:1 complexation stoichiometry between an analyte and a selector is obeyed. It follows that the equation needs further refinement for other complexation stoichiometry, which however goes beyond the scope of this paper.

Comparison between Eqs. (5) and (6) reveals that Tiselius' equation, Eq. (5), results from the generalized NLTEM model, yet with an amendment that the molar fractions of the individual forms (with respect to the given analyte) should be evaluated at the limit of $C_A \to 0$. Consequently, the total (analytical) concentration of the selector should be always supplied into Wren and Rowe's (and similar) equation(s). We discuss elsewhere [40] that from the experimental perspective, this effective mobility is observed through fitting analyte's peak by the HVL function distribution profile and reading the so-called a_1 parameter from the fit [40]. Any nonlinear curve fitting software or our automated tool CEval [34], can be used for this purpose.

3.1.3. Consequences for data evaluation

For the experimental verification, we used a BGE consisting of 10 mM tricine and 5.15 mM lithium (pH = 8.14). β-CD was used as the selector and R-FLU as the analyte. Flurbiprofen is a weak acid that is fully dissociated at the given pH. Fig. 1 shows variations of R-FLU effective electrophoretic mobility, $\mu_{\text{eff, }A}$, as a function of β-CD concentration. Effective electrophoretic mobilities were evaluated from experimental peaks by CEval software [34]. Experimental data (black triangles) were fitted with the classical Wren and Rowe's equation, Eq. (4), (green solid line). The complexation parameters as resulted from the fit are: $\mu_{\text{R-FLU}} = -(22.18 \pm 0.15)\cdot 10^{-9}$ m^2 s^{-1} V^{-1}, $\mu_{(\text{R-FLU-}\beta\text{-CD})} = -(9.95 \pm 0.09)\cdot 10^{-9}$ m^2 s^{-1} V^{-1} and $K'_{(\text{R-FLU-}\beta\text{-CD})} = 4700 \pm 231$ M^{-1}. These parameters are apparent, valid for the given experiment, albeit they are in accordance with our previous measurements [22].

The parameters were supplied to a PM 6 calculation. No correction for ionic strength was chosen because the complexation parameters used as input data are already measured at the actual ionic strength. The viscosity correction was not used either in order to make the PM 6 calculation comparable with the analytical solution (the influence of the viscosity is practically imperceptible for low selector concentrations [41]). PM 6 numerically solves all equilibria in the system, constructs the electromigration and the communication matrices, evaluates the mobility matrix $\mathbf{M}_0$ at the composition of the BGE and reports the obtained eigenvalues as mobilities of system and analyte peaks. Notice that PM 6 does not apply any of the approximations that we adopted in order to observe the analytical solution to the equations (i.e., it does not need the constituents to be strong electrolytes and it does account for

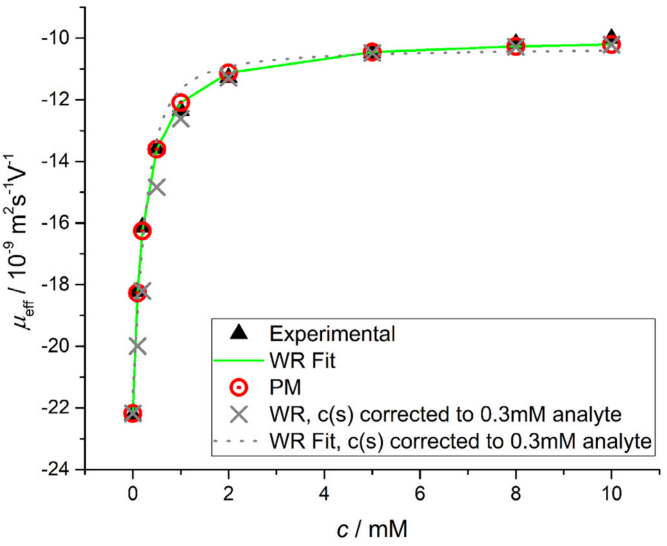

Fig. 1. Variations of R-FLU effective electrophoretic mobility as a function of β-CD concentration in Tricine/Li buffer (non-interacting). "Experimental" (black triangles): experimental data; "WR Fit" (green solid line): data fitting with Eq. (4); PM (red circles): PM 6 calculation with parameters obtained from "WR Fit"; "WR, c(s) corrected to 0.3 mM analyte" (gray crosses): calculation according to Eq. (4), when the total concentration of the selector, $\boldsymbol{c_S}$, is replaced with a concentration of the free selector, $\boldsymbol{c_{(S)}}$, assuming interaction of the selector with 0.3 mM of the analyte; "WR Fit, c(s) corrected to 0.3 mM analyte" (gray dashed line): data fitting with Eq. (4) when the total concentration of the selector, $\boldsymbol{c_S}$, is replaced with the concentration of the free selector, $\boldsymbol{c_{(S)}}$.

autoprotolyzis of water, cf. Section 3.1.1 Analytical solution). The resulting effective electrophoretic mobilities are plotted for the analyte with red circles in Fig. 1. The PM 6 calculation follows the green curve of the classical Wren and Rowe's equation exactly.

In the next step, we adapted Wren and Rowe's equation to take the free amount of the selector, $c_{(S)}$, instead of the total amount, C_S, into account. The free selector concentration, $c_{(S)}$, was calculated assuming consumption of the total portion of the selector, C_S, by its interaction with 0.3 mM of the analyte (the injected amount). First, we calculated effective electrophoretic mobilities of the analyte that would result from the adapted Wren and Rowe's equation using the complexation parameters obtained from the original fit. The resulting values are depicted with gray crosses in Fig. 1. The values differ significantly from the effective electrophoretic mobilities resulting from the NLTEM theory, i.e., the PM 6 calculation, at low C_S concentrations. This calculation illustrates that eigenvalues of the matrix $\mathbf{M}_0$ do certainly not depend on the selector consumption by the analyte. Finally, we subjected the experimental data to nonlinear fitting by the adapted Wren and Rowe's equation. The best fit is depicted with gray dashed line in Fig. 1. The original fit, which does not compensate for the selector consumption (the green solid line), reflects the curvature of the experimental data visibly better.

3.1.4. Cyclodextrin package

The complete NLTEM model provides information of not only mobilities of system and analyte zones but also their composition. It results, in direct contradiction with any attempt to compensate for the low selector concentration, as discussed above, that the amount of the selector inside the analyte zone can actually increase due to complexation. This is caused by the fact that the selector is mobilized by the interaction with the analyte. Thus the analyte takes a portion of the selector along its path through the separation system. Since measured with cyclodextrin as the selector, we call this phenomenon a cyclodextrin package. This effect was addressed already by Poppe in 1999 [42], and was independently observed experimentally by online-NMR detection by Almeide and Larive in 2005 [43]. Yet, it was not further investigated by any theoretical or systematic experimental study, likely since the theory was not available until now, and because most selectors only absorb around 200 nm, and their absorbance usually interferes with analyte absorbance (while online NMR detection is not commonly available setup).

To observe the selector profile during the measurements, we purchased a mono-derivatized β-cyclodextrin with a chromofore. This monoaminophenyl-β-cyclodextrin (MAPH-β-CD) has UV/VIS spectra with maxima at 200, 245 and 290 nm. Our model system consisted of CHES at pH 11.44 (5 mM LiOH) as a negatively charged analyte and of neutral MAPH-β-CD as a selector. The following complexation parameters of the charged form of CHES were measured: $K'_{(\mathrm{CHES-MAPH\text{-}\beta\text{-}CD})^-} = 1200 \pm 200\ M^{-1}$ and $\mu_{(\mathrm{CHES-MAPH\text{-}\beta\text{-}CD})^-} = -(10.6 \pm 0.1) \cdot 10^{-9}\ \mathrm{m^2 s^{-1} V^{-1}}$. The effective electrophoretic mobility of CHES at the actual ionic strength (4.96 mM) is $\mu_{\mathrm{CHES}} = -(19.7 \pm 0.1) \cdot 10^{-9}\ \mathrm{m^2\ s^{-1}\ V^{-1}}$. The complexation constant of the neutral form is unknown, but it does not affect the calculation in any way because the analyte is fully charged at this pH. A calibration curve of the MAPH-β-CD absorbance response as a function of MAPH-β-CD concentration was measured at 245 nm. According to this calibration, the experimental electropherogram was replotted in terms of concentration scale, which allowed us to directly compare the concentration values inside the cyclodextrin package.

Fig. 2 shows the comparison between the concentration-scaled experimental electropherogram at 245 nm and the MAPH-β-CD concentration profile from PM 6. The peak on the right corresponds to the analyte zone, showing the cyclodextrin package – the increased amount of the selector inside the analyte zone. The cyclodextrin package is compensated by the corresponding decrease of concentration of cyclodextrin inside the stationary system peak. There is a nearly perfect agreement with the PM 6 electropherogram, especially in terms of peak height. The experimental peak only exhibits a slightly more diffusive front boundary. For the system peak, the agreement is not as good. However, the behavior of the system zones with zero electrophoretic mobility value in CZE is questionable, and other effects may affect the cyclodextrin profile, such as partial dissociation of the cyclodextrin OH^- groups or its interaction with the capillary wall (notice the baseline profile behind the system peak). Nevertheless, such hypotheses would require further investigation. This experiment aimed at the

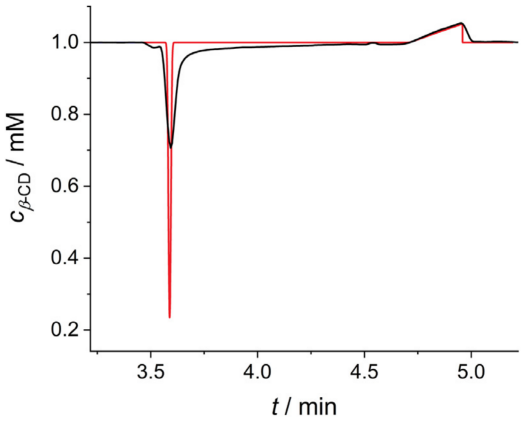

Fig. 2. Experimental electropherogram (black) recalculated to the concentration scale according to the measured calibration curve (245 nm) compared with the PM 6 electropherogram (red). The concentration profile of MAPH-β-CD shows the zero system peak (left) and the cyclodextrin package in the analyte zone (right). BGE consisted of 5 mM LiOH and 1 mM MAPH-β-CD, with 1 mM CHES as the analyte. L_{tot} = 48.9 cm, L_{det} = 40.4 cm, id = 50 µm. Injection zone 1.38 mm, voltage +10 kV.

cyclodextrin package, which was successfully confirmed, and further examination of the cyclodextrin distribution along the capillary goes beyond our primary intention. We rather leave the observed disagreement between the profile of the stationary system zone and its PM 6 prediction as an example of the limitations of the ideal model.

3.2. Selector interacting with the analyte and with a BGE constituent

We continue with an example of two complex-forming equilibria, when the selector interacts not only with an analyte but also with another BGE constituent. Complexation with the analyte is described by complexation constant K'_{AS}, Eq. (1), and complexation with the BGE constituent is described by complexation constant K'_{XS}. The complexed form of the selector (XS) also participates in the conductivity term and the electroneutrality condition, even though the selector is neutral. This leads to a rather complicated structure of the final mobility matrix, $\mathbf{M}_0$. We provide the structures of the matrices in Supplementary material.

3.2.1. Analyte

Eq. (6), along with its derivation in Supplementary material, tells us that the effective electrophoretic mobility of the analyte is governed by its molar fractions (with respect to the total amount of the analyte) in the BGE when $C_A \to 0$, regardless of the actual structure of the final mobility matrix, $\mathbf{M}_0$. The limit $C_A \to 0$ signifies that we should first calculate the equilibrium composition of all forms in the BGE (without the presence of any analyte). Then, we supply concentrations of these individual forms into equations governing their interaction with the analyte as constants, unaffected by the presence of the analyte. This situation is identical to that of deliberating, e.g., the degree of dissociation of a weak acidic analyte in a BGE of a given pH, and it considerably simplifies the process of derivation of the effective electrophoretic mobility of the analyte.

Interaction of the analyte with the selector is governed by Eq. (1). When no interaction between the selector an another BGE constituent existed (Section 3.1), the limit $C_A \to 0$ implied $c_{(S)} \to C_S$. This allowed us to supply the total concentration of the selector into Eq. (1), and subsequently arrive at Wren and Rowwe's Eq. (4). When the selector interacts with a BGE constituent, the same reasoning involves,

$$C_A \to 0: \; c_{(S)} \to c_{(S)}^{\mathrm{BGE}} = \left[\frac{1}{2}\left(\frac{\sqrt{\left(K'_{XS}C_X - K'_{XS}C_S - 1\right)^2 + 4K'_{XS}C_X} - 1}{K'_{XS}C_S} - \frac{C_X}{C_S} + 1\right)\right] C_S \quad (7)$$

where $c_{(S)}^{\mathrm{BGE}}$ is the equilibrium concentration of the free form of the selector in the BGE. When plugging $c_{(S)}^{\mathrm{BGE}}$ instead of C_S into the original Wren and Rowe's formula, the resulting equation represents the electrophoretic mobility of the analyte in a system in which the selector interacts both with a BGE constituent and with the analyte. Based on the exact values of C_X and K'_{XS}, the variation of analyte effective electrophoretic mobility as a function of C_S, using Eq. (7) in Eq. (4), may look either like an S-shaped curve or a hyperbola.

It can be easily seen that the term in the square brackets in Eq. (7) takes a role of a "correction factor" of the complexation constant K'_{AS} when supplied into Wren and Rowe's equation. This factor itself, however, changes with varying the concentration of the selector, C_S. It attains values from $(1 + K'_{XS}C_X)^{-1}$ to 1, at $C_S \to 0$ and $C_S \to \infty$, respectively. These limits show that the modified Wren and Rowe's curve coalesces with the original Wren and Rowe's curve (as if no selector-BGE interaction occurred) at high C_S concentrations where $\mu_{\mathrm{eff},A}$ approaches the value of $\mu_{(AS)}$. On the other hand, the modified curve differs from the original one at low to middle-range selector concentrations, where it can be a source of error when affinity constants are determined in interfering buffers. We plotted these curves for a large number of combinations of C_X and K'_{XS} values (data not shown). The hyperbolic shape was more commonly found over the S-shaped curve. Thus, the systematic error in the complexation constant K'_{AS} may be very difficult to discover from the electrophoretic mobility function alone because the experimental data can still be fitted with the hyperbolic (Wren and Rowe's – like) formula to an extent good enough to mistake any visible imperfections for a mere random experimental error.

For experimental verification, we used a system consisting of CHES/Li (10/5.15 mM) buffer, β-CD as selector and R-FLU as analyte. PM 6 calculation requires the complexation parameters for CHES measured at the actual ionic strength (5.15 mM), which we retrieved from our previous paper [21], and are: $\mu_{\mathrm{CHES}} = -22.23 \cdot 10^{-9}$ m^2 s^{-1} V^{-1}, $\mu_{(\mathrm{CHES}\text{-}\beta\text{-}\mathrm{CD})^-} = -(7.9 \pm 0.2) \cdot 10^{-9}$ m^2 s^{-1} V^{-1}, $K'_{(\mathrm{CHES}\text{-}\beta\text{-}\mathrm{CD})^-} = 460 \pm 10$ M^{-1} and $K'_{\mathrm{CHES}\text{-}\beta\text{-}\mathrm{CD}} \sim 30$ M^{-1}. Since Eq. (7) is based on Wren and Rowe's formula, only fully charged components are considered. In our case, the charged form of CHES has a significantly higher complexation constant; thus, we only consider the complexation with this form in Eq. (7) and PM 6 calculations and ignore the complexation with the neutral form. We also assume that the acid-base equilibria are not affected by the ongoing complexation equilibria in the BGE in the case of Eq. (7) (PM 6 calculation inevitably covers this effect). Thus the equilibrium concentration of CHES anion at the given pH of the BGE, $c_{(X^-)} = 5.11$ mM, is supplied for C_X into Eq. (7).

The results are presented in Fig. 3. Effective mobilities were evaluated from the electropherograms by CEval software [34]. Experimental data (black triangles) were fitted with the modified Wren and Rowe's equation, Eq. (4) with $C_S \equiv c_{(S)}^{BGE}$, Eq. (7), (green solid line). The complexation parameters as resulted from the fit are: $\mu_{\mathrm{R\text{-}FLU}} = -(22.90 \pm 0.09) \cdot 10^{-9}$ m^2 s^{-1} V^{-1}, $\mu_{(\mathrm{R\text{-}FLU}\text{-}\beta\text{-}\mathrm{CD})} = -(10.45 \pm 0.07) \cdot 10^{-9}$ m^2 s^{-1} V^{-1} and $K'_{(\mathrm{R\text{-}FLU}\text{-}\beta\text{-}\mathrm{CD})^-} = 5170 \pm 180$ M^{-1}. These parameters are apparent, valid for the given experiment only, albeit they are in accordance with that obtained in the non-interacting buffer (Section 3.1.3 and ref. [22]). The parameters were supplied to PM 6 calculation. No

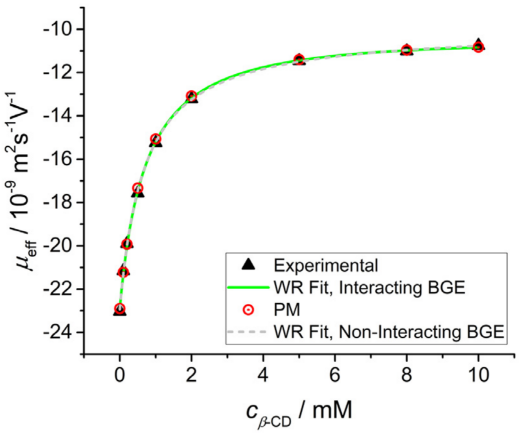

Fig. 3. Variation of R-FLU effective electrophoretic mobility as a function of β-CD concentration, in CHES/Li buffer (interacting); "Experimental" (black triangles): experimental data, "WR Fit, Interacting BGE" (green solid line): data fitting with Eq. (4), when the total concentration of the selector, C_S, is replaced with a concentration of the free selector in the BGE, $c_{(S)}^{\mathrm{BGE}}$, Eq. (7); "WR Fit, Non-Interacting BGE" (gray dashed line): data fitting with Eq. (4).

correction for ionic strength was chosen because the complexation parameters used as input data are already measured at the actual ionic strength. The viscosity correction was not used either in order to make the PM 6 calculation comparable with the analytical solution (the influence of the viscosity is practically imperceptible for low selector concentrations [41]). The resulting effective mobilities are plotted for the analyte with red circles in Fig. 3. The PM 6 calculation confirms that the modified Wren and Rowe's equation is in exact agreement with the full numerical NLTEM solution (as performed by PM 6).

Finally, we subjected the experimental data to nonlinear fitting by the original Wren and Rowe's equation. The best fit is depicted with gray dashed line in Fig. 3, and the resulting parameters are: $\mu_{\text{R-FLU}} = -(22.93 \pm 0.08) \cdot 10^{-9}$ m^2 s^{-1} V^{-1}, $\mu_{(\text{R-FLU-}\beta\text{-CD})} = -(9.93 \pm 0.08) \cdot 10^{-9}$ m^2 s^{-1} V^{-1} and $K'_{(\text{R-FLU-}\beta\text{-CD})^-} = 1460 \pm 40$ M^{-1}. The complexation constant becomes significantly biased compared to the values previously obtained in the non-interacting buffer (Section 3.1.3 and ref. [21]), in spite of the fact that the goodness of fit is indistinguishable for the two curves, the modified (correct) and the original (not correct) Wren and Rowe's equation. In contrast to the complexation constant, both fits yield practically the same values of mobilities of the free analyte and the analyte-selector complex. This confirms our theoretical discussion outlined above.

3.2.2. System peaks

The behavior of system peaks in interacting electrolytes has been previously observed and compared with simulations [22], but not described theoretically until now. The generalized NLTEM model allows us to find an analytical solution to mobilities of system peaks in BGEs composed of two strong electrolyte constituents (an ion and a counter-ion) and a neutral selector that interacts with one of these constituents. We provide the structure of the underlying matrices in Supplementary material. It results that out of the three stationary system peaks (cf. Section 3.1.1), one of the system peaks becomes mobilized: $\lambda(\mathbf{M}_{0[\boldsymbol{AS},\boldsymbol{XS}]}) = \{0; 0; \mu_{\text{eff},A}; \mu_{sys}\}$, where the subscript [*AS, XS*] indicates interaction of the selector with both analyte and BGE ion constituents, $\mu_{\text{eff, }A}$ is the effective electrophoretic mobility of the analyte as discussed earlier (Section 3.2.1), and μ_{sys} is the nonzero electrophoretic mobility of one of the system peaks, the exact formula for which is too convoluted for any theoretical discussion (cf. Supplementary material).

It should be noticed, that the analytical solution is limited to BGEs consisting of exclusively strong electrolytes and it does further adopt the approximation of excluding water ions form the consideration. These approximations are not very realistic since BGE is typically composed as a buffer. Buffering systems with complexation equilibria are reflected in NLTEM by a highly non-trivial structure of the communication matrix because the complexation (even with a neutral selector) interfere with acid-base equilibria and, consequently, affects also the electroneutrality condition. If a neutral selector is added to a buffering BGE and the selector does not interact with any another BGE constituent, the system peaks in the original buffering BGE remain unaffected and only the trivial stationary system peak arises as in the case of Section 3.1.1. If the interaction between the selector and a buffering BGE constituent is allowed, not only the stationary system peak gets mobilized as suggested by the simplified analytical solution, but also mobilities of other system peaks in the buffering BGE are affected. Only numerical solution to NLTEM by means of PM 6 calculation can solve this problem.

For experimental investigation, we used two different systems, one with a neutral selector and second with a charged selector. The former system consists of 5 mM benzoic acid (interacting with the

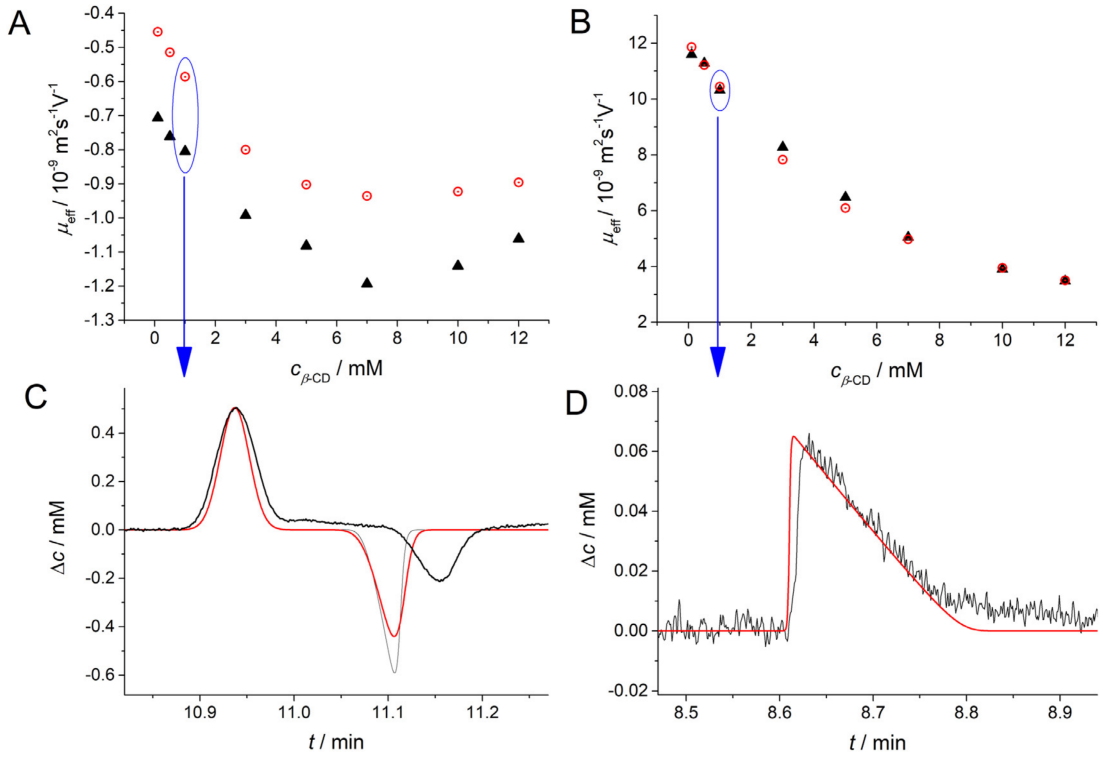

Fig. 4. Variation of the effective electrophoretic mobility of anionic (A) and cationic (B) system peaks as a function of β-CD concentration. Experimental values (black triangles) are compared with PeakMaster calculations (red circles). Furthermore, we show the respective electropherograms for one β-CD concentration (1 mM). (C) Zero system peak (positive) and anionic system peak (negative) at 1 mM β-CD in the BGE. Experimental electropherogram (black) compared with PeakMaster (red) and with Simul 5 Complex simulation (gray). Experimental data were re-calibrated so that the zero system peak height fits the PeakMaster result. (D) Cationic system peak at 1 mM β-CD in the BGE. Experimental electropherogram (black) compared with PeakMaster (red). Experimental data were re-calibrated so that the zero system peak height fits the PeakMaster result. No simulation for the cationic peak was performed because it would be too computationally challenging.

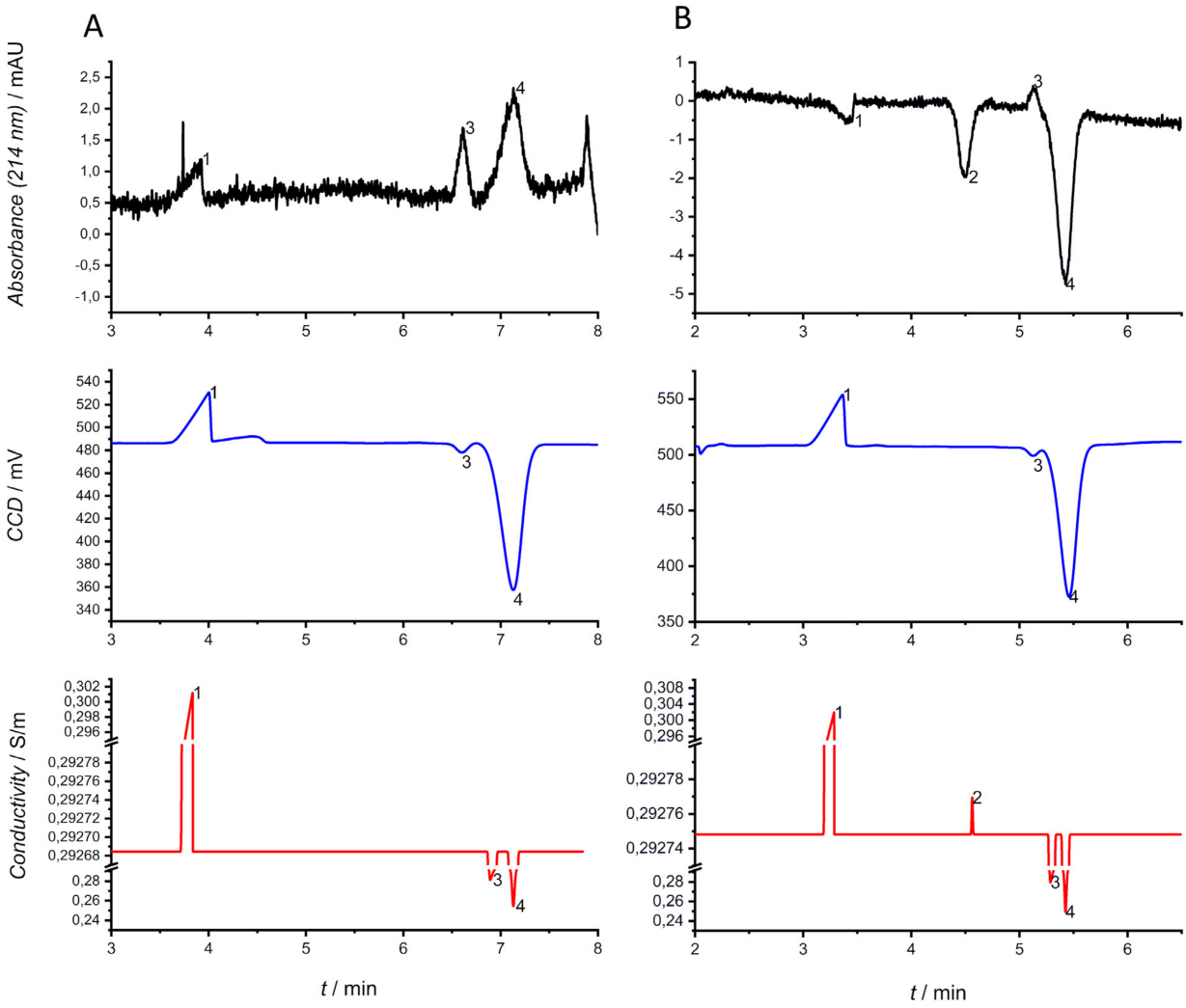

Fig. 5. System peaks in BGE consisting of (A) 30 mM acetic acid, 15 mM LiOH, 25 mM PA-β-CD · HCl, and (B) the same system with additional 0.3 mM HB in BGE. Experimental electropherograms, DAD, 214 nm (black) and CCD (blue) compared with PeakMaster (red). The peaks are numbered from low to high migration times. All peaks are system peaks. Peak number 4 is the stationary system peak. The y-scale in PeakMaster electropherogram is broken in order to make the system peak 2 visible in Panel B. The peak is below the limit of detection in experimental CCD (the blue trace) albeit it is detectable at 214 nm (the black trace). The x-scale of experimental data from CCD were re-scaled for visual comparison since the position of the CCD detector differs from that of the DAD detector (cf. Supplementary material for details).

selector) and 3 mM lithium (pH = 4.39) as BGE. β-CD was used as the selector. No analyte was present, and only disturbed BGE samples were injected (composition outlined in Table S1, Supplementary material.). We used complexation parameters evaluated for an ionic strength of 5.15 mM from our previous publication [21]. The values are: $\mu_{(\text{benzoic-}\beta\text{-CD})^-} = -(9.9 \pm 0.1) \cdot 10^{-9}$ m^2 s^{-1} V^{-1}, $K_{(\text{benzoic-}\beta\text{-CD})^-} = 29 \pm 1$ M^{-1} and $K'_{(\text{benzoic-}\beta\text{-CD})} = 460 \pm 20$ M^{-1}.

The original benzoic acid/Li buffer produces two system peaks, one stationary and one cationic. The addition of β-CD to the buffer severely slows the cationic system peak and gives rise to a new anionic system peak. The third system peak keeps electrophoretic mobility close to zero. A closer observation of the behavior of the anionic peak with the increase in β-CD concentration shows that its electrophoretic mobility first increases and then decreases. Such phenomena have not been described until now. We compare the experimental mobilities of both cationic and anionic system peaks with the PM 6 output. This comparison, including electropherograms, is shown in Fig. 4. Both system peaks show a difference (approx. 0.25 electrophoretic mobility unit) between experimental and PM 6 electrophoretic mobility values (Panels A and B, black triangles and red circles, respectively). This difference is much more visible for the anionic peak because its electrophoretic mobility values are very low. System peaks are extremely sensitive to all complexation parameters, thus this difference likely results from the uncertainty of the determination of complexation parameters. However, the electrophoretic mobility trends predicted by the NLTEM model are clearly followed by experimental data.

We compared the anionic peak in BGE with 1 mM β-CD between the PM 6 calculation and a simulation by Simul 5 Complex [31] in Fig. 4 (Panel C, red solid and gray lines, respectively). Both peaks have the same mobilities (positions at time axis), which confirms that the PM 6 calculation approximates the full solution to the underlying set of partial differential equations correctly and that the slight disagreement with experimental data likely stems from a bias in the complexation parameters. Finally, we compared the shapes of the system peaks as predicted by PM 6 with that obtained experimentally and for the anionic peak also with the simulation by Simul 5 Complex (only one simulation for 1 mM β-CD due to computational demands), Fig. 4 (Panels C and D). An excellent agreement is observed for the faster (cationic) system peak. The slower (anionic) system peak, which is much more sensitive to the calculation input parameters and experimental conditions,

is depicted with not so good, yet still practically acceptable, precision. The slight difference in peak shape as predicted by PM 6 and Simul 5 Complex is caused by the interaction between zones before they separate, which is not covered by the generalized NLTEM model in PM 6 due to the approximation of an immediate separation of all zones [33].

Second, we investigated a system with BGE consisting of 30 mM acetic acid and 15 mM LiOH and 25 mM PA-β-CD hydrochloride (positively charged) as the selector. 0.3 mM hydrobenzoin was added to BGE, as a complexing compound (but not a buffering one). No analyte was present this time either, only disturbed BGE was injected. We used complexation parameters evaluated for an ionic strength of 40 mM from our previous publication [28]. The respective values are:

$$\mu_{(HB-PA-\beta-CD)^+} = (7.671 \pm 0.053) \cdot 10^{-9} \mathrm{m^2 s^{-1} V^{-1}}$$

and

$$K'_{(HB-PA-\beta-CD)^+} = 140.3 \pm 2.6\ \mathrm{M^{-1}}.$$

Notice that the situation is rather reversed compared to the usual setup in this experiment. The cyclodextrin concentration in the BGE is constant while hydrobenzoin is being added as an interacting constituent. The original buffer with the selector (no hydrobenzoin) produces four system peaks (chlorides from the PA-β-CD hydrochloride present the fourth BGE constituent). Only one of the four system zones is stationary. Since now the cyclodextrin is not a neutral compound, its presence invokes a mobile system peak even if it does not interact with any other BGE constituent. One of the system peaks migrates too fast towards the anode and thus will not reach the detector. Consequently, two cationic system peaks, numbered as 1 and 3, are observed, (Fig. 5A). With the addition of the hydrobenzoin, one more system peak, numbered as 2, appears (Fig. 5B).

In the previous case (neutral selector added into the BGE), the system peak with almost zero electrophoretic mobility got mobilized upon addition of the selector into the BGE and its electrophoretic mobility changed gradually (forth and back) with increasing concentration of the selector. In this second case, when the charged selector is already present in the system and a neutral complexing constituent is added to the BGE, the system peak with a significantly nonzero electrophoretic mobility pops up immediately. The electrophoretic mobility of that system peak is governed by the amount of the charged selector (cyclodextrin) present in the system. PeakMaster predicts that the system peak occurs with the same migration time even when hydrobenzoin concentration is set to effectively zero (nevertheless, the amplitude of the peak would be infinitesimal in such a case).

The amplitude of this system peak (with 0.3 mM hydrobenzoin in the BGE) on the conductivity profile is too small, so it cannot be detected by CCD. However, the concentration of the absorbing compounds changes inside the system zone, so we detect the peak at 214 nm (although we can't compare the concentration profile with PeakMaster this time, since the absorbance profile is a result of several contributions). Nevertheless, the agreement on predicted electropherogram (peak positions) with PeakMaster is very good, as seen from Fig. 5 (predicted $\mu_{sys} = 5.94 \cdot 10^{-9}$ m^2 s^{-1} V^{-1}, experimental $\mu_{sys} = 6.49 \cdot 10^{-9}$ m^2 s^{-1} V^{-1}).

4. Conclusion

The generalized NLTEM model provides a useful insight into the complexation equilibria in EKC systems. The fundamental equation introduced by Tiselius in 1930 can be derived from the generalized NLTEM model. The derivation shows that Tiselius' equation should be always evaluated at the limit of zero concentration of the analyte. Specifically, any correction of a selector concentration for its presumable consumption by the analyte-selector complexation equilibrium is not justified in EKC. To the contrary, concentration of a selector may even increase in the zone of the analyte, as predicted by generalized NLTEM and confirmed experimentally, as the so-called cyclodextrin package.

If the selector interacts not only with the analyte but also another BGE constituent, determination of the complexation constant between the selector and the analyte may be severely compromised. A modified Wren and Rowe's equation was derived based on the previous conclusion about the Tiselius' equation for such systems. Yet, it was shown that the modified equation can easily result in the same hyperbolic trend as the original Wren and Rowe's formula, which makes it particularly difficult to discover the side-interaction just from the experimental data alone.

When the selector is added to BGE, a new system peak appears. If the selector does not interact with BGE constituents, other system peaks related to the given BGE composition remain unaffected. For systems with interacting BGEs, even the neutral selector gives generally rise to a non-stationary system peak and also mobilities of the other system peaks may change considerably. We have observed that, rather surprisingly, this electrophoretic mobility of a system peak may not be a monotonic function of the selector concentration. When a charged selector is present, not only a new system peak appears due to the presence of the extra charged constituent in the BGE, but stationary system peak(s) may also gain fairly nonzero electrophoretic mobility if the selector interacts with other BGE constituent(s).

We investigated the systems with fully charged analytes and neutral or fully charged selectors in this paper, all interacting exclusively with 1:1 stoichiometry. These systems allowed us to demonstrate all phenomena expected in EKC, albeit the theory and software are applicable to general equilibria when any number of ampholytic analytes or BGE constituent(s) interact with any number of possibly ampholytic selectors in any ionization state and with any stoichiometry. The main limitation is seen in determining all input parameters to such systems. Determining the two complexation constants of a monovalent week electrolyte with a single form of a selector can already be a difficult task. Considering even more interacting forms would present a real experimental challenge. Another limitation is application of ionic strength corrections in environments with highly charged selectors (such as common charged cyclodextrin derivatives), which hits the limits of the theoretical models used for small molecules (i.e. Debye-Hückel and Onsager-Fuoss theories). On the other hand, generalized NLTEM can be easily formulated for micellar systems, too, the mode of EKC to be implemented in future versions of PeakMaster software.

All effects were confirmed experimentally and compared with the new version of our software, PeakMaster 6. Analytical formulas derived from NLTEM, calculations by means of PM 6, and experimental results generally showed a very good agreement. Thus, this paper justifies using PeakMaster software for complexing CZE systems.

Declaration of Competing Interest

The authors declare that they have no known competing financial interests or personal relationships that could have appeared to influence the work reported in this paper.

Acknowledgment

The support of the Czech Science Foundation, Grant Agency of the Czech Republic, 18-11776S and Grant Agency of Charles University, Grant No. 116217 is gratefully acknowledged.

Supplementary materials

Supplementary material associated with this article can be found, in the online version, at doi:doi:10.1016/j.chroma.2019.460595.

References

[1] S. Terabe, K. Otsuka, T. Ando, Electrokinetic chromatography with micellar solution and open-tubular capillary, Anal. Chem. 57 (4) (1985) 834–841.
[2] P. Dubský, M. Dvořák, M. Ansorge, Affinity capillary electrophoresis: the theory of electromigration, Anal. Bioanal. Chem. 408 (2016) 8623–8641.
[3] Q. Zhu, G.K. Scriba, Advances in the use of cyclodextrins as chiral selectors in capillary electrokinetic chromatography: fundamentals and applications, Chromatographia 79 (21–22) (2016) 1403–1435.
[4] S. Surapaneni, K. Ruterbories, T. Lindstrom, Chiral separation of neutral species by capillary electrophoresis evaluation of a theoretical model, J. Chromatogr. A 761 (1–2) (1997) 249–257.
[5] S.A.C. Wren, Theory of chiral separation in capillary electrophoresis, J. Chromatogr. A 636 (1993) 57–62.
[6] G. Chalumot, C. Yao, V. Pino, J.L. Anderson, Determining the stoichiometry and binding constants of inclusion complexes formed between aromatic compounds and β-cyclodextrin by solid-phase microextraction coupled to high-performance liquid chromatography, J. Chromatogr. A 1216 (2009) 5242–5248.
[7] G.K.E. Scriba, Selected fundamental aspects of chiral electromigration techniques and their application to pharmaceutical and biomedical analysis, J. Pharm. Biomed. Anal. 27 (2001) 373–399.
[8] Y.Y. Rawjee, D.U. Staerk, G. Vigh, Capillary electrophoretic chiral separations with cyclodextrin additives. I. acids: chiral selectivity as a function of pH and the concentration of β-cyclodextrin for fenoprofen and ibuprofen, J. Chromatogr. A 635 (1993) 291–306.
[9] Y.Y. Rawjee., R.L. Williams, G. Vigh, Capillary electrophoretic chiral separations using cyclodextrin as resolving agent. II. bases: chiral selectivity as a function of pH and the concentration of β-cyclodextrin, J. Chromatogr. A 652 (1993) 233–245.
[10] P. Dubský, L. Müllerová, M. Dvořák, B. Gaš, Generalized model of electromigration with 1:1 (analyte:selector)complexation stoichiometry: part I. theory, J. Chromatogr. A 1384 (2015) 142–146.
[11] H. Poppe, Overloading and interaction phenomena in electrophoretic separations, Anal. Chem. 64 (1992) 1908–1919.
[12] M. Štědrý, M. Jaroš, B. Gaš, Eigenmobilities in background electrolytes for capillary zone electrophoresis I. system eigenpeaks and resonance in systems with strong electrolytes, J. Chromatogr. A 960 (2002) 187–198.
[13] M. Štědrý, M. Jaroš, ..K. Včeláková, B. Gaš, Eigenmobilities in background electrolytes for capillary zone electrophoresis: II. eigenpeaks in univalent weak electrolytes, Electrophoresis 24 (2003) 536–547.
[14] M. Štědrý, M. Jaroš, V. Hruška, B. Gaš, Eigenmobilities in background electrolytes for capillary zone electrophoresis: III. linear theory of electromigration, Electrophoresis 25 (2004) 3071–3079.
[15] V. Hruška, M. Štědrý, K. Včelákovám J. Lokajová, E. Tesařová, M. Jaroš, B. Gaš, Eigenmobilities in background electrolytes for CZE. V. intensity (amplitudes) of system peaks, Electrophoresis 27 (23) (2006) 4610–4617.
[16] M. Jaroš, V. Hruška, M. Štědrý, I. Zusková, B. Gaš, Eigenmobilities in background electrolyte for capillary zone electrophoresis: IV. computer program PeakMaster, Electrophoresis 25 (18-19) (2004) 3080–3085.
[17] V. Hruška, M. Riesová, B. Gaš, A nonlinear electrophoretic model for PeakMaster: I. mathematical model, Electrophoresis 33 (2012) 923–930.
[18] M. Riesová, V. Hruška, B. Gaš, A nonlinear electrophoretic model for PeakMaster: II. experimental verification, Electrophoresis 33 (6) (2012) 931–937.
[19] V. Hruška, J. Svobodová, M. Beneš, B. Gaš, A nonlinear electrophoretic model for PeakMaster: part III. electromigration dispersion in systems that contain a neutral complex-forming agent and a fully charged analyte. Theory, J. Chromatogr. A 1267 (2012) 102–108.
[20] M. Beneš, J. Svobodová, V. Hruška, M. Dvořák, I. Zusková, B. Gaš, A nonlinear electrophoretic model for PeakMaster: part IV. electromigration dispersion in systems that contain a neutral complex-forming agent and a fully charged analyte. Experimental verification, J. Chromatogr. A 1267 (2012) 109–115.
[21] M. Riesová, J. Svobodová, Z. Tošner, M. Beneš, E. Tesařová, B. Gaš, Complexation of buffer constituents with neutral complexation agents: part I. impact on common buffer properties, Anal. Chem. 85 (2013) 8518–8525.
[22] M. Beneš, M. Riesová, J. Svobodová, E. Tesařová, P. Dubský, B. Gaš, Complexation of buffer constituents with neutral complexation agents: part II. practical impact in capillary zone electrophoresis, Anal. Chem. 85 (2013) 8526–8534.
[23] P. Debye, E. Hückel, Zur theorie der electrolyte, Physik. Z. 24 (1923) 185–206.
[24] P. Debye, E. Hückel, Zur Theorie der Elektrolyte: (2): Das Grenzgesetz für die Elektrische Leiftfahrigkei, Physik. Z. 24 (1923) 305–325.
[25] L. Onsager, On the theory of electrolytes. II, Phys. Z. 28 (1927) 277–298.
[26] D. Koval, V. Kašička, J. Jiráček, M. Collinsová, T.A. Garrow, Analysis and characterization of phosphinic pseudopeptides by capillary zone electrophoresis, Electrophoresis 23 (2002) 215–222.
[27] P.M. Nowak, M. Woźniakiewicz, P. Kościelniak, Seven approaches to elimination of the inherent systematic errors in determination of electrophoretic mobility by capillary electrophoresis, Anal.Chem. 89 (2017) 3630–3638.
[28] M. Beneš, I. Zusková, J. Svobodová, B. Gaš, Determination of stability constants of complexes of neutral analytes with charged cyclodextrins by affinity capillary electrophoresis, Electrophoresis 33 (6) (2012) 1032–1039.
[29] J. Caslavska, M.C. Breadmore, W. Thormann, Dynamic high-resolution computer simulation of isotachophoretic enantiomer separation and zone stability, Electrophoresis 35 (2014) 625–637.
[30] W. Thormann, L. Chankvetadze, M. Gumustas, B. Chankvetadze, Dynamic computer simulation of electrophoretic enantiomer migration order and separation in presence of a neutral cyclodextrin, Electrophoresis 35 (2014) 2833–2841.
[31] V. Hruška, M. Beneš, J. Svobodová, I. Zusková, B. Gaš, Simulation of the effects of complexformation equilibria in electrophoresis: I. mathematical model, Electrophoresis 33 (2012) 938–947.
[32] M.C. Breadmore, J.P. Quirino, W. Thormann, Insight into the mechanism of transient trapping in micellar electrokinetic chromatography, Electrophoresis 32 (2011) 542–549.
[33] M. Malý, M. Dovhunová, M. Dvořák, G.S. Gerlero, P.A. Kler, V. Hruška, P. Dubský, Generalized model of the linear theory of electromigration and its application to electrokinetic chromatography: theory and software PeakMaster 6—Next generation, Electrophoresis 40 (2019) 683–692.
[34] P. Dubský, M. Ördögová, M. Malý, M. Riesová, CEval: all-in-one software for data processing and statistical evaluations in affinity capillary electrophoresis, Journal of Chromatography A 1445 (2016) 158–165.
[35] A. Tiselius, Nova Acta Regiae Soc Sci Ups 4 (1930), Ser IV 7, 1–107, pp. 26.
[36] J. Boonleang, J.F. Stobaugh, New single isomer negatively charged β-cyclodextrin derivatives as chiral selectors in capillary electrophoresis, Electrophoresis 34 (8) (2013) 1232–1240.
[37] S.G. Penn, E.T. Bergstrom, I. Knights, G. Liu, A. Ruddick, D.M. Goodall, Capillary electrophoresis as a method for determining binding constants: application to the binding of cyclodextrins and nitrophenolatest, J. Phys. Chem. 99 (11) (1995) 3875–3880.
[38] S.G. Penn, E.T. Bergstrom, D.M. Goodall, J.S. Loran, Capillary electrophoresis with chiral selectors: optimization of separation and determination of thermodynamic parameters for binding of tioconazole enantiomers to cyclodextrins, Anal. Chem. 66 (18) (1994) 2866–2873.
[39] T. Le Saux, A. Varenne, P. Gareil, Peak shape modeling by Haarhoff-Van der Linde function for the determination of correct migration times: a new insight into affinity capillary electrophoresis, Electrophoresis 26 (2005) 3094–3104.
[40] M. Dvořák, P. Dubský, M. Dovhunová, B. Gaš, The dynamics of band (peak) shape development in capillary zone electrophoresis in light of the linear theory of electromigration, Electrophoresis 40 (2019) 668–682.
[41] L. Müllerová, P. Dubský, B. Gaš, Separation efficiency of dual-selector systems in capillaryelectrophoresis, J. Chromatogr. A 1330 (2014) 82–88.
[42] H. Poppe, System peaks and non-linearity in capillary electrophoresis and high-performance liquid chromatography, J. Chromatogr. A 831 (1999) 105–121.
[43] V.K. Almeida, C.K. Larive, Insights into cyclodextrin interactions during samplestacking using capillary isotachophoresis with on-linemicrocoil NMR detection, Magn. Reson. Chem. 43 (2005) 755–761.

Publication III

Michal Malý[1]
Milan Boublík[1]
Marijana Pocrnić[2]
Martin Ansorge[1]
Kateřina Lorinčíková[1]
Jana Svobodová[3]
Vlastimil Hruška[3]
Pavel Dubský[1]
Bohuslav Gaš[1]

[1]Faculty of Science, Department of Physical and Macromolecular Chemistry, Charles University in Prague, Prague, Czech Republic
[2]Department of Chemistry, Faculty of Science, University of Zagreb, Zagreb, Croatia
[3]Agilent Technologies Deutschland GmbH & Co. KG, Liquid Phase Separations Division, Waldbronn, Germany

Received July 29, 2019
Revised October 3, 2019
Accepted October 19, 2019

Research Article

Determination of thermodynamic acidity constants and limiting ionic mobilities of weak electrolytes by capillary electrophoresis using a new free software AnglerFish

Thermodynamic acidity constants (acid or acid-base dissociation constants, sometimes called also as ionization constants) and limiting ionic mobilities (both of them at defined temperature, usually 25°C) are the fundamental physicochemical characteristics of a weak electrolyte, that is, weak acid or weak base or ampholyte. We introduce a novel method for determining the data of a weak electrolyte by the nonlinear regression of effective electrophoretic mobility versus buffer composition dependence when measured in a set of BGEs with various pH. To correct the experimental data for zero ionic strength we use the extended Debye-Hückel model and Onsager-Fuoss law with no simplifications. Contrary to contemporary approaches, the nonlinear regression is performed on limiting mobility data calculated by PeakMaster's correction engine, not on the raw experimental mobility data. Therefore, there is no requirement to perform all measurements at a constant ionic strength of the set of BGEs. We devised the computer program AnglerFish that performs the necessary calculations in a user-friendly fashion. All thermodynamic pKa values and limiting electrophoretic mobilities for arbitrarily charged substances having any number of ionic forms are calculated by one fit. The user input consists of the buffer composition of the set of BGEs and experimentally measured effective mobilities of the inspected weak electrolyte.

Keywords:
Capillary electrophoresis / Dissociation constant / Limiting mobility / Nonlinear regression / Software
DOI 10.1002/elps.201900283

1 Introduction

An acidity dissociation constant and electrophoretic mobilities are the fundamental physicochemical constants that characterize an ionic constituent (by ionic constituent we understand a weak electrolyte, i.e., a weak acid or base). Both of the constants determine the effective mobility of the constituent in the electromigration movement and in this way have a direct impact on the quality of separation in electromigration separation methods–CZE and ITP. In fact, both constants depend on the ionic strength of the solution. The ionic strength I is the quantity assessing the contributions of Coulombic interaction of all ionic species in the solution, including H^+ and OH^- ions, and is defined as: $I = 1/2 \sum_{i=1}^{n} c_i z_i^2$, where c_i and z_i is the concentration and the charge number of the i-th ionic species, n is the number of all ionic species in solution. The mobility and acidity dissociation constant (pKa) converge to some values when decreasing the ionic strength, that is, when decreasing the concentration of ionic species to zero. Such limiting values are called limiting ionic mobilities and thermodynamic pKa constants and characterize the particular constituent. They are defined for infinitely diluted solutions and therefore are unavailable to be measured directly.

Accurate and precise knowledge of limiting mobilities and thermodynamic constants is however essential in multiple fields of chemistry, not only in electromigration, and much scientific effort has been devoted to development of methods for their determination. Most of these methods do not utilize the set of the measurements of quantities with gradually decreasing ionic strength, but rather rely on a theoretical model of the dependence of the quantities on ionic strength.

The development of such models goes back to the history of physical chemistry. It was Debye and Hückel who proposed the theory of activity coefficients dependent on ionic strength [1, 2]. The theory has been used with various modifications to the present time. It explains how to obtain the activity

Correspondence: Michal Malý, Faculty of Science, Department of Physical and Macromolecular Chemistry, Charles University in Prague, Prague, Czech Republic
E-mail: michal.maly@natur.cuni.cz

Abbreviation: **GMP**, guanosine monophosphate

Color online: See article online to view Figs. 13 in color.

coefficient γ_i of the ion to calculate the activity $a_i = \gamma_i\ c_i$ of the i-th ionic species from the concentrations c_i at a finite ionic strength I. When the activities of the ionic species are known, the true thermodynamic dissociation constants of the ionic constituents (acid or bases) can be determined.

The dependence of the electrophoretic mobility on ionic strength is, however, more complicated. While the activity coefficient regards only the static influence of the ionic atmosphere, the electrophoretic mobility has to take into consideration also the dynamics of forming an ionic atmosphere, as the ionic constituents are in forced movement. The theory by Onsager and Fuoss [3] takes into account two phenomena connected with the electromigration of ionic constituents: the electrophoretic and relaxation effects. It even derives for electrolytes composed of more than two ionic species that the relaxation effect depends not only simply on ionic strength but also on the mobility ratios and on the ratios of concentrations in which the various ions are present. Onsager and Fuoss call this phenomenon the "mixture effect" and show that the mixture effect is greater the more the mobility ratios deviate from unity. The mixture effect plays an inevitable role in electrolytes in CE, where typically three ions are present in the peak: the separated ion, the co-ion and the counter ion of the BGE. The mixture effect is significant in highly acidic or alkaline electrolytes, as the mobilities of hydroxonium and hydroxide ions are extraordinarily high when compared to other ions.

Long before CE and isotachophoresis, the methods for the direct determination of mobilities and dissociation constants were introduced, a number of papers were published on the dependence of molar conductivity and transport numbers on ionic strength. This is reviewed in the classic book by Robinson and Stokes [4].

As mentioned above, the electromigration separation methods, ITP and CZE, can be used not only for the separation of analytes but also for the determination of the mobilities and pKa constants of various constituents. Here a substantial contribution was made by Hirokawa and coworkers [5–13], who published a great deal of reliable data obtained by ITP. The advantage of ITP is its separation ability, which enables us to determine the mobilities of several constituents at once, even without purification. Further advantage of ITP for such measurements is its accuracy, as it works in a hydrodynamically closed system, which eliminates bulk electroosmotic flow, a possible source of experimental errors. Due to a stacking effect the edges of the zones remain sharp. The approach by Hirokawa involved computer-assisted data fitting and then correcting both pKa and limiting mobilities for ionic strength. The Debye-Hückel law [1, 2] was used to calculate the true thermodynamic pKa constants, while the limiting mobilities were calculated using the Onsager equation [14].

One of the first approaches based on CZE measurements was proposed by Beckers et al. [15]. Beckers' method naturally uses the fact that effective electrophoretic mobility is the weighted average of the actual ionic mobilities of all dissociation states of a given compound where the weights are molar fractions of each dissociation state. Beckers showed that the pKa and limiting mobility of a monovalent acid or base can be calculated by measuring its effective mobility in two systems with different pH, provided that the pH and ionic strength of both systems is known. True pKa values are again calculated using the Debye-Hückel law and the limiting mobilities are calculated from ionic equivalent conductance.

Cai et al. from the group of El Rassi [16] were the first to combine effective mobility measurements by CZE with nonlinear regression. In this case, the effective mobility of the analyte is measured in several buffers with different pH. The obtained set of pH versus effective mobility data points is then fitted with a model appropriate for the analyte. Ionic mobilities and pKa constants are parameters of the fit. A considerable advantage of this approach is the fact that the overall procedure remains the same regardless of the number of dissociation states of the analyte. The only thing that needs to be adjusted is the equation describing the theoretical dependence of the effective mobility on pH. Such an equation is, however, fairly simple to derive so long as the possible dissociation states of the studied substance are known. Other advantages include high robustness against experimental error, proper error estimation of the fitted parameters and the ease of automation. Even though ionic mobilities are also obtained from the fit, Cai proposed no means of how to calculate limiting mobilities from the experimental data. Cai's approach has been further extended for multivalent substances [17] and applied to wide variety of substances [18, 19].

For the purposes of true thermodynamic pKa determination it is convenient to define a sort of acidity constants as so-called mixed constant [20, 21]. The mixed acidity constant is defined as a function of activity of hydroxonium ions and concentrations of the two consecutive ionic forms of a given compound. This is advantageous because activity of hydroxonium ions can be measured directly by calibrated pH electrodes. As such, this mixed constant is already partially corrected for ionic effects.

Andrassi et al. [22] performed a comparative study of pKa determination using CZE and potentiometric titration. They concluded that CZE is advantageous due to its ability to both separate and characterize a substance, thus greatly reducing the effect of any impurities that might be present in a sample. Additionally, it can work with very small sample volumes and even allows for the characterization of multiple substances simultaneously.

While calculation of true pKa using the Debye-Hückel law is straightforward, there is no equally simple and universal formula for the calculation of limiting mobilities. Presently used methods for determination of limiting mobilities that utilize CZE use some form of the Pitts equation [23,24]. The Pitts equation, Ref. [25], is an extension of the Onsager-Fuoss [3] law and uses various additional parameters whose value must be determined beforehand. The means of how to get the values of these parameters vary from semi-empirical approaches to rather complicated experiments that require specialized equipment.

There were many attempts to use CZE to determine both pKa and ionic mobilities, see, for example, Refs. [26–28]. Šlampová et al. [27, 28] attempted to correct both pKas and ionic mobilities for ionic effects. Šlampová's approach was limited to singly charged weak electrolytes and required that all experimental data be measured at the same ionic strength. A Microsoft Excel spreadsheet has been provided for automatic data evaluation.

All the works on the determination of limiting ionic mobilities and thermodynamic pKa constants by electromigration methods have used the following approach: determination of the actual ionic mobilities and apparent pKa constants from the sets of experimental data and then correcting them for zero ionic strength using the Debye-Hückel theory and some modification of the Onsager equation for mobilities. Such an approach requires using a set of measurements at constant ionic strength, which is difficult or even impossible to reach at very low or very high pH, where either hydroxonium or hydroxide ions significantly contribute to the ionic strength. In fact, the approach is principally incorrect, as the experimentally available effective mobility is dependent both on the ionic mobility and pKa constant. Moreover, it is difficult to make a proper correction of mobilities when two pKa constants of a constituent are close together because in this case the pKa constants also influence each other and so do the limiting mobilities.

Our group introduced two software tools for the simulation and prediction of electromigration behavior and for method development–PeakMaster [29–32] and Simul [33]. Both tools use as the input data the set of limiting ionic mobilities and thermodynamic pKa constants, which is known as the Hirokawa database [6]. Both software tools also enable one to perform the correction of (i) activity coefficients influencing pKa using the Debye-Hückel theory [1, 2] and (ii) mobilities using the theory by Onsager and Fuoss [3]. This way they can simulate the real behavior of ions quite precisely.

In the present work, we propose adapting the ionic strength corrections used in PeakMaster for the inverse task: to determine the limiting mobilities and true thermodynamic pKa constants of a constituent from the set of experimental data of effective mobilities of the constituent obtained by electrophoresis using a set of background electrolytes with various pH. The procedure for obtaining the limiting mobilities and thermodynamic pKa constants will be a nonlinear regression of the set of experimental mobility data. Contrary to contemporary approaches, the nonlinear regression is performed on limiting mobility data calculated by the PeakMaster's correction engine, not on the raw experimental mobility data. This enables us to calculate by one fit both the true thermodynamic pKa values and limiting electrophoretic mobilities for arbitrarily charged substances with any number of ionic forms. There is no requirement to perform all measurements at the same ionic strength of the set of BGEs.

We have developed the freeware program AnglerFish for the user-friendly input of experimental data and the comfortable obtaining of results.

2 Theory

2.1 Corrections for ionic strength

As was shown by Debye and Hückel [1, 2] and Onsager and Fuoss [3], even low concentrations of ions in a solution lead to observable deviation of the expected ideal behavior of solutions. These deviations cause differences between the observed and expected dissociation constants and changes in conductivity, which in turn are a result of the reduced ionic mobilities of all ions. The Debye-Hückel and Onsager-Fuoss theories consider ions to be infinitely small uniformly charged particles.

In our software tools PeakMaster and Simul we apply the Davies' [34] modification of the extended Debye-Hückel formula for the ionic activity coefficient γ_z of an ion with the charge number z at a temperature of 25°C:

$$\log\ \gamma_z = -\frac{0.50925\ z^2\ \sqrt{I}}{1+1.5\ \sqrt{I}} + 0.1\ z^2 I, \tag{1}$$

where z is the charge number of the ion and I is the ionic strength expressed in mol/L.

For the correction of mobility for ionic strength, u_j, we use the equations derived by Onsager and Fuoss [3] taking into account effects stemming from nonequilibrium thermodynamics. We have rewritten the equations into contemporary notation and presently used units for better clarity:

$$u_j = u_j^{\infty} - \left(B_1 z_j u_j^{\infty} \sum_{n=0}^{5} C_n R_j^{(n)} + B_2 \left|z_j\right|\right) \frac{\sqrt{\Gamma}}{1+Ba\sqrt{\frac{\Gamma}{2}}}$$

$$B_1 = \frac{e^3}{12\pi}\sqrt{\frac{N_A \nu}{(\varepsilon k T)^3}},\ B_2 = \frac{e^2}{6\pi\eta}\sqrt{\frac{N_{A\nu}}{\varepsilon k T}},\ \Gamma = \sum_{i=1}^{s}\Gamma_i,$$

$$\Gamma_i = c_i z_i^2, \tag{2}$$

where u_j^{∞} and z_j are the limiting ionic mobility and charge number of the j-th ionic species, respectively, c_j is the concentration of the j-th ionic species, e is the elementary charge, $N_{A\nu}$ is the Avogadro constant, ϵ and η is the permittivity and dynamic viscosity of the solution, respectively, k is the Boltzmann constant, T is the absolute temperature, and s is the overall number of all ionic species in the solution. For the $Ba/\sqrt{2}$ term, the value of 1.5 $\mathrm{mol}^{-1/2}\mathrm{dm}^{3/2}$ is employed.

C_n are the coefficients of the series

$$C_0 = \frac{1}{2}\left(2-\sqrt{2}\right) \text{ and } C_n = -\frac{\sqrt{2}}{2}\binom{1/2}{n} \text{ for } n \geq 1 \tag{3}$$

Column vectors $R^{(n)}$ are defined by means of the recursion formulas

$$R_j^{(n)} = \sum_{\sigma=1}^{s} (2\mathbf{H}-\mathbf{I})_{j\sigma} R_{\sigma}^{(n-1)}$$

$$R_j^{(0)} = z_j - \frac{\sum_{i=1}^{s} z_i \mu_i}{\sum_{i=1}^{s}\left|\frac{z_i}{u_i^{\infty}}\right|\mu_i}\left|\frac{z_j}{u_j^{\infty}}\right|$$

$$\mu_i = \frac{\Gamma_i}{\Gamma} \tag{4}$$

H is the matrix with the elements h_{ji}

$$h_{ji} = \delta_{ji}\left(\sum\nolimits_i \mu_i \frac{\omega_i}{\omega_i + \omega_j}\right) + \mu_i \frac{\omega_i}{\omega_i + \omega_j}, \omega_j = \frac{u_j^\infty}{|e_j|} \tag{5}$$

where δ_{ji} is the Kronecker delta, e_j is the charge of j-th ion, $e_j = e\, z_j$, where e is the elementary charge, and **I** is the unit matrix.

This way it is possible to calculate the so-called actual effective mobilities of an analyte when all parameters of the BGE and the analyte are known–their limiting ionic mobilities and the thermodynamic pKa constants of all constituents included.

But our task is inversed:

i. We have an analyte, the thermodynamic pKa constant(s) and mobility(ies) of which are to be determined.
ii. We have a background electrolyte with a known composition, where all limiting mobilities and thermodynamic constants pKa of all its constituents are known. This enables us to calculate using PeakMaster: (a) the pH based on the activity of the hydroxonium ions and (b) ionic strength of the background electrolyte.
iii. We prepare a set of such BGE s with various pH.
iv. We measure by CZE the effective mobilities of the analyte in the set of the background electrolytes above.
v. Using a nonlinear regression, we fit the set of the mobilities of the analyte by the Henderson-Hasselbalch equation, in the analogous way, as in Ref. [16]. The substantial difference is that we correct the measured mobilities of the analyte for ionic strength effects using the PeakMaster correction engine, Eqs. (1–5), inversely. The correction is hardcoded in the fitting function, so in our approach the Henderson-Hasselbalch equation fits directly the limiting ionic mobilities and thermodynamic constants of the compound. In the single fitting procedure, the fitted parameters are both the limiting ionic mobilities and thermodynamic pKa constants of the analyte. These parameters are the results.

2.2 AnglerFish computer program

One obvious drawback of treating the entire buffer as an independent variable by multi-purpose tools such as Origin, MATLAB, QtiPlot, Gnuplot, etc. that are commonly used in the electrophoretic community for the nonlinear fitting of experimental mobility, is that the fitting cannot simply use both the Henderson-Hasselbalch equation and correction procedure by Debye-Hückel and Onsager-Fuoss. Specifically, the Onsager-Fuoss correction is nontrivial and it requires knowledge of the exact buffer composition. A specialized computer program that accepts experimentally obtained effective mobilities and composition of buffers as input is needed.

To take full advantage of the approach suggested above we have devised the computer program AnglerFish. Input data for the program consists of (i) the composition of a series of buffers, (ii) effective mobilities measured experimentally in each entered buffer and (iii) initial estimates of the pKa and limiting mobilities. The program then performs a nonlinear regression using the Levenberg-Marquardt algorithm [35, 36] to calculate the thermodynamic pKa constants and limiting ionic mobilities. Since the program knows the exact composition of every buffer, the proper correction for ionic effects using the Debye-Hückel law for pKa and the Onsager-Fuoss law for limiting mobilities is applied at every step of the regression. This enables the calculation of the true thermodynamic values of all pKa constants and eliminates the need to perform the entire series of measurements in buffers of the same ionic strength. The AnglerFish program is derived from the PeakMaster 6 [32] program and both programs provide a common user interface which allows for the user-friendly input and output of parameters and displaying a graph with the experimental and fitted values of mobilities.

The expected procedure of use is to design a series of buffers by means of PeakMaster, run the experiments, import the composition of buffers and measured actual effective mobilities into AnglerFish, and fit the results. The program and a user guide can be downloaded from the ECHMET group website [37], the source code is available on GitHub [38].

3 Materials and methods

3.1 Chemicals

All used chemicals were of analytical grade purity. Lithium hydroxide monohydrate, β-alanine, CHES, MOPS, MES, glycine, acetic acid, formic acid, phosphoric acid, histidine, guanosine monophosphate (GMP), all of them from Sigma Aldrich. Water for preparation of all solutions was deionized by Watrex Ultrapur system (Prague, Czech Republic). All running buffers were filtrated using Minisart syringe filters (Sartorius Stedim Biotech, Goettingen, Germany), pore size 0.45 mm.

All experiments were performed using Agilent 7100 CE equipment operated under ChemStation software (Agilent Technologies, Waldbronn, Germany). Detection was performed with the built-in DAD. Fused silica capillary (50 µm i.d. 375 µm o.d.) was provided by Polymicro Technologies (Phoenix, AZ). The experiments were performed in bare capillaries with a total lengths and effective lengths to the DAD detector around 50 and 41.5 cm, respectively. The new capillary was flushed first with 1 M sodium hydroxide and then with de-ionized water for 10 min and 10 min with actual BGE.

A sets of 33 buffers with calculated properties by PeakMaster was prepared. Buffers covered pH range of 1.5–12 in ionic strengths of 10 mM. pH coverage for all the buffers is summarized in Table 1. All BGEs as well as sample matrix were prepared by mixing appropriate amounts of buffer component stock solutions and deionized water. Injected samples composed of 0.1–0.5 mM of GMP and DMSO were dissolved in the measured BGE. DMSO was used to track the velocity

Table 1. Set of buffers and their pH range

Buffer composition	pH range
Phosphoric acid	1.5–2.3
Phosphoric acid/LiOH	2–3.1
Formic acid/LiOH	2.9–4.1
Acetic acid/LiOH	3.8–5
MES/LiOH	5.3–6.2
MOPS/LiOH	6.2–7.4
Tricine/LiOH	7.3–8.6
Glycine/LiOH	8.9–10.4
CHES/LiOH	8.5–9.3
β-Alanine/LiOH	9.7–11.7
LiOH	11.6–12.6

of electroosmotic flow. Hydrodynamic injection of 10 mbar × 15 s was applied. Additional pressure was used if there was a need to modulate the velocity of EOF. Applied voltage was 15 kV keeping flowing current below 15 µA. Measurements were performed in triplicates and evaluated by CEval 0.6h6 [39] computer program.

3.2 Data fit algorithm

The software performs a nonlinear fit to calculate the thermodynamic pKa and limiting mobilities. The algorithm performs sanity checks of the fitted parameters to ensure that they are physically sensible. The first check is to make sure that pKa(n) > ··· > pKa(p), where pK(n) is pK of the form with the lowest charge and pK(p) the pK of the form with the highest charge.

The second check concerns limiting mobilities and can be described as follows: $0.55\ u_{\text{base}} + u_{z-1} < u_z < 1.2\ u_{\text{base}} + u_{z-1}$ for basic and as $0.55\ u_{\text{base}} + u_{z+1} < u_z < 1.2\ u_{\text{base}} + u_{z+1}$ for acidic ionic forms, where u_{base} is either u_{-1} or u_{+1} depending on whether the acidic or basic forms are evaluated. This reflects the generally valid rule that each additional charge increases the overall mobility of a substance by approximately the same amount. AnglerFish provides the option of disabling the limiting mobilities sanity check. The sanity check of pKas cannot be disabled. Initial estimates for fits, both in Origin and AnglerFish, were estimated from experimental curves.

4 Results and discussion

It is not the purpose of this paper to present thermodynamic pKa constants and limiting mobilities of a number of various compounds. Instead, we will demonstrate the abilities of AnglerFish by calculating the data for one multivalent ionic constituent–GMP, which is a trivalent weak anionic compound. The set of buffers summarized in Table 1 was prepared to have the same ionic strength close to 10 mM. Buffers of the same ionic strength were prepared to allow for the fair comparison between the "classic" procedure and AnglerFish.

Our intention here is to compare the classic procedure for the determination of thermodynamic pKa constants and limiting mobilities of an ionic compound by electrophoresis with the new one based on the new approach.

(i) The classic procedure we used was based on this approach: we measured the set of effective mobility data of the compound for various pH of the BGEs and fitted these raw experimental mobility data by the Henderson-Hasselbalch equation with the Origin software. This way obtained apparent mixed pKa constants we corrected for zero ionic strength using the Debye-Hückel equation, Eq. (1). To make the comparison with AnglerFish fair, we corrected the actual mobilities for zero ionic strength by "manual iteration" by means of the PeakMaster software. This "manual iteration" procedure is explained further below.

(ii) The procedure by AnglerFish is based simply on the input of the compositions of the set of BGEs and corresponding measured effective mobilities.

4.1 Classic procedure

The set of 99 couples of the measured pH of 33 BGEs (every measurement was repeated three times) and the corresponding measured effective mobilities of GMP were entered into the Origin environment into the so-called Book. The data were analyzed and depicted by one of Origin's tools, the Nonlinear Curve Fit, using the Henderson-Hasselbalch function, which was manually inserted. The Levenberg-Marquardt algorithm was used for the nonlinear fit. The output in the form of a Graph is shown in Fig. 1.

All effective mobilities dependent on pH are depicted by crosses. The figure also displays the fitting Henderson-Hasselbalch curve in red and the fitted parameters calculated by Origin in the inlay: the actual ionic mobilities and apparent mixed pKa constants. These values are to be corrected for ionic strength.

4.1.1 Correction of pKa constants

The dissociation steps of GMP are as follows:

$$\mathrm{GMP} \underset{\mathrm{H^+}}{\rightleftharpoons} \mathrm{GMP^-} \underset{\mathrm{H^+}}{\rightleftharpoons} \mathrm{GMP^{2-}} \underset{\mathrm{H^+}}{\rightleftharpoons} \mathrm{GMP^{3-}}$$

and corresponding dissociation equations for mixed dissociation constants K_z^{mix} are:

$$K_1^{\text{mix}} = \frac{c\left(\mathrm{GMP^-}\right) \cdot a\left(\mathrm{H^+}\right)}{c\left(\mathrm{GMP}\right)}$$

$$K_2^{\text{mix}} = \frac{c\left(\mathrm{GMP^{2-}}\right) \cdot a\left(\mathrm{H^+}\right)}{c\left(\mathrm{GMP^-}\right)} \tag{6}$$

$$K_3^{\text{mix}} = \frac{c\left(\mathrm{GMP^{3-}}\right) \cdot a\left(\mathrm{H^+}\right)}{c\left(\mathrm{GMP^{2-}}\right)}$$

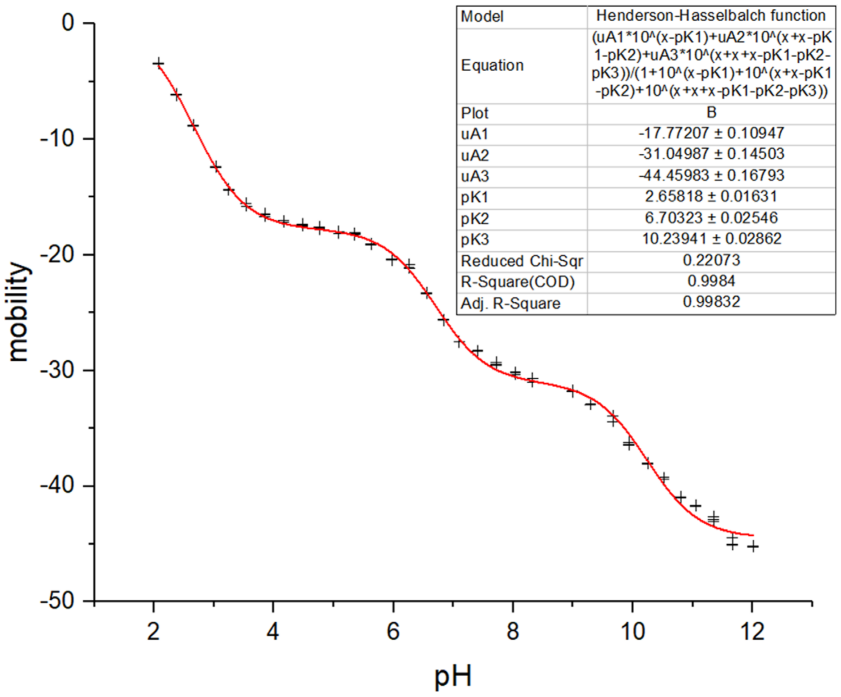

Figure 1. Origin's output of nonlinear regression analysis of effective mobility dependence on pH of the BGE for GMP. Crosses: experimental data. Curve: fitting function. The Henderson-Hasselbalch fitting function and fitted parameters are depicted in the inlay.

According to equation Eq. (1), the activity coefficients for mono-, di- and three-valent ions for the electrolytes with ionic strengths I of 0.01 mol/L are: $\gamma_1 = 0.9051$, $\gamma_2 = 0.6712$, $\gamma_3 = 0.4078$, respectively. The true thermodynamic dissociation constants are expressed exclusively by means of activities, $a_i = \gamma c_i$, instead of concentrations. The relation between the thermodynamic K_z and apparent K_z^{mix} mixed dissociation constants is therefore $K_1 = \gamma_1 K_1^{mix}$, $K_1 = \frac{\gamma_2}{\gamma_1} K_2^{mix}$, $K_3 = \frac{\gamma_3}{\gamma_2} K_3^{mix}$, so correspondingly for pKa constants

$$\begin{aligned} \mathrm{pK}_1 &= \mathrm{pK}_1^{mix} - \log(\gamma_1) \\ \mathrm{pK}_2 &= \mathrm{pK}_2^{mix} - \log(\gamma_2) + \log(\gamma_1) \\ \mathrm{pK}_3 &= \mathrm{pK}_3^{mix} - \log(\gamma_3) + \log(\gamma_2) \end{aligned} \quad (7)$$

Using formulas in Eqs. (7) the corrected pKa values for GMP are: $\mathrm{pK}_1 = 2.7015$, $\mathrm{pK}_2 = 6.8331$, $\mathrm{pK}_3 = 10.4558$.

4.1.2 Correction of mobilities

All data on mobilities in this paper is given in electrophoretic units, that is, 10^{-9} $\mathrm{m^2V/s}$. The correction of mobilities for zero ionic strength was accomplished by manual iteration by means of the PeakMaster software. In PeakMaster we first input as the BGE a highly alkaline electrolyte composed of lithium hydroxide to assure that any anionic analyte will be fully dissociated. The concentration of lithium used was 10.130 mM to achieve an ionic strength of 10.000 mM. Then we build the GMP as the analyte by steps, starting from a hypothetical univalent form. We entered the value 2.7015 obtained in the above paragraph as the pKa(-1) and manually iteratively adjusted the limiting mobility u(-1) to obtain the effective mobility of the compound of –17.772, as fitted by Origin, see Fig. 1. The resulting limiting mobility u(-1) was 20.538. These actions were repeated when adding the second and third valency with pKa 6.8331 and 10.4558, successively. The resulting corrected mobilities are u(-1) = 20.538, u(-2) = 37.178, u(-3) = 55.620.

4.2 Procedure by AnglerFish

The same set of 99 couples of the measured pH of 33 BGEs including their compositions and corresponding measured effective mobilities of GMP were placed into the window of the AnglerFish environment, see Fig. 2.

The software then requires initial estimates of mobilities of all ionic forms, here say 45, 27, and 17, and pKa constants, here say 10.4, 6.7, and 2.8. The calculation of limiting mobilities and thermodynamic constants is carried out by simply clicking the Fit button. The resulting graphical window is shown in Fig. 3, the fitted parameters in Fig. 4.

Notice that the blue squares in Fig. 3 are the fitted values of the actual effective mobilities. They do not have to necessarily form a smooth curve (when using BGEs with different ionic strengths) as it was in the classic procedure, where the fitting function was the Henderson-Hasselbalch function.

The comparison of the limiting values obtained by both approaches is shown in Table 2.

4.3 Discussion

It is obvious from Table 2 that all results obtained by AnglerFish have lower standard deviations. It is a natural consequence of the fact that the Henderson-Hasselbalch function is exact only for true thermodynamic dissociation

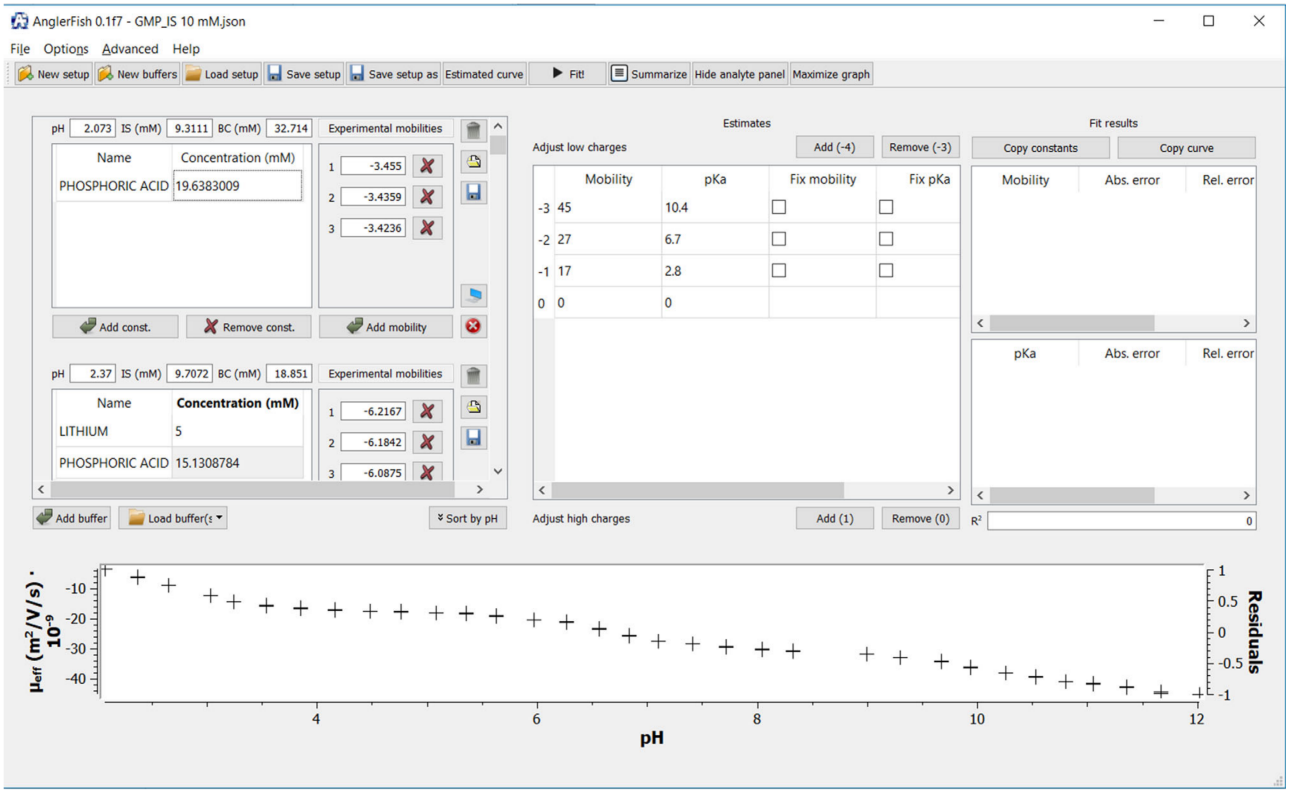

Figure 2. Input window of AnglerFish. Crosses: experimental data. Subwindows in the upper left corner: compositions of BGEs. Subwindow in the middle upper part: initial estimates.

Table 2. Limiting ionic mobilities and thermodynamic pKa constants. In the classic approach: first fitted by Origin, then manually corrected. In the AnglerFish approach: fitted directly

	Classic approach		AnglerFish	
	Mobility	S.D.	Mobility	S.D.
u_1	20.538	0.109	20.696	0.034
u_2	37.178	0.145	38.140	0.050
u_3	55.620	0.168	57.458	0.051
	pKa	S.D.	pKa	S.D.
pK_1	2.7015	0.0163	2.6986	0.0048
pK_2	6.8331	0.0255	6.7638	0.0080
pK_3	10.4558	0.0286	10.2056	0.0093
R^2		0.99832		0.99947

R^2: coefficient of determination.

constants and limiting ionic mobilities. Thus, it does not fit the experimental data correctly before its correction to the thermodynamic (limiting) values.

Moreover, as a matter of fact, any effective mobility obtained by measurement is dependent more or less on all parameters of the compound. Therefore, it is not entirely right to correct the values of the actual ionic mobilities and apparent pKa constants for zero ionic strength independently, one by one, as is done in the classic procedure.

There is one more important aspect of using AnglerFish which employs the Onsager-Fuoss correction procedure described in Ref. [3]. As already mentioned, this procedure considers the mixture effect. In alkaline BGEs at pH around 12 or more, the anions are composed mostly of highly mobile hydroxide ions. The mixture effect of fast hydroxide ions speeds up the negative GMP^{3-} ions, so their mobility is extraordinarily higher. This is well recognized by AnglerFish and the fitted points lie close to experimental points at a high pH of around 12. On the other hand, in the classic approach by Origin the fitted curve deviates from the experimental points in this region; compare Figs. 1 and 3.

Another advantage of the proposed approach is that the buffers in the set need not necessarily have the same ionic strength as each of them is treated individually. This is especially useful for buffers with either highly acidic or highly alkaline pH, for example, it is principally impossible to prepare a buffer for pH less than two having the ionic strength equal to or less than 0.01 mol/L.

As mentioned above, the input data for AnglerFish regarding buffers is simply the compositions of these buffers. The software includes the same database of pKa constants and mobilities of many constituents, as Simul and PeakMaster have–the Hirokawa database. From the composition of the buffer can be then calculated its corresponding pH. However,

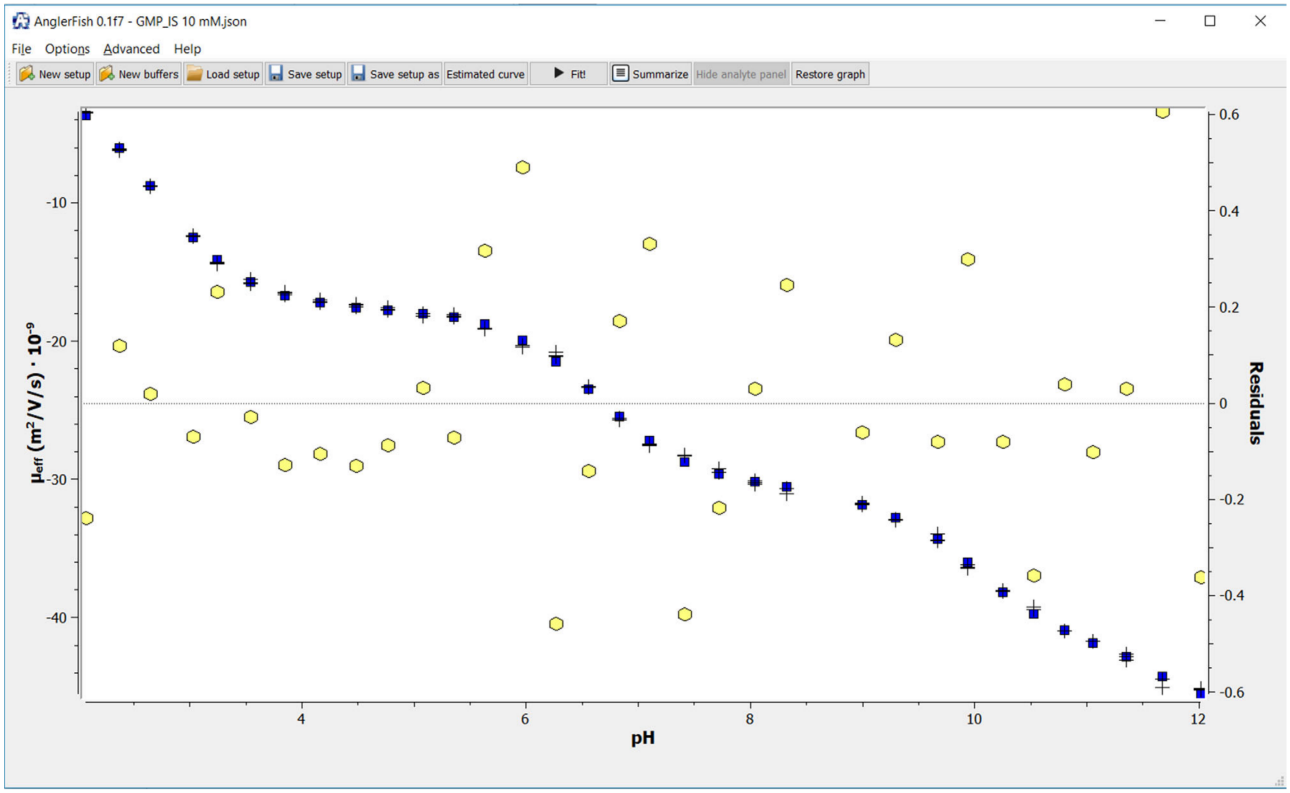

Figure 3. Output graphical window of AnglerFish. Crosses: experimental data. Full squares: fitted mobilities, values on left axis. Hexagons: residuals of the fit, values on right axis.

Fit results

Copy constants | Copy curve

	Mobility	Abs. error	Rel. error (%)
-3	57.4576	0.0507771	0.0883732
-2	38.1399	0.0500545	0.131239
-1	20.6956	0.0336282	0.16249

	pKa	Abs. error	Rel. error (%)
-3	10.2056	0.00926394	0.0907734
-2	6.76373	0.00795214	0.11757
-1	2.69858	0.00482898	0.178946

R^2 0.99947

Figure 4. Output window of AnglerFish – fitted limiting mobilities and thermodynamic constants together with their standard deviations. R^2: coefficient of determination.

the calculated pH may differ from the pH measured. Moreover, often some chemicals used for the preparation of buffers cannot be weighed with maximum precision, especially liquid chemicals, such as phosphoric or acetic acid. Therefore, we decided to adopt the following strategy: (i) the pH measured by a calibrated pH meter and (ii) the amount of one of the constituents of the buffer, the one which can be reliably weighed, are the basic entries of the buffer composition. The corresponding amount of the second constituents of the buffer is calculated by the software. This way we are able to reach the maximum correctness of the input data.

To the authors' best knowledge, when utilizing the Onsager-Fuoss correction, Eqs. (2–5), the ionic strength of all used buffers should not exceed 20 mM to achieve acceptable accuracy. As we came to recognize, for a higher ionic strength and charge numbers of measured compounds higher than two the correction can fail and yield deviated results.

5 Concluding remarks

We have introduced an improved method for the determination of thermodynamic acidity dissociation constants and limiting ionic mobilities by the nonlinear fit of effective mobility versus buffer composition dependence. The method uses the extended Debye-Hückel model and Onsager-Fuoss law with no simplifications and does not require maintaining constant ionic strength in all experiments. We devised a computer program that performs the necessary calculations in a fully automated fashion. The user input consists of the buffer composition and experimentally measured effective mobilities.

The authors gratefully acknowledge the financial support of the Czech Science Foundation, GAČR Grant No. 18–11776S, Agilent Technologies Research Gift No. 4135, and the CEEPUS project No. CIII-RO-0010-13-1819.

The authors have declared no conflict of interest.

6 References

[1] Debye, P., Hückel, E., *Physik. Z.* 1923, *24*, 185–206.

[2] Debye, P., Hückel, E., *Physik. Z.* 1923, *24*, 305–325.

[3] Onsager, L., Fuoss, R. M., *J. Phys. Chem.* 1932, *36*, 2689–2778.

[4] Robinson, R. A., Stokes, R. H., *Electrolyte Solutions*, Dover Publications, Mineola, New York, 2nd revised ed., 2002.

[5] Hirokawa, T., Kiso Y., *J. Chromatogr.* 1982, *248*, 341–362.

[6] Hirokawa, T., Nishimo, M., Aoki, N., Kiso, Y., Sawamoto, Y., Yagi, T., Akiyama, J., *J. Chromatogr.* 1983, *271*, D1–D106.

[7] Hirokawa, T, Kiso, Y., *J. Chromatogr.* 1982, *252*, 33–48.

[8] Hirokawa, T., Nishino, M., Kiso, Y., *J. Chromatogr.* 1982, *252*, 49–65.

[9] Hirokawa, T., Kobayashi, S., Kiso, Y. *J. Chromatogr.* 1985, *318*, 195–210.

[10] Hirokawa, T., Gojo, T., Kiso, Y., *J. Chromatogr.* 1986, *369*, 59–81.

[11] Hirokawa, T., Tsuyoshi, T., Kiso, Y., *J. Chromatogr.* 1978, *408*, 27–41.

[12] Hirokawa, T., Gojo, T., Kiso, Y., *J. Chromatogr.* 1987, *390*, 201–223.

[13] Hirokawa, T., Kiso, Y., Gaš, B., Zusková, I., Vacík, J., *J. Chromatogr.* 1993, *628*, 283–308.

[14] Onsager, L., *Phys. Z.* 1927, *28*, 277.

[15] Beckers, J. L., Everaerts, F. M., Ackermans, M. T., *J. Chromatogr.* 1991, *537*, 407–428.

[16] Cai, J., Smith, J. T., El Rassi, Z., *J. High Resol. Chromatogr.* 1992, *15*, 30–32.

[17] Poole, S. K., Patel, S., Dehring, K., Workman, H., Poole, C. F., *J. Chromatogr. A* 2004, *1037*, 445–454.

[18] Šolínová, V., Kašička, V., Koval, D., Česnek, M., Holý, A., *Electrophoresis* 2006, *27*, 1006–1019.

[19] Nowak, P., Wozniakiewicz, M., Koscielniak, P., *J. Chromatogr A* 2015, *1377*, 1–12.

[20] Koval D., Kašička, V., Jiráček, V., Collinsová, M., *Electrophoresis* 2003, *24*, 774–781.

[21] Včeláková, K., Zusková, I., Kenndler, E., Gaš, B., *Electrophoresis* 2004, *25*, 309–317.

[22] Andrasi, M., Buglyo, P., Zekany, L., Gaspar, A., *J. Pharm. Biomed. Analysis* 2007, *44*, 1040–1047.

[23] Aupiais, J., Delorme, A., Baglan, N., *J. Chromatogr. A* 2003, *994*, 199–206.

[24] Li, D., Fu, S., Lucy, C. A., *Anal. Chem.* 1999, *71*, 687–699.

[25] Pitts, D., *Proc. R. Soc. Lond. A* 1953, *217*, 43–70.

[26] Tůmová, T., Monincová, L., Čeřovský, V., Kašička, V., *Electrophoresis* 2016, *37*, 3186–3195.

[27] Šlampová, A., Boček, P., *Electrophoresis* 2008, *29*, 538–541.

[28] Šlampová, A., Křivánková, L., Gebauer, P., Boček, P., *J. Chromatogr. A* 2009, *1216*, 3637–3641.

[29] Jaroš, M., Včeláková, K., Zusková, I., Gaš, B., *Electrophoresis* 2002, *23*, 2667–2677.

[30] Jaroš, M., Hruška, V., Štědrý, M., Zusková, I., Gaš, B., *Electrophoresis* 2004, *25*, 3080–3085.

[31] Hruška, V., Riesová, M., Gaš, B., *Electrophoresis* 2012, *33*, 923–930.

[32] Malý, M., Dovhunová, M., Dvořák, M., Gerlero, G. S., Kler, P. A., Hruška V., Dubský, P., *Electrophoresis* 2019, *40*, 683–692.

[33] Hruška, V., Jaroš, M., Gaš, B., *Electrophoresis* 2006, *27*, 984–991.

[34] Davies, C. W., *Ion Association*, Butterworths, London, 1962.

[35] Levenberg, K., *Quart. Appl. Math.* 1944, *2*, 164–168.

[36] Marquardt, D. W., *J. Soc. Indust. Appl. Math.* 1963, *11*, 431–441.

[37] https://echmet.natur.cuni.cz/

[38] https://github.com/echmet/AnglerFish

[39] Dubský, P., Ördögová, M., Malý, M., Riesová, M., *J. Chromatogr. A* 2016, *1445*, 158–165.

Publication IV

Martin Ansorge[1]
Bohuslav Gaš[1]
Milan Boublík[1]
Michal Malý[1]
Jana Šteflová[1,2]
Vlastimil Hruška[2]
Gyula Vigh[3]

[1]Department of Physical and Macromolecular Chemistry, Faculty of Science, Charles University, Prague, Czech Republic
[2]Agilent Technologies Deutschland GmbH, Waldbronn, Germany
[3]Chemistry Department, Texas A&M University, College Station, TX, USA

Received October 4, 2019
Revised November 5, 2019
Accepted November 7, 2019

Research Article

CE determination of the thermodynamic pK_a values and limiting ionic mobilities of 14 low molecular mass UV absorbing ampholytes for accurate characterization of the pH gradient in carrier ampholytes-based IEF and its numeric simulation

Fourteen low molecular mass UV absorbing ampholytes containing 1 or 2 weakly acidic and 1 or 2 weakly basic functional groups that best satisfy Rilbe's requirement for being good carrier ampholytes ($\Delta pK_a = pKa_{monoanion} - pKa_{monocation} < 2$) were selected from a large group of commercially readily available ampholytes in a computational study using two software packages (ChemSketch and SPARC). Their electrophoretic mobilities were measured in 10 mM ionic strength BGEs covering the $2 < pH < 12$ range. Using our Debye-Hückel and Onsager-Fuoss laws-based new software, AnglerFish (freeware, https://echmet.natur.cuni.cz/software/download), the effective mobilities were recalculated to zero ionic strength from which the thermodynamic pK_a values and limiting ionic mobilities of the ampholytes were directly calculated by Henderson-Hasselbalch equation-type nonlinear regression. The tabulated thermodynamic pK_a values and limiting ionic mobilities of these ampholytes (pI markers) facilitate both the overall and the narrow-segment characterization of the pH gradients obtained in IEF in order to mitigate the errors of analyte ampholyte pI assignments caused by the usual (but rarely proven) assumption of pH gradient linearity. These thermodynamic pK_a and limiting mobility values also enable the reality-based numeric simulation of the IEF process using, for example, Simul (freeware, https://echmet.natur.cuni.cz/software/download).

Keywords:
Capillary isoelectric focusing / Limiting ionic mobility / pH Gradient linearity / pI Marker / Thermodynamic acid dissociation constant
DOI 10.1002/elps.201900381

1 Introduction

According to a seminal paper of Rilbe [1], for a successful IEF separation in a natural pH gradient, the following conditions have to be met. First, the anode compartment of the electrophoretic device has to be filled with an acidic solution (the anolyte, e.g. 20 mM H_3PO_4). Second, the separation compartment has to be filled with a mixture of carrier ampholytes (ampholytes for which it holds that $\Delta pK_a = pKa_{monoanion} - pKa_{monocation} < 2$). Third, the cathode compartment has to be filled with a base (the catholyte, e.g. 20 mM NaOH). Fourth, convective disturbances have to be absent or suppressed in the system (either by using an anti-convective medium or a capillary as the separation compartment). Fifth, a sufficiently large DC voltage has to be applied between the anode and the cathode for a sufficiently long period of time to allow any and all of the initially cationic and anionic carrier ampholytes in the mixture to migrate out of sections of the separation compartment in which the local pH value is different from their isoelectric point value. (Since Rilbe considered the isoelectric point value to be very close to the isoprotic point value–which he calculated as $(pKa_{monocation} + pKa_{monoanion})/2$–the symbol p$I$, and the term p$I$ value, became loosely–and interchangeably–used in the literature to designate either "iso" value.)

Once all these conditions are fulfilled, adjacent, individual carrier ampholyte bands form across the separation compartment such that the pH in the successive bands increases

Correspondence: Prof. Bohuslav Gaš, Department of Physical and Macromolecular Chemistry, Faculty of Science, Charles University, Prague, Czech Republic
E-mail: bohuslav.gas@natur.cuni.cz

Abbreviations: **3MHIS**, 3-methylhistidine; **DNS-Cl**, dansylchloride; **DNS-IDA**, dansylated iminodiacetic acid; **GLYHIS**, glycyl-histidine; **ICIEF**, Imaging capillary isoelectric focusing; **IDA**, iminodiacetic acid; **LAB**, labetalol; **LBB**, Leucoberbelin blue I dye; **SERO**, serotonin

Color online: See the article online to view Figs. 1, 3–5 in color.

monotonously from that in the anolyte to that in the catholyte. If the concentration of the carrier ampholyte in its band is sufficiently high, the pH approaches the isoprotic/isoelectric value of the individual carrier ampholyte such that, to quote Rilbe [2], "... my contemplated pH gradients should be stable indefinitely.".

When a number of ampholytic analyte molecules are mixed with the carrier ampholytes prior to the separation, they also participate in the formation of the natural pH gradient and end up in segments of the separation compartment where the pH corresponds to their respective p*I* value. Since the p*I* value (however defined) of an ampholytic analyte is considered an important material characteristic, it would be valuable if it could be obtained from the IEF experiment itself. It is possible to take fractions from the focused carrier ampholyte train when IEF is carried out in a conventional density gradient column (even when it is miniaturized, see, e.g. [3]) or in a multicompartmental electrolyzer (see, e.g. [4]), or in a free-flow electrophoretic device (see, e.g. [5]) and measure their pH. One can also measure, post focusing, the pH along the surface of an IEF gel with a specialized glass electrode (see, e.g. [6]). However, there is no convenient direct way to do either of these when the separation compartment is a capillary, even if the focusing position of the analyte band is detectable. The usual solution to this conundrum is an indirect one: two or more additional ampholytes with known p*I* values (the so-called p*I* markers) that are readily detectable at the end of the IEF process (by whatever detector is used in the instrument) are added to the carrier ampholyte mixture and their known p*I* values are plotted against their relative focusing positions between the anode and the cathode. The resulting graph is deemed to represent the shape of the pH profile in the separation compartment and is commonly referred to as the pH gradient. Being an indirect method, the accuracy of this representation is ill-defined and depends on the often assumed–yet rarely proven–local linearity of the pH gradient between the adjacent p*I* markers. In principle, the use of a larger number of p*I* markers can lead to a more accurate the description of the shape of the pH gradient.

Historically, both proteins and small ampholytic molecules with consensus p*I* values have been used as p*I* markers (for an extensive list of early references and their fair critique, see, e.g. [7]). In CIEF, the use of small ampholytic markers is preferred, because multiple analytical methods can be applied for the determination and cross-validation of their p*I* values. In addition to finding such p*I* markers by scouring catalogues of fine chemicals (see, e.g. [8]), many groups have synthesized families of p*I* markers such as, e.g. substituted nitrophenols [7, 9–11], monoalkylpiperidine amides of fluorescein [12], azo dyes [13], oligopeptides [6, 14], and ampholytic trisulfonamido pyrenes [15].

Most of the time, the pK_a values associated with the monocationic and monoanionic forms of the p*I* markers are determined experimentally and the p*I* values are calculated as their arithmetic average according to Rilbe's equation (vide supra), yielding the isoprotic point value. The respective pK_a values can be obtained, among others, from potentiometric titrations (see, e.g. [7]), pH-dependent spectroscopic measurements (see, e.g. [12, 13]) or pH-dependent capillary electrophoretic effective mobility measurements (see, e.g. [16–18]). Alternatively, the p*I* value can be determined directly from pH-dependent pressure-mediated capillary electrophoretic measurements [19] (which can also provide the respective pK_a and limiting electrophoretic mobility values of the p*I* markers).

Table 1. Stock BGE compositions and their corresponding pH ranges, c_{stock} stands for concentration of the stock solution

Buffering constituent	c_{stock} mol/dm^3	Titrant	pH range
Phosphoric acid	0.5	–	2
Phosphoric acid	0.5	LiOH	2.30–3.00
Formic acid	1	LiOH	3.00–4.00
Acetic acid	2	LiOH	4.00–5.15
MES	0.5	LiOH	5.15–6.15
MOPS	0.5	LiOH	6.15–7.30
Tricine	1	LiOH	7.30–8.50
CHES	1	LiOH	8.50–9.50
β-Alanine	1	LiOH	9.50–11.70
Lithium	0.5	–	11.70–12.00

The first objective of the work reported in this paper was to identify a set of low molecular mass p*I* markers suitable for characterization of the pH gradient in the 3 < pH < 10 range that (i) have well-defined structure and contain no more than two acidic and two basic functional groups, (ii) are commercially available (or are very easy to prepare) with adequate purity, at relatively low cost. The second objective was then to determine their respective thermodynamic pK_a and limiting electrophoretic mobility values to facilitate their use (i) for characterization of the shape of the pH gradient in IEF and, (ii) in reality-based numeric simulation of IEF separations with programs such as Simul [20, 21] (freeware, https://echmet.natur.cuni.cz/software/download).

2 Materials and methods

2.1 Chemicals

2.1.1 BGEs

Water used for the preparation of all solutions was purified by Rowapur and Ultrapur (Watrex, San Francisco, CA, USA). The BGE constituents were chosen to buffer in the 2 < pH < 12 range. BGEs were prepared by mixing appropriate amounts of the stock solutions shown in Table 1 according to PeakMaster 6 [22] (freeware, https://echmet.natur.cuni.cz/software/download), and then diluted with deionized water to 10 mM ionic strength. In all cases, 0.5 M lithium hydroxide was used as the titrant, except at pH 2 where pure phosphoric acid and at pH 12 where

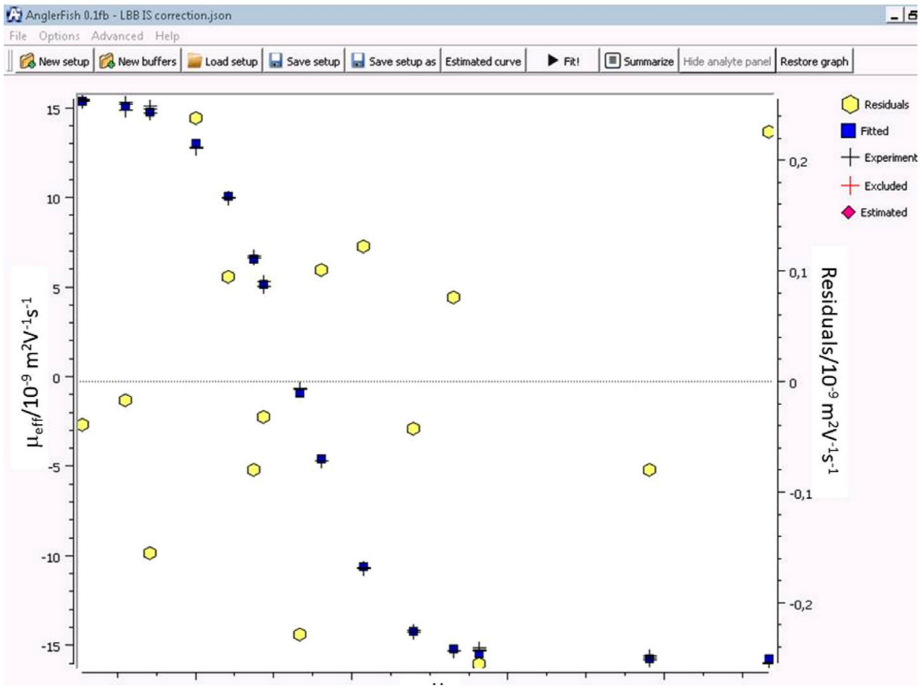

Figure 1. Comparison of the measured effective mobility values (symbol black +) and those calculated by AnglerFish (symbol blue square) using the thermodynamic pK_a and limiting ionic mobility values of Leucoberbelin Blue I, LBB (left vertical axis) as a function of pH (horizontal axis). The yellow hexagon symbols show the residuals, that is, the differences between the average experimental values and the calculated values (right vertical axis, in 10^{-9} $m^2/V/s$ units).

pure lithium hydroxide were used. All BGEs were filtered through 0.45 µm syringe filters (Whatman, GE Healthcare, Chicago, IL, USA). All chemicals used for the stock solutions were of analytical grade purity. Phosphoric acid was purchased from Lachema (Brno, Czech Republic), formic acid, acetic acid (AcOH), MES, MOPS, *N*-(2-hydroxy-1,1-bis(hydroxymethyl)ethyl)glycine (Tricine), CHES, β-alanine and lithium hydroxide were supplied by Sigma-Aldrich (Prague, Czech Republic). The pH of every BGE was measured by a PHM 240 pH/ION Meter (Radiometer Analytical, HACH, Loveland, CO, USA), calibrated with IUPAC buffers of pH 1.679, 4.005, 7.000, 10.012, and 12.450 (Radiometer, Copenhagen, Denmark).

2.1.2 Commercially available low molecular mass ampholytes used as p*I* markers

These ampholytes were purchased from Sigma-Aldrich (Prague, Czech Republic). Their names and abbreviations (in parentheses) are as follows: 3-methylhistidine (3MHIS), 4-(4-aminophenyl)butyric acid, epinephrine (EPI), glycylhistidine (GLYHIS), labetalol (LAB), leucoberbelin blue I dye (LBB), metanephrine (MEPI), norepinephrine (NEPI), serotonin (SERO), and tyramine (TYRA) (purchased as chloride salt).

2.1.3 p*I* markers prepared by dansylation of amino acids

Aspartic acid (ASP), γ-aminobutyric acid, glutamic acid, and iminodiacetic acid (IDA), were dansylated by dansylchloride (DNS-Cl) (all from Sigma-Aldrich, Prague, Czech Republic) according to the procedure in [23] yielding dansylated ASP, dansylated GABA, dansylated GLU, and dansylated IDA (DNS-IDA). Briefly, a 1 mM stock solution of the selected amino acid was prepared in 40 mM aqueous lithium carbonate and its pH was adjusted to 9.2 with hydrochloric acid. A 5.5 mM DNS-Cl solution was prepared in acetonitrile (Sigma-Aldrich, Prague, Czech Republic) and 1 mL of it was added rapidly to 2 mL of the amino acid stock solution, mixed for 2 min, then kept in a dark place at room temperature for 60 min. Subsequently, the reaction mixture was applied onto a silica gel column, hydrolysed DNS-Cl was removed from it with a 1:4 methanol:chloroform eluent, followed by the elution of the dansylated amino acid by a 1:1 methanol:chloroform eluent, while the inorganic compounds stayed on the silica gel.

2.2 Capillary electrophoretic experiments

The effective electrophoretic mobilities of the p*I* markers in different pH BGEs were measured by CE using an Agilent CE 7100 system equipped with a diode array detector and operated via ChemStation software (Agilent Technologies, Waldbronn, Germany). In order to minimize analyte-capillary wall interactions, multiple capillaries with different inner surface coatings were used including (i) bare fused silica capillaries (50 µm i.d., 56 and 71.5 cm effective lengths), (ii) fluorocarbon-coated µSil capillaries (75 µm i.d., 56 cm effective length) and PVA-coated capillaries (50 µm i.d., 56 cm effective length, all from Agilent Technologies, Waldbronn, Germany), and (iii) dynamically-coated triple layer Polybrene

Table 2. Thermodynamic pK_a data and their respective standard deviations for the p*I* markers calculated by AnglerFish from the experimentally measured pH-dependent effective mobilities. Values marked with asterisk (*) are values estimated with insufficient accuracy due to too few data points at high pH. pK_{CC}, pK_C, pK_A, and pK_{AA} denote the pK_a of the +2, +1, –1, and –2 charged species, respectively. Values in the last three columns were calculated as $\Delta pK_a = pK_A - pK_C$ [1], $-dz/dpH = \ln(10)/(1 + 0.5(10^{(pK_A - pK_C)/2)})$ [7] and $pI = (pK_A + pK_C)/2$ [1], respectively

Name	pK_{CC}	σ	pK_C	σ	pK_A	σ	pK_{AA}	σ	ΔpK_a	$-dz/dpH$	p*I*
DNS-IDA	–	–	2.30	0.07	3.68	0.09	4.84	0.09	1.38	0.67	2.99
DNS–ASP	–	–	2.75	0.01	3.93	0.02	5.13	0.02	1.18	0.78	3.34
DNS–GLU	–	–	2.96	0.02	4.02	0.03	5.29	0.04	1.06	0.85	3.49
DNS–GABA	–	–	3.57	0.01	4.83	0.01	12.53*	–	1.26	0.73	4.20
4APBA	–	–	4.26	0.01	5.45	0.01	–	–	1.19	0.78	4.86
LBB	–	–	4.70	0.01	5.83	0.01	–	–	1.13	0.81	5.27
GLYHIS	2.22	0.06	6.77	0.01	8.32	0.01	–	–	1.55	0.58	7.55
3MHIS	2.04	0.4	6.50	0.01	8.91	0.01	–	–	2.41	0.26	7.71
LAB	–	–	7.32	0.01	9.65	0.01	–	–	2.33	0.28	8.49
NEPI	–	–	8.62	0.04	9.80	0.05	–	–	1.18	0.78	9.21
EPI	–	–	8.62	0.03	10.02	0.07	12.88*	–	1.40	0.66	9.32
MEPI	–	–	9.11	0.01	10.33	0.03	–	–	1.22	0.76	9.72
TYRA	–	–	9.50	0.04	10.84	0.05	–	–	1.34	0.69	10.17
SERO	–	–	10.01	0.02	11.15	0.03	–	–	1.14	0.81	10.58

4APBA, 4-(4-aminophenyl)butyric acid; DNS-ASP, dansylated aspartic acid; 3MHIS, 3-methylhistidine; DNS-GABA, dansylated γ-aminobutyric acid; DNS-GLU, dansylated glutamic acid; DNS-IDA, dansylated iminodiacetic acid; EPI, epinephrine; GLYHIS, glycyl-histidine; LAB, labetalol; LBB, Leucoberbelin blue I dye; MEPI, metanephrine; NEPI, norepinephrine; SERO, serotonin; TYRA, tyramine

capillaries (50 µm i.d., 71.5 cm effective length, made in our laboratory according to [24]. Briefly, a bare fused silica capillary was rinsed with 1 M NaOH (Sigma-Aldrich, Prague, Czech Republic) solution for 30 min, then with deionized water for 10 min, then sequentially with aqueous 5%, w/v Polybrene, 3%, w/v dextran sulfate and again with 5%, w/v Polybrene solutions for 20 min each.

All CE experiments were performed at a constant 25°C temperature and +15 kV voltage (except with the Polybrene-coated capillary, where –15 kV was used). All capillaries were preconditioned prior to the CE measurements: the bare fused silica capillaries were rinsed with 0.1 M NaOH solution for 10 min, deionized water for another 10 min and with the respective BGEs for 5 min, whereas the fluorocarbon- and PVA-coated capillaries were rinsed with 10 mM phosphoric acid prior to deionized water, 10 min each. When switching BGEs, the capillaries were flushed with the new BGE for 5 min, then for 1 min before each run. The sample was an aqueous solution of the analyte at a concentration of 0.1 mg/mL and 0.08%, v/v DMSO as an EOF marker. The sample was injected by applying 20 mbar pressure for 5 s. All measurements were performed in triplicates.

2.3 Imaging capillary isoelectric focusing experiments

Imaging capillary isoelectric focusing (ICIEF) experiments were carried out on a CEInfinite instrument equipped with an on-line whole column imaging detector operating at 280 nm wavelength (Advanced Electrophoresis Solutions, Cambridge, ON, Canada). The separation cassette contained a 100 µm i.d. fluorocarbon-coated capillary (50 mm scanned length) between the two electrode reservoirs (containing 0.3 M phosphoric acid and 0.2 M lithium hydroxide, respectively). IDA and arginine (ARG), used as sacrificial ampholytes [25] were purchased from Sigma-Aldrich (Prague, Czech Republic).

The carrier ampholyte stock solution consisted of 5 mL of 0.25%, w/v aqueous methylcellulose (1500 cP / 2%, w/w, aq) solution, 300 µL of 0.2 M IDA (anodic sacrificial ampholyte [25]), 100 µL of 0.5 M ARG (cathodic sacrificial ampholyte [25]), and 150 µL of AES SH 3–10 carrier ampholyte mixture (Advanced Electrophoresis Solutions Ltd., Cambridge, ON, Canada), resulting in nominal 10.8 mM IDA and 9 mM ARG concentrations in the carrier ampholyte stock solution. A p*I* marker stock solution containing each marker at a concentration of 1 mg/mL was prepared and 1 µL of it was added to 0.5 mL of the carrier ampholyte mixture, resulting in individual p*I* marker concentrations of 2 µg/mL.

The sample-containing carrier ampholyte solutions were filled into the ICIEF capillary manually by introducing 0.8 mL of air into the headspace of the 2 mL sample vial through its tightly closed septum for 3 min. The length of time has been experimentally verified to be sufficient for complete replacement of the content of the whole capillary with a fresh solution. ICIEF measurements were made at ambient temperature. The applied voltage was set to 1 kV for 1 min, followed by a step change to 3 kV for 4 min. Whole column images were taken in 10 s intervals.

Table 3. Limiting ionic mobility data of the p*I* markers calculated by AnglerFish from the experimentally measured pH-dependent effective mobilities. Values marked with asterisk (*) are values estimated with insufficient accuracy due to too few data points at high pH. u_{CC}, u_C, u_A, and u_{AA} stand for the limiting ionic mobility of the +2, +1, –1, and –2 charged species in 10^{-9} $m^2/V/s$ units. Δu is the difference between the absolute values of limiting mobilities of the monocationic and monoanionic species (i.e., $\Delta u = |u_C|-|u_A|$)

Name	u_{CC}	σ	u_C	σ	u_A	σ	u_{AA}	σ	$\Delta u = \|u_C\|-\|u_A\|$
DNS-IDA	–	–	21.6	1.2	−18.6	2.1	−39.4	0.2	3.0
DNS–ASP	–	–	20.9	0.1	−18.4	0.4	−40.5	0.1	2.5
DNS–GLU	–	–	20.6	0.2	−19.2	0.8	−40.0	0.1	1.4
DNS–GABA	–	–	22.0	0.1	−21.3	0.1	−46.7*	–	0.7
4APBA	–	–	26.9	0.1	−26.6	0.1	–	–	0.3
LBB	–	–	18.4	0.1	−18.6	0.1	–	–	−0.2
GLYHIS	51.9	1.8	25.3	0.1	−25.0	0.1	–	–	0.3
3MHIS	42.5	6.8	27.4	0.2	−26.6	0.1	–	–	0.8
LAB	–	–	19.3	0.1	−19.1	0.1	–	–	0.2
NEPI	–	–	26.4	0.3	−26.2	0.6	–	–	0.2
EPI	–	–	25.7	0.2	−22.6	1.3	−50*	–	3.1
MEPI	–	–	25.1	0.1	−20.9	1.1	–	–	4.2
TYRA	–	–	30.0	0.3	−27.0	0.7	–	–	3
SERO	–	–	28.1	0.2	−24.0	0.5	–	–	4.1

4APBA, 4-(4-aminophenyl)butyric acid; DNS-ASP, dansylated aspartic acid; 3MHIS, 3-methylhistidine; DNS-GABA, dansylated γ-aminobutyric acid; DNS-GLU, dansylated glutamic acid; DNS-IDA, dansylated iminodiacetic acid; EPI, epinephrine; GLYHIS, glycyl-histidine; LAB, labetalol; LBB, Leucoberbelin blue I dye; MEPI, metanephrine; NEPI, norepinephrine; SERO, serotonin; TYRA, tyramine.

3 Results and discussion

Based on prior experience with low molecular mass ampholytic p*I* markers in one of our laboratories [17, 19, 25, 26], corroborated by structure-based pK_a predictions by SPARC (SPARC 2018, ARChem, Danielsville, GA, USA, www.archemcalc.com) and ChemSketch (ACD/Labs, 2017.2.1, Advanced Chemistry Development, Toronto, ON, Canada, www.acdlabs.com), a series of relatively inexpensive, commercially available or simple-to-synthesize p*I* marker candidates were selected for the CE measurements of their pH-dependent effective mobilities, from which their pK_a and electrophoretic mobility values could be calculated. However, due to the ionic strength dependence of the measured effective mobilities, a direct nonlinear regression fit of the data by the Henderson-Hasselbalch equation [27] yields only the apparent pK_a and apparent ionic mobilities. Our laboratory recently devised a new model and new software, called AnglerFish [28] (freeware, https://echmet.natur.cuni.cz/software/download), for the direct determination of the thermodynamic pK_a and limiting ionic mobility values of weak electrolytes by nonlinear regression of the experimental data. The program uses the Debye-Hückel [29–31] and Onsager-Fuoss [32] laws to calculate thermodynamic pK_a and limiting ionic mobilities. First, using both the experimentally measured pH and the actual buffer compositions of the set of BGEs as input data, the program recalculates the effective mobilities by the correction engine to the corresponding infinite-dilution, limiting mobility values, followed by nonlinear regression using the Henderson-Hasselbalch equation which yields, in one fit, both the thermodynamic pK_a values and the limiting ionic mobilities. This approach is universally valid within the limitations of the Debye-Hückel and Onsager-Fuoss laws.

As an example, Fig. 1 shows the measured effective mobility values (symbol +) and those calculated by AnglerFish (symbol blue square) using the thermodynamic pK_a and limiting ionic mobility values of Leucoberbelin Blue I, LBB (left vertical axis) as a function of pH (horizontal axis). The yellow hexagon symbols show the residuals, that is, the differences between the average experimental values and the calculated values (right vertical axis, in 10^{-9} $m^2/V/s$ units). Similar graphs were obtained for the other p*I* markers as well.

The calculated thermodynamic pK_a and limiting ionic mobility data of all of the p*I* markers obtained by AnglerFish are shown in Tables 2 and 3. The last three columns in Table 2 list the ΔpK_a and –d*z*/dpH values of the markers (characterizing their focusing ability), along with their p*I* values. Eleven out of the 14 p*I* markers have $\Delta pK_a < 1.5$ values (i.e., they are excellent focusers), the remaining three have acceptable focusing speeds, $1.55 < \Delta pK_a < 2.41$ (GLYHIS, 3MHIS, and LAB). Table 3 lists the limiting ionic mobility data, where u_{CC}, u_C, u_A, and u_{AA} stand for the limiting ionic mobility of the +2, +1, –1, and –2 charged species in 10^{-9} $cm^2/V/s$ units and Δu is the difference between the absolute values of limiting mobilities of the monocationic and monoanionic species (i.e., $\Delta u = |u_C|-|u_A|$). The limiting mobilities of the monocharged ions are in the $18 < |u| < 30$ range (in 10^{-9} $m^2/V/s$ units), in agreement with what is found for similar structures in Hirokawa's database [33] implemented in PeakMaster 6 what is typically used in computer simulations of CIEF, for example, [34]. Interestingly though, and contrary to what is typically used in the numeric simulation of CIEF, the limiting mobilities of the monocations are larger than those of the

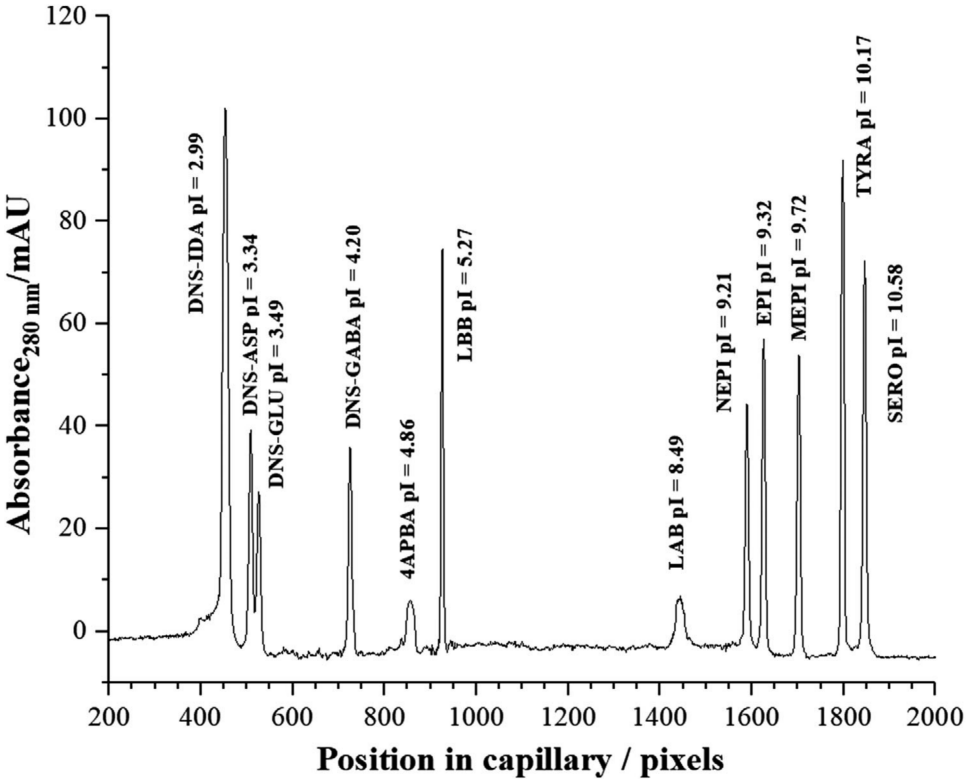

Figure 2. Image of the 12 focused ampholytes detectable at 280 nm and serving as potential p*I* markers, distributed alongside the pH gradient obtained with the SH AES carrier ampholyte mixture. For experimental conditions see Section 2.3.

monoanions (see the last column of Table 3) for 13 out of the 14 p*I* markers studied. For about half of the p*I* markers that mobility difference is as large as 10 to 15%, for the rest it is in the 1 to 2% range.

These p*I* markers were used in CIEF experiments to trace the shape of the pH gradient obtained with the SH AES carrier ampholyte mixture in a CEInfinite instrument. The p*I* markers that are detectable by the full column imaging photometric detector at 280 nm (12 of the 14, since GLYHIS and 3MHIS are not visible at 280 nm, only at 230 nm) were added to the prepared carrier ampholyte solution and focused as described in Section 2.3 The UV absorbance at 280 nm recorded as a function of position in the capillary is shown in Fig. 2. The 50 mm long capillary is imaged across 2050 pixels of the detector. The rise above the steady baseline at 400 pixels indicates that the 0 to 400 pixels portion of the capillary is filled with the focused anodic sacrificial ampholyte, IDA [25]. The initial concentration of IDA in the 2050 pixels long capillary that was 10.8 mM, increased in the 0 to 400 pixels segment to a steady 55.4 mM value (10.8 mM × 2050/400) after focusing. The 190 pixels long section of the capillary between pixels 1860 and 2050 is filled with the cathodic sacrificial ampholyte, ARG, whose 9 mM initial concentration was increased to about 97 mM by the focusing step (9 mM × 2050/190). The p*I* markers are found between 400 and 1860 pixels in the capillary: their names and p*I* values (from Table 2) are listed on the labels next to the respective peaks. Though the concentrations (in mg/mL) of the markers in the feed solution were identical, the peak height values are different due to their different molecular masses, molar absorbances at 280 nm and their slightly different peak widths.

The shape of the pH gradient created from the SH AES carrier ampholyte mixture (Fig. 2) is deduced from the respective p*I* values and peak maximum positions in the capillary of the p*I* markers, as shown in Fig. 3. In the IDA zone (IDA pI = 2.33, symbol red **×**) the pH, calculated by PeakMaster 6 is 2.4 (blue solid line), slightly higher than the p*I* value of IDA, and the buffering capacity is high (57 mM), predicting a sharp boundary between the anodic sacrificial ampholyte (anodic blocker [25]) and the focused carrier ampholyte train. The most acidic p*I* marker, DNS-IDA (pI = 3.02, symbol red **+**) is only about 30 pixels away from this boundary, indicating a relatively steep change in pH (about 0.7) and confirming the absence of significant amounts of carrier ampholytes with pI < 3 in the SH AES 3–10 carrier ampholyte mixture.

At the cathodic side end of the capillary that is filled with ARG (pI = 11.36), the pH calculated by PeakMaster for the 97 mM ARG concentration is only 10.9 (blue solid line), and the buffering capacity is only 4.4 mM, due to the relatively large ΔpK_a of ARG (4.88). Thus, the boundary between the focused carrier ampholyte train and ARG is expected to be less sharp than the boundary with IDA. SERO (pI = 10.61) is a good marker to indicate the beginning of the ARG zone.

Figure 3 shows that the pH gradient between the most acidic p*I* marker, DNS-IDA (pI = 3.02) and the most basic p*I* maker, SERO (pI = 10.61) is nonlinear. One of the factors that leads to this nonlinearity is ITP that is contemporaneous

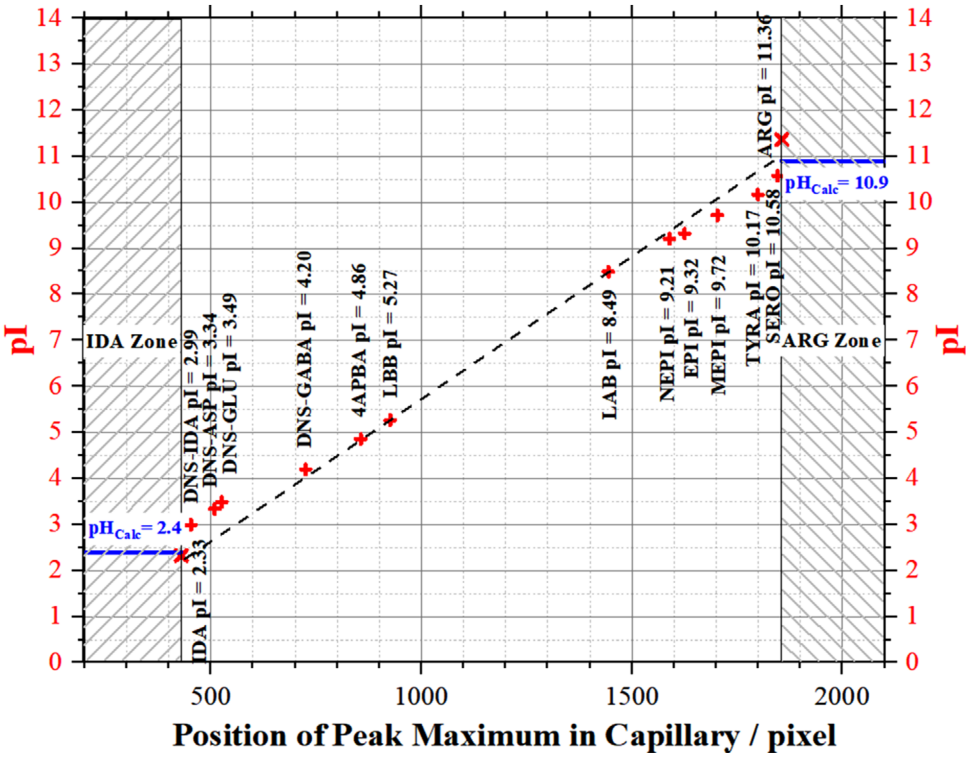

Figure 3. pH profile of the focused SH AES 3–10 carrier ampholyte mixture calculated from the focusing positions of the p*I* markers in Fig. 2 and their p*I* values in Table 2, indicating a nonlinear pH gradient. The rapid increases of pH at the beginning and end of the pH gradient are caused by the boundaries at the IDA- and ARG-filled zones. The pH values in these zones were calculated by PeakMaster using the focused IDA and ARG concentrations (see text) and the pK_a values of IDA from Ref. [35] and of ARG from Ref. [36].

with focusing: it continuously removes the most extreme p*I* components into the respective electrode compartments [34] and over time also alters the width of the focused carrier ampholyte bands. For wide-range carrier ampholytes ($3 <$ p$I < 10$), the extent of change is initially least noticeable in the p*I* range nearest to (and equidistant from) p*I* 7. Thus, by connecting a straight line through the coordinates of the two p*I* markers closest to pH 7 in Fig. 3, LBB (p$I = 5.26$) and LAB (p$I = 8.49$), one can find the approximate slope of the hypothetical linear pH gradient one would find in the absence of ITP, as shown by the black dashed line in Fig. 3. Obviously, the farther away one is from p*I* 7, the shallower the actual slope becomes, until one reaches the boundaries of the anodic and cathodic blockers, wherein there is a rapid change toward the actual pH value of the focused blocker solutions.

The results in Fig. 3 clearly indicate that the common practice of fitting a "best straight line" through the p*I* versus position scatter graph of the focused p*I* makers leads to a systematically incorrect description of the pH profile of the focused carrier ampholyte train.

Since this work provided not only the thermodynamic pK_a values, but also the limiting ionic mobilities, they can be used for reality-based numeric simulation of the IEF process. Therefore, a simulation run was set up using Simul [21]. In the simulation the separation channel had a total length of 72 mm with 1000 grid points and was segmented into three parts in the ratio of 1:6:1. The first and the last parts served as the electrode compartments and contained 0.3 M phosphoric acid and 0.2 M lithium hydroxide, respectively, as anolyte and catholyte. The middle part contained 181 uni-univalent hypothetical carrier ampholytes with increasing values of pK_a, starting from an anionic pK_a of 3.5 to an anionic pK_a of 10.8 with Δp$K_a = 1$ between the anionic and cationic forms, and a pK_a step of 0.0406 for each following ampholyte. The cationic and anionic mobilities of all ampholytes were set to 20×10^{-9} m^2/V/s, their concentrations to 0.1 mM. The p*I* markers occupied the same part of the separation channel as the carrier ampholytes at time zero, but their concentration was set to 0.01 mM. The thermodynamic pK_a and limiting mobility values of the p*I* markers were taken from Tables 2 and 3. The applied voltage was 100 V for 3002 s, which was sufficient for formation of the pH gradient. The results of the simulation are shown in Fig. 4. The tall peaks belong to the carrier ampholytes (only every 10th is shown, starting with the p$I = 3$ one at the IDA zone boundary), the short peaks belong to the 14 p*I* markers, starting with DNS-IDA at the IDA boundary. The pH trace (light purple) shows four plateaus (corresponding to zones of H_3PO_4, IDA, ARG, and LiOH). The horizontal red line shows the maximum possible concentration of any carrier ampholyte that is mostly untouched yet by bidirectional ITP. Notice that the extent of zone expansion–contraction at the low and high p*I* ends of the carrier ampholyte train are different. The pH profile obtained by the simulation and the superimposed p*I* values of the markers from Table 2 and the focusing positions of their peak maxima from Fig. 4 are shown in Fig. 5. Figure 5 closely resembles Fig. 3 indicating that the main source of pH nonlinearity is bidirectional isotachophoresis that accompanies IEF and alters both the concentration and width of the focused carrier ampholyte zones. This effect is more pronounced at the low

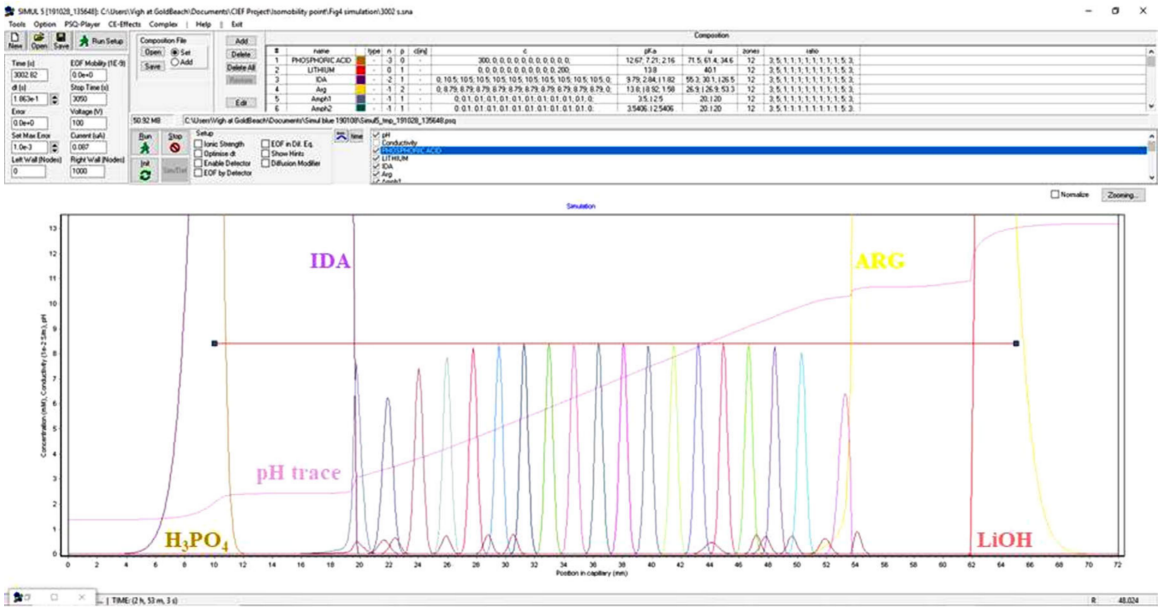

Figure 4. Simulated ICIEF separation of the 14 p*I* markers from Tables 2 and 3. For the simulation conditions, see the text. H_3PO_4 (ochre), IDA (dark purple), ARG (yellow) and LiOH (reddish brown) concentration traces are off-scale, their boundaries pointing toward the middle of the capillary are labeled. pH profile: light purple trace. Tall peaks: carrier ampholytes, every 10th is shown, starting at p*I* 3. Low peaks: 14 p*I* markers of this study starting with DNS-IDA (p*I* = 2.99). For direct compatibility with Fig. 2 (experimental CIEF trace), p*I* markers GLYHIS and MHIS that are not detectable at 280 nm are not shown. Horizontal red line: maximum concentration of carrier ampholyte peaks mostly unaffected yet by ITP.

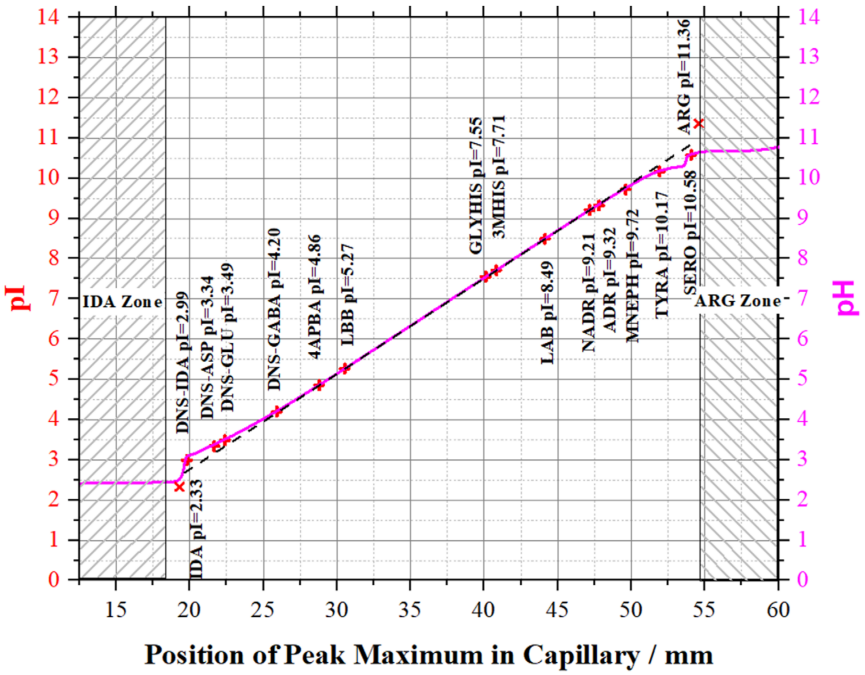

Figure 5. pH profile calculated during simulation of the ICIEF separation of the p*I* markers in Fig. 4 along with the superimposed p*I* values from Table 2.

and high pH extremes of the pH gradient. The agreement between Fig. 3 (obtained with an actual carrier ampholyte mixture SH AES 3–10) and Fig. 5 (obtained with a hypothetical, ideal carrier ampholyte mixture containing only 181 species) is remarkable and reinforces the notion that the practice of using a linear model to describe the shape of the pH gradient is untenable.

4 Concluding remarks

The pH-dependent electrophoretic mobilities of 14 low molecular mass UV absorbing ampholytes containing 1 or 2 weakly acidic and 1 or 2 weakly basic functional groups (p*I* markers) were measured by CE in 10 mM ionic strength background electrolytes in the $2 < pH < 12$ range. The measured

effective mobilities were recalculated to zero ionic strength from which the thermodynamic pK_a values and limiting ionic mobilities of the p*I* markers were directly calculated by a Henderson-Hasselbalch equation-type nonlinear regression with the help of our Debye-Hückel and Onsager-Fuoss laws-based new software, AnglerFish. Except for LAB, all of the p*I* markers that can be detected at 280 nm have $\Delta pK_a < 1.5$ and $-dz/d(pH) > 0.66$, that is, they are rapid focusers. The thermodynamic pK_a values and limiting ionic mobilities of 12 of the 14 markers that are visible at 280 nm were used to characterize the shape of the pH gradients obtained in full column imaging isoelectric focusing experiments. They also enabled the numeric simulation of the IEF process of a hypothetical ideal carrier ampholyte mixture with Simul and revealed that the nonlinearities experimentally observed with an actual carrier ampholyte mixture and in a simulated ICIEF system with a hypothetical ideal carrier ampholyte mixture (identical ΔpK_a, identical initial concentration and identical limiting mobility values) were very similar and were caused by the bidirectional isotachophoretic process that unavoidably accompanies IEF.

The authors gratefully acknowledge the financial support of the Czech Science Foundation, GAČR Grant No. 18–11776S and Agilent Foundation Research Gift No. 4135. Advanced Electrophoresis Solutions Ltd., Cambridge, ON, Canada is gratefully acknowledged for lending their imaging CIEF instrument CEInfinite for these experiments and providing the AES SH 3–10 carrier ampholyte mixture.

The authors have declared no conflict of interest.

5 References

[1] Rilbe, H., *Ann. N. Y. Acad. Sci.* 1973, *209*, 11–22.

[2] Rilbe, H., *Electrophoresis* 1984, *5*, 1–17.

[3] Frederiksson, S., *Anal. Biochem.* 1972, *70*, 575–585.

[4] Righetti, P. G., Wenisch, E., Faupel, M., *J. Chromaotgr.* 1989, *475*, 293–307.

[5] Weber, G., Boček, P., *Electrophoresis* 1996, *17*, 1896–1910.

[6] Shimura, K., Wang, Z., Matsumoto, H., Kasai, K., *Electrophoresis* 2000, *21*, 603–610.

[7] Šlais, K., Friedl, Z., *J. Chromatogr. A* 1994, *661*, 249–256.

[8] Righetti, P. G., Gianazza, E., *J. Chromatogr.* 1977, *137*, 171–181.

[9] Šlais, K., Friedl, Z., *J. Chromatogr. A* 1995, *695*, 113–122.

[10] Caslavska, J., Molteni, S., Chmelik, J., Šlais, K., Matulik, F., Thormann, W., *J. Chromatogr. A* 1995, *680*, 549–559.

[11] Friedl, Z., Šlais, K., *Chem. Listy* 1997, *91*, 679–680.

[12] Šlais, K., Horká, M., Nováčková, J., Friedl, Z., *Electrophoresis* 2002, *23*, 1682–1688.

[13] Šťastná, M., Trávníček, M., Šlais, K., *Electrophoresis* 2005, *26*, 53–59.

[14] Shimura, K., Kamiya, K., Matsumoto, H., Kasai, K., *Electrophoresis* 2002, *74*, 1046–1053.

[15] Vigh, G., Li, M., US Patent 9,689,841, 2017.

[16] Klepárník, K., Šlais, K., Boček, P., *Electrophoresis* 1993, *14*, 475–479.

[17] Lalwani, S., Tutu, E., Vigh, G., *Electrophoresis* 2005, *26*, 2047–2055.

[18] Šolínová, V., Kašička, B., *Electrophoresis* 2013, *34*, 2655–2665.

[19] Glukhovskiy, P. V., Vigh, G., *Electrophoresis* 1998, *19*, 3166–3170.

[20] Hruška, V., Jaroš, M., Gaš, B., *Electrophoresis* 2006, *27*, 984–991.

[21] Hruška, V., Beneš, M., Svobodová, J., Zusková, I., Gaš, B., *Electrophoresis* 2012, *33*, 938–947.

[22] Malý, M., Dovhunová, M., Dvořák, M., Gerlor, G. S., Kler, P. A., Hruška, V., Dubský, P., *Electrophoresis* 2019, *40*, 683–692.

[23] Tahupi, Y., Schmidt, D. E., Lindner, W., Karger, B. L., *Anal. Biochem.* 1981, *115*, 123–129.

[24] Katayama, H., Ishihama, Y., Asakawa, N., *Anal. Chem.* 1998, *70*, 5272–5277.

[25] North, R., Vigh, G., *Electrophoresis* 2008, *29*, 1077–1081.

[26] Lalwani, S., Tutu, E., Vigh, G., *Electrophoresis* 2005, *26*, 2503–2510.

[27] Cai, J., Smith, J. T., *J. High Resolut. Chromatogr.* 1992, *15*, 30–32.

[28] Malý, M., Boublík, M., Pocrnić, M., Ansorge, M., Lorinčíková, K., Svobodová, J., Hruška, V., Dubský, P., Gaš, B., *Electrophoresis* 2020, *41*, https://doi.org/10.1002/elps.201900283.

[29] Debye, P., Hückel, E., *Physik. Z.* 1923, *24*, 185–206.

[30] Debye, P., Hückel, E., *Physik. Z.* 1923, *24*, 305–325.

[31] Davies, C. W., *Ion Association*, Butterworths, London, 1962.

[32] Onsager, L., Fuoss, R. M., *J. Phys. Chem.* 1932, *36*, 2689–2778.

[33] Hirokawa, T., Nishimo, M., Aoki, N., Kiso, Y., Sawamoto, Y., Yagi, T., Akiyama, J., *J. Chromatogr.* 1983, *271*, D1–D106.

[34] Mosher, R. A., Thormann, W., *Electrophoresis* 1990, *11*, 717–723.

[35] Bossi, A., Righetti, P. G, *Electrophoresis* 1997, *18*, 2012–2018.

[36] Fitch, C. A., Platzer, G., Okon, M., Garcia-Moreno, B., McIntosh L. P., *Protein Sci.* 2015, *24*, 752–761.

